

INTERACTIONS OF Cu^{2+} WITH PHOSPHATIDYLSERINE AND THEIR
BIOLOGICAL IMPLICATIONS

A Dissertation

by

XIAO CONG

Submitted to the Office of Graduate and Professional Studies of
Texas A&M University
in partial fulfillment of the requirements for the degree of

DOCTOR OF PHILOSOPHY

Chair of Committee,	Paul S. Cremer
Co-Chair of Committee,	David H. Russell
Committee Members,	Gregory D. Reinhart
	Christian Hilty
Head of Department,	François P. Gabbaï

May 2015

Major Subject: Chemistry

Copyright 2015 Xiao Cong

ABSTRACT

Phosphatidylserine (PS) lipids in cell membranes play significant roles in cell apoptosis, blood clotting and neurodegenerative disorders such as Alzheimer's disease (AD). A novel fluorescence quenching assay based on lipid bilayer-coated microfluidic platform was developed to investigate the interactions of PS, Cu^{2+} and PS-related proteins on membranes. PS in supported lipid bilayers (SLBs) was found to bind Cu^{2+} and the resulting $\text{Cu}(\text{PS})_2$ complex could quench a broad spectrum of lipid-bound fluorophores in a reversible and pH-dependent fashion.

This quenching assay was subsequently combined with other spectroscopy techniques to explore how Cu^{2+} -binding affinity changes as a function of PS surface density. The apparent binding affinity of Cu^{2+} to PS got enhanced by about five orders of magnitude as the PS density in SLBs was increased from 1.0 to 20 mol %. Despite the effect of binding valency change from monovalent to bivalent, this binding enhancement was primarily attributed to the greatly amplified Cu^{2+} concentration in the double layer of the surface with a high PS density, since Cu^{2+} -binding preserves the surface charges.

Cu^{2+} -PS interactions have numerous biological implications under specific physiological or pathological conditions. Herein two typical examples were investigated. First one involves the interactions of β -amyloid peptides ($\text{A}\beta$), Cu^{2+} and lipid membranes. $\text{A}\beta$ is an important biomarker of Alzheimer's disease (AD) while $\text{A}\beta$ -binding of transition metal ions can promote its pathological assembly. We applied our

fluorescence assay and mass spectrometry (MS) to mimic how A β acquires Cu²⁺ from cell membranes in AD brains where copper level is generally reported to be depressed. The Cu²⁺ detachment by A β was detected by monitoring the recovery of the fluorescent signal quenched by Cu(PS)₂ complex. This Cu²⁺ transfer behavior can be confirmed by MS detection of different complexes. The results could assist clarifying the membrane-related neurotoxicity of A β and copper homeostasis at pathological conditions. The combination of fluorescence and MS can be further applied in investigations of other Cu²⁺-mediated interactions between proteins and membranes. Another biological implication is about the effect of Cu²⁺-PS binding on lipid oxidations. With PS in vesicles, the oxidation of surrounding unsaturated phosphatidylcholine (PC) lipids was inhibited, which implies that PS in the membranes might protect other lipids against the Cu²⁺-catalyzed oxidation.

ACKNOWLEDGEMENTS

I would like to express my deepest appreciation to my committee chair, Dr. Paul S. Cremer and co-chair, Dr. David H. Russell. I consider myself to be so fortunate to have both of them as my advisors and to have such a unique “a-tale-of-two-cities” experience in two warm research families. I once felt lost and struggled to make choices when Dr. Cremer decided to move to Penn State in my third year of PhD study. Then they offered me a great collaborative research platform to let me work half-by-half in each group, which enabled me to learn so much from both research families. I have benefited a lot from their guidance, wisdom, advices and most importantly, their passion and enthusiasm for science. When I felt frustrated and depressed, they always cheered me up and helped me build up my self-confidence. Without their encouragement, support and help, this dissertation would not have been possible. In addition, thanks also go to my committee members Dr. Christian Hilty and Dr. Gregory D. Reinhart for their insightful comments and suggestions throughout my PhD study.

I am also grateful to work with so many talented researchers over the years. Special thanks go to Dr. Tinglu Yang, Dr. Christopher Monson, Dr. Aaron Robison and Dr. Da Huang for their guidance and helpful discussions on fluorescence study; to Matthew Poyton for all his help, encouragement and teamwork throughout my PhD study and paper writing; to Dr William Russell, Dr. Yohannes Rezenom, Dr. Shu-hua Chen and John Patrick for their guidance and help on mass spectrometry learning; to all the Cremer group members for giving me a wonderful memory of the first two years in

Texas and the last two summers in Penn State; to all the Russell group members for all the joy and warmth they brought in springs and falls. I also want to extend my gratitude to the department faculty and staff, especially Sandy Manning, Julie Zercher, Evamarie Capareda as well as Dana Hosko in PSU who helped me with document works for my summer research in Penn State. Thanks to my friends for making my time at Texas A&M a wonderful experience. Thanks also go to the National Institutes of Health, the Office of Naval Research and Robert A. Welch Foundation that provided the funding for my research.

Finally I would like to thank my family for their unconditional love, understanding and support. I feel so blessed to have my wonderful parents, Wenjuan Jiang and Dr. Yang Cong, and my parents-in-law, Hongsong Wang and Yongqiang Xin. They always believe in me and encourage me to follow my heart to pursue my dream. My husband, Dongyue Xin, has always been a constant source of love, concern, support and strength since we met in the winter of 2007 in college. We felt so lucky to get the offer letters from Texas A&M together and we supported each other throughout our PhD studies all these years. He is the one who shows up when I am in trouble, the one whose shoulder I can cry on, the one who gives brilliant suggestions for my research and the one who always cares for me and pushes me to achieve my goal. I am thankful for sharing the entire amazing journey with him.

NOMENCLATURE

SLBs	Supported Lipid Bilayers
SUVs	Small Unilamellar Vesicles
PDMS	Polydimethylsiloxane
POPC	1-palmitoyl-2-oleoyl- <i>sn</i> -glycero-3-phosphocholine
POPS	1-palmitoyl-2-oleoyl- <i>sn</i> -glycero-3-phospho-L-serine
DOPS	1,2-dioleoyl- <i>sn</i> -glycero-3-phospho-L-serine
DLPS	1,2-dilauroyl- <i>sn</i> -glycero-3-phospho-L-serine
DPPS	1,2-dipalmitoyl- <i>sn</i> -glycero-3-phospho-L-serine
GM ₁	Ganglioside (bovine)
Cardiolipin	1,1',2,2'-tetramyristoyl cardiolipin
DOPG	1,2-dioleoyl- <i>sn</i> -glycero-3-phospho-(1'- <i>rac</i> -glycerol)
DPPG	1,2-dipalmitoyl- <i>sn</i> -glycero-3-phospho-(1'- <i>rac</i> -glycerol)
POPG	1-palmitoyl-2-oleoyl- <i>sn</i> -glycero-3-phospho-(1'- <i>rac</i> -glycerol)
DOPA	1,2-dioleoyl- <i>sn</i> -glycero-3-phosphate
DSPA	1,2-distearoyl- <i>sn</i> -glycero-3-phosphate
TR-DHPE	Texas Red 1,2-dihexadecanoyl- <i>sn</i> -glycero-3-phosphoethanolamine
Tail-labeled NBD-PC	1-palmitoyl-2-{12-[(7-nitro-2-1,3-benzoxadiazol-4-yl)amino]dodecanoyl}- <i>sn</i> -glycero-3-phosphocholine

Tail-labeled NBD-PS	1-palmitoyl-2-{12-[(7-nitro-2-1,3-benzoxadiazol-4-yl)amino]dodecanoyl}- <i>sn</i> -glycero-3-phosphoserine
Head-labeled NBD-PS	1,2-dioleoyl- <i>sn</i> -glycero-3-phospho-L-serine-N-(7-nitro-2-1,3-benzoxadiazol-4-yl)
Rhodamine-DHPE	Lissamine Rhodamine B 1,2-dihexadecanoyl- <i>sn</i> -glycero-3-phosphoethanolamine
Fluorescein-DHPE	N-(Fluorescein-5-thiocarbamoyl)-1,2-dihexadecanoyl- <i>sn</i> -glycero-3-phosphoethanolamine
Bodipy-DHPE	N-(4,4-difluoro-5,7-dimethyl-4-bora-3a,4a-diaza-s-indacene-3-propionyl)-1,2-dihexadecanoyl- <i>sn</i> -glycero-3-phosphoethanolamine

TABLE OF CONTENTS

	Page
ABSTRACT	ii
ACKNOWLEDGEMENTS	iv
NOMENCLATURE	vi
TABLE OF CONTENTS	viii
LIST OF FIGURES	x
LIST OF TABLES	xii
CHAPTER	
I INTRODUCTION	1
Cell Membranes and Supported Lipid Bilayers	1
Properties and Biological Functions of Phosphatidylserine	
Lipids and Copper Ions	3
Detecting Ligand-Receptor Interactions by Fluorescent Sensing	
on Microfluidic Platform Combined with Other Analytical	
Techniques.....	5
II DEVELOPING A FLUORESCENCE QUENCHING ASSAY FOR THE	
DETECTION OF PHOSPHATIDYLSERINE- Cu^{2+} INTERACTIONS.....	9
Introduction	9
Experimental Section.....	11
Results	15
Discussions.....	29
III UNQUENCHABLE SURFACE POTENTIAL DRAMATICALLY	
ENHANCES Cu^{2+} BINDING TO PHOSPHATIDYLSERINE LIPIDS.....	31
Introduction	31
Experimental Section.....	34
Results	39
Discussions.....	53

CHAPTER	Page
IV BETA AMYLOID-METAL ION-MEMBRANE INTERACTIONS UNDER COPPER-DEFICIENT PATHOLOGICAL CONDITIONS	59
Introduction	59
Experimental Section.....	63
Results and Discussions	65
Conclusion.....	76
V THE EFFECTS OF Cu ²⁺ -PHOSPHATIDYLSERINE BINDING ON LIPID OXIDATIONS	77
Introduction	77
Experimental Section.....	79
Results and Discussions	82
VI CONCLUSIONS	98
REFERENCES.....	101

LIST OF FIGURES

	Page
Figure 1.1. The structure of phosphatidylserine (PS) lipid	4
Figure 1.2. Schematic representation of the fluorescence sensing experiments set up on microfluidic devices.....	8
Figure 2.1. The PS-mediated Cu^{2+} quenching reaction.....	11
Figure 2.2. Fluorescence images from parallel lipid bilayers in a microfluidic device.....	16
Figure 2.3. The Cu^{2+} -PS quenching response as a function of pH.....	18
Figure 2.4. UV/Vis and fluorescence spectra of vesicles containing PS..	19
Figure 2.5. A Stern-Volmer plot to determine Cu^{2+} -PS binding stoichiometry.....	21
Figure 2.6. A Job's plot showing the binding stoichiometry of the Cu^{2+} -PS complex.....	22
Figure 2.7. The reversible quenching-dequenching process with a varying pH..	24
Figure 2.8. The quenching of TR-DHPE with various divalent metal chlorides and silver nitrate.....	27
Figure 3.1. Schematic representation of the change of K_{Dapp} with the PS density on SLBs (top) and the binding reaction equation (bottom).....	34
Figure 3.2. (A) Fluorescence images and (B) line scans from lipid bilayers in a multi-channel microfluidic device.....	41
Figure 3.3. Non-competitive binding curves of SLBs containing 1.0 to 7.5 mol % PS.....	43
Figure 3.4. Competitive binding curves of SLBs containing 7.5 to 20 mol % PS.....	45
Figure 3.5. VSFS spectra of DPPS monolayers with divalent metal ions..	51

	Page
Figure 3.6. The negative mode ESI-MS spectra of PS-contained vesicles without or with Cu^{2+} ..	52
Figure 3.7. K_{Dapp} and K_{Dint} values plotted as a function of PS surface density.....	56
Figure 4.1. Schematic diagram of the proposed mechanism of $\text{A}\beta$ - Cu^{2+} -membrane interactions.....	62
Figure 4.2. (A) Fluorescence images and (B) line scans from two parallel microfluidic channels with Cu^{2+} and $\text{A}\beta_{1-16}$..	67
Figure 4.3. Fluorescence response over time showing fluorescence dequenching caused by $\text{A}\beta$ swiping Cu^{2+} ..	69
Figure 4.4. The graphic summary of normalized fluorescence intensity of SLBs containing PS with Cu^{2+} -quenching and $\text{A}\beta_{1-16}$ dequenching.....	72
Figure 4.5. The graphic summary of normalized fluorescence intensity showing $\text{A}\beta_{1-42}$ has the similar ability to grab Cu^{2+} compared with $\text{A}\beta_{1-16}$	73
Figure 4.6. The negative mode ESI-MS spectra of PS-contained vesicles with CuCl_2 and $\text{A}\beta_{1-16}$	75
Figure 5.1. The reconstructed-ion chromatograms (RIC) of the vesicles containing 70 mol % DLPC and 30 mol % PLiPC incubated with Cu^{2+} over different time periods.....	84
Figure 5.2. The proposed formation mechanism of PLiPC radicals susceptible to oxidations.....	85
Figure 5.3. The RIC of the vesicles containing 70 mol % DLPC and 30 mol % PLiPC incubated for 24 hours without Cu^{2+} or with Cu^{2+} and BHT..	89
Figure 5.4. A comparison of the oxidation percentages of vesicles without or with PS over time.....	91
Figure 5.5. A graphic summary showing the comparison of oxidation percentages of PLiPC mixed with different kinds of lipids.....	94
Figure 5.6. A graphic summary showing the comparison of oxidation percentages of PLiPC when different Cu^{2+} -binding reagents were added..	96

LIST OF TABLES

	Page
Table 2.1. Lipids and fluorophores tested for Cu^{2+} quenching	28
Table 3.1. Binding constants of non-competitive binding curves for 1.0 to 7.5 mol % PS and competitive binding curves for 7.5 to 20 mol % PS	44
Table 3.2. The calculated σ , ψ_0 and surface charge-adjusted dissociation constants K_{Dint} for Cu^{2+} binding of SLBs containing 1.0~20 mol % PS	55
Table 5.1. Oxidation products and their possible structures	87

CHAPTER I

INTRODUCTION

Cell Membranes and Supported Lipid Bilayers

Cell membranes play crucial roles in a lot of fundamental biological processes. They usually consist of the lipid bilayer as a core structure and the associated functional proteins such as integral proteins and peripheral proteins.¹ In mammalian cells, glycerophospholipids are the main components of the membranes, which account for about 70% of the total lipid content, while the other 30% are cholesterol, sphingomyelin, and glycosphingolipids.² Differences in lipid compositions in general will affect the charge density and permeability of cell membranes. Specifically, certain lipids are involved in the protein-membrane binding, cell signaling and biosynthetic pathways while the malfunctions of these processes are closely related to diseases.²⁻⁴ Therefore, it is necessary to achieve a better understanding of the properties and functions of specific lipids to further elucidate the molecular basis of those biological events and facilitate the discovery of new therapeutics.

Supported lipid bilayers (SLBs) have been well recognized as model systems to study the properties of cell membranes and the protein-membrane interactions.⁵⁻⁸ Compared with black lipid membranes or suspended lipid membranes, SLBs are superior in their stability and more accessible to the surface characterization techniques

such as atomic force microscope (AFM), fluorescence microscope and quartz crystal microbalance (QCM), due to the immobilization of the analytes on the solid surface.⁹⁻¹² Furthermore, the two-dimensional membrane fluidity is maintained in SLBs owing to a 10~20 Å layer of trapped water lubricant between the solid substrate and the bilayers.^{6,13} Therefore, the redistribution and reorganization of the surface constituent are attainable, which allows for the investigations of multivalent ligand-receptor interactions, cell signaling and lipid trafficking. For example, a pentavalent carbohydrate-protein interaction on membranes, the ganglioside GM₁ binding of cholera toxin B-subunit (CTB), has been explored on SLBs in microfluidic devices.⁹ The results surprisingly showed a 10-fold weaker binding affinity as the GM₁ density was increased from 0.02 to 10.0 mol %. This inhibition of CTB binding on GM₁-enriched membranes is caused by the hydrogen-bonding interactions between adjacent glycolipid headgroups, resulting in the clustering of GM₁ which disturbs the binding.^{9,14} During this study, the fluidic lipid bilayers formed on glass surface provide an applicable ligand presentation platform which can be visualized by fluorescence microscope and AFM.

SLBs can be formed on a variety of solid substrates, such as glass, quartz, mica, gold and titanium oxide.^{6,12,15-17} Three methods are generally used to form SLBs.⁶ The first approach is vesicle adsorption and fusion. After incubating with the solid support, lipid vesicles in aqueous solutions can spontaneously adhere to the substrate and fuse to form the lipid bilayers.¹⁸ The second way is through a layer-by-layer lipid deposition on solid surface based on Langmuir-Blodgett technology.¹³ Additionally, a combinative method can be applied, in which a monolayer is firstly transferred to the surface via

Langmuir–Blodgett method followed by vesicle fusion to form the upper layer of SLBs.¹⁹ The first method is easier and more versatile while the other two are usually employed to form asymmetric SLBs.⁶

Properties and Biological Functions of Phosphatidylserine Lipids and Copper Ions

Phosphatidylserine (PS) is one of the most abundant negatively charged phospholipids in cell membranes (structure shown in Figure 1.1).² It can be found in a variety of cells and plays an important role in apoptosis, blood clotting and embryonic development, which can be attributed to its unique physical and biochemical identities.^{2,20-23} PS density varies significantly throughout various cellular membranes and moreover, PS lipids are asymmetrically distributed between two leaflets of an individual membrane bilayer.² For example, PS preferentially resides in the cytoplasmic leaflet of plasma membrane due to the action of aminophospholipid flippases, whereas the translocation of PS from the inner to outer leaflet is usually associated with cell apoptosis.^{2,21,24} Carrying one negative charge at physiological pH, PS is known to form complexes with metal ions such as Ca^{2+} and Mg^{2+} through the carboxyl and phosphate groups.²⁵⁻²⁹ These interactions are assumed to be relatively weak with equilibrium dissociation constants generally measured in mM~M range.^{25,28,30} Despite an abundance of studies on Ca^{2+} -PS binding, there is far less known about how transition metal ions interact with PS.^{26,31}

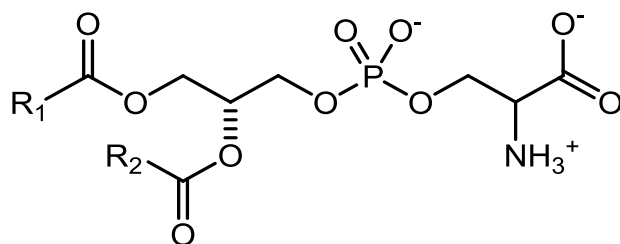


Figure 1.1. The structure of phosphatidylserine (PS) lipid

Transition metal ions are essential for the activities of various enzymes and influence a number of medically relevant events.^{32,33} Copper is the third most abundant transition metal in human body and it is redox-active.³² Generally, the distribution of copper ions within cells is strictly regulated by enzymes and chaperons while the labile Cu^{2+} is toxic to cells and closely linked to neurodegenerative disorders such as Wilson's disease and Alzheimer's disease.^{33,34} However, many questions still remain concerning copper ion homeostasis and how it contributes to disease.

Cu^{2+} is generally found to bind negatively charged residues of proteins as well as the lone electron pairs of nitrogen on histidine, lysine, arginine and N-terminus.³⁵⁻³⁸ Decades ago, in an initiative study, Cu^{2+} was found to form a complex with PS in 1:2 ratio at the interface of organic/aqueous solution.²⁶ Further studies indicated that Cu^{2+} -PS interactions have numerous biological implications, such as the PS-dependent protein-membrane binding and the oxidative damage of cell membranes.^{2,39} The consequences of these interactions are probably more pronounced when PS lipids are flipped from the inner to outer leaflets of plasma membranes during apoptosis or other biological processes, which increase the exposed PS density on cell membranes and

enable the direct contact of PS with a Cu^{2+} -rich environment.^{24,40} Therefore, it is appealing to study the properties and functions of Cu^{2+} -PS binding in these biological events. Previous studies of Cu^{2+} -PS focused upon detecting the effect of divalent cations (Ca^{2+} and/or Cu^{2+}) binding on molecular motions of PS in a water-methanol-chloroform mixed solvent.²⁶ However, Cu^{2+} -PS interactions had only been characterized with mM Cu^{2+} concentrations using atomic absorption spectroscopy (AAS) and electron spin resonance spectroscopy (ESR).²⁶ This inspired us to develop a generally applicable and more sensitive fluorescence-based assay which allows us to detect physiological levels of Cu^{2+} and investigate the interactions of Cu^{2+} and the negatively-charged PS on lipid bilayers.

Detecting Ligand-Receptor Interactions by Fluorescent Sensing on Microfluidic Platform Combined with Other Analytical Techniques

Ligand-receptor interactions are essential to various biological processes including cell signaling, pathogen recognition and inflammatory response.^{3,41} Understanding these interactions on a molecular basis and how they are associated with membrane chemistry should provide insights into the elucidation of biological processes and the targeted drug design. Fluorescence sensing methods based on microfluidic devices have been established by our group to investigate the ligand–receptor interactions on lipid membranes.^{42,43} This lab-on-a-chip technique on a microfluidic

platform allows for a rapid, high-throughput and low-sample-volume analysis with an unprecedented signal-to-noise ratio.

The microfluidic devices are fabricated from oxygen plasma-cleaned polydimethylsiloxane (PDMS) patterns and annealed glass coverslips. After loading the small unilamellar vesicles (SUVs) into each of the channels in microfluidic devices and incubating them for thirty minutes, the lipid bilayers can be formed through vesicle adsorption and fusion.^{44,45} Incorporating lipid-bound fluorophores into the lipid bilayers enables us to visualize parallel channels and create a real-time *in situ* detection on the SLBs. The buffer solutions containing proteins, drug molecules or metal ions can be continuously introduced to the lipid bilayers through a gravity-driven flowing method (Figure 1.2). The equilibrium can be established quickly at high sample concentrations while it might take as long as several hours for samples in low concentrations (pM~nM) to reach equilibrium. Usually, only microliters to milliliters of samples are required for the detection. The data from lipid bilayers with different lipid compositions or protein concentrations can be acquired simultaneously in multiple channels to generate binding curves.

This fluorescence method can be combined with other analytical techniques to address the research questions and provide more in-depth information for ligand-receptor interactions. In this dissertation, several other spectroscopy techniques such as dynamic light scattering (DLS), ultraviolet–visible spectroscopy (UV/Vis), fluorometry and vibrational sum-frequency spectroscopy (VSFS) were employed in different projects. For example, VSFS based on sum frequency generation (SFG) was used to elucidate

surface-specific water molecules at a lipid monolayer/water interface involving cation-lipid interactions and measure the surface charges.⁴⁶⁻⁴⁸ Besides, electrospray ionization mass spectrometry (ESI-MS) and liquid chromatography–mass spectrometry (LC-MS) also play big parts in the studies into ion-lipid and ion-peptide binding as well as the lipid oxidation chemistry. Given the ability of ESI-MS to manipulate large molecular ions through soft ionization mode, the binding complexes can be examined in a straightforward way to confirm their structures and stoichiometry.^{49,50} The lipid oxidation products at different conditions can be quantitatively measured by LC-MS, which helps us to investigate if these metal ion-lipid interactions can promote or disrupt the oxidation damage of the membranes.⁵¹

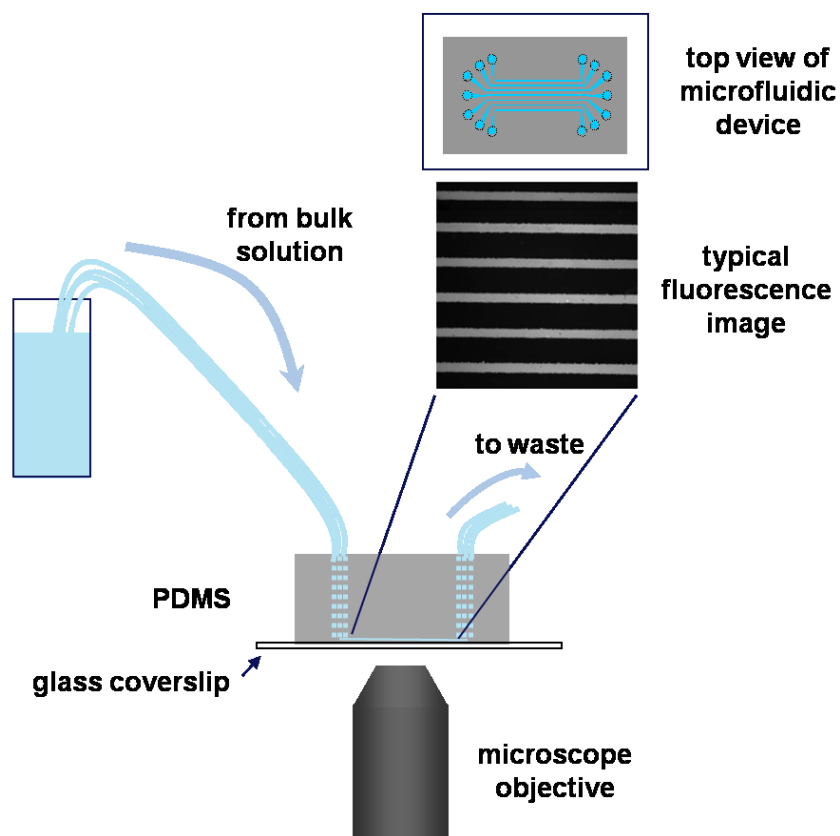


Figure 1.2. Schematic representation of the fluorescence sensing experiments set up on microfluidic devices. The microfluidic device consisted of a patterned PDMS block adhered to a glass coverslip. Top view of the device was shown in the right top, as well as a typical fluorescent image obtained from lipid bilayers in multiple channels. The fabrication procedure for the device was described in the experimental section in Chapter II. For binding detections, buffer solutions containing proteins, metal ions or drug molecules were flowed into each channel by several Teflon tubes through each inlet port to interact with SLBs. Flow through the device was gravity driven with an average flow rate at $\sim 100 \mu\text{L/h}$ in each channel. The consumed buffer drained from each outlet port to waste container. The fluorescence of each channel was monitored by an inverted epifluorescence microscope.

CHAPTER II

DEVELOPING A FLUORESCENCE QUENCHING ASSAY FOR THE DETECTION OF PHOSPHATIDYLSERINE- Cu^{2+} INTERACTIONS*

Introduction

Phosphatidylserine (PS) lipids are found in a wide variety of cell types, but are typically only present in moderate abundance. In eukaryotic systems, they account for approximately 5-10 mol % of phospholipid content.² Moreover, PS is unevenly distributed within cells. For example, it is enriched in the inner leaflet of the plasma membrane and depleted in the outer leaflet.^{2,20} It is essentially absent in mitochondrial membranes.^{2,52} A number of proteins interact specifically with PS and it is an important signaling molecule in clotting, apoptosis, and embryonic development.^{2,23,53-57} PS bears a negative charge at physiological pH and is known to form complexes with metal ions such as Ca^{2+} , Mg^{2+} and Cu^{2+} .^{25,58,59} These interactions are assumed to be relatively weak with equilibrium dissociation constants that have been generally measured in the mM range for Ca^{2+} . The presence of Ca^{2+} mediates a number of protein-PS interactions and therefore the Ca^{2+} -PS interaction has been relatively well studied.^{25,60-63} There have been far fewer investigations of Cu^{2+} -PS interactions, although it is known that at mM concentrations Cu^{2+} forms a 1:2 complex with PS in solutions containing water, methanol, and chloroform.⁵⁹

*Reprinted with permission from “Phosphatidylserine Reversibly Binds Cu^{2+} with Extremely High Affinity” by Monson, C. F.; Cong, X.; Robison, A. D.; Pace, H. P.; Liu, C. M.; Poyton, M. F.; Cremer, P. S. *Journal of the American Chemical Society* **2012**, *134*, 7773. Copyright 2012 by American Chemical Society.

Cu^{2+} is necessary for the proper activity of various enzymes, but uncomplexed Cu^{2+} is toxic to cells.^{64,65} Indeed, in healthy cells the total copper ion concentration is generally around 100 μM , but the free copper ion concentration is so low that on average there is less than one free ion per cell.⁶⁶ Thus, copper is tightly regulated with copper chaperones responsible for the delivery of copper ions to copper-binding enzymes and the vast majority of the copper delivery is in the form of Cu^+ .^{65,67} Excessive copper has been linked to Wilson's disease and a number of medically relevant events are influenced by copper ions, including the outcome of vascular injury and the onset of prion disease.^{68,69} Cu^{2+} has also been proposed for use as an anti-tumor agent.⁷⁰

Using a fluorescence quenching assay, we report herein that PS binds Cu^{2+} on lipid bilayers in a reversible fashion. The Cu^{2+} -PS system forms a one metal ion-to-two PS lipid complex and is observed to quench a variety of lipid-bound fluorophores as illustrated schematically in Figure 2.1. Fluorescence quenching takes place at basic pH values and unquenching occurs under acidic conditions. The 1:2 Cu^{2+} -PS complex has a number of implications for biological processes. For example, the PS-enriched inner plasma membrane may serve as a Cu^{2+} scavenger or as a location for copper-dependent reactions at high environmental Cu^{2+} levels.

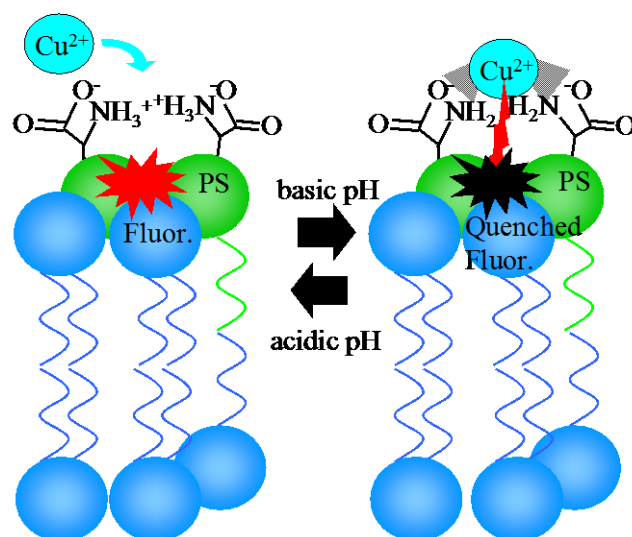


Figure 2.1. The PS-mediated Cu^{2+} quenching reaction. At basic pH values, Cu^{2+} binds to 2 PS molecules and quenches nearby fluorophores (red to black in the diagram). The reaction can be reversed by lowering the pH.

Experimental Section

Vesicle Preparation

Phospholipid vesicles were prepared using the freeze-thaw/extrusion method.^{71,72} Lipids were mixed in chloroform at the desired ratio and then the chloroform was evaporated in a stream of N_2 gas. The dried lipids were put under vacuum for at least four hours to remove any remaining solvent. The lipid mixture was rehydrated with Tris buffer (100 mM NaCl, 10 mM tris(hydroxymethyl)aminomethane, pH 7.4), subjected to ten freeze/thaw cycles in liquid nitrogen and warm water, and then extruded through a track etched polycarbonate membrane with 100 nm pores (Whatman, Florham Park, NJ). The vesicles were diluted to 1 mg/mL with Tris buffer and stored at 4 °C until use. The

average size of the vesicles was found to be 100 ± 20 nm by dynamic light scattering (90Plus Particle Size Analyzer, Brookhaven Instrument Corp., Holtsville, NY).

Glass Cleaning

Glass coverslips (Corning, Inc., Corning, NY, 24 x 40 mm No. 1.5) were cleaned by boiling in a 1:5 solution of 7X (MP Biomedicals, Solon, OH) and purified water. The slides were extensively rinsed with 18 M Ω water (Barnstead Nanopure water purification system, Thermo Scientific), blown dry with filtered air, and annealed at 530 °C for five hours.⁴²

Microfluidic Fabrication

Microfluidic devices were fabricated from polydimethylsiloxane (PDMS, Sylgard 184, Dow Corning, Midland, MI) and clean glass coverslips using previously reported procedures.⁴² Briefly, HF etching was performed on a glass plate protected by photolithographically patterned photoresist (MICROPOSIT S1813, Shipley Corp. Marlborough, MA) to form a master. PDMS was mixed in a 10 part base to 1 part polymerizer mass ratio, degassed under vacuum for 1 hour, poured over the master, and baked at 100 °C for 2 hours. Access holes were punched with a polished needle. The devices were assembled by pressing together an oxygen plasma-cleaned PDMS body and an oxygen plasma-cleaned glass cover slip and heating to 100 °C for 1 minute.

Bilayer Formation

SLBs were formed via the vesicle fusion method.⁷³⁻⁷⁵ Fourteen microliters of vesicle solution were injected via a pipette into each channel of a freshly prepared microfluidic device. In all runs, the largest lipid component of the vesicles was 1-palmitoyl-2-oleoyl-*sn*-glycero-3-phosphocholine (POPC, Avanti Polar Lipids, Alabaster, AL). A fluorescent lipid was also present, typically Texas Red 1,2-dihexadecanoyl-*sn*-glycero-3-phosphoethanolamine (TR-DHPE, Invitrogen, Carlsbad, CA) at either 0.1 or 1.0 mol % along with 0 to 30 mol % PS. 1,2-dioleoyl-*sn*-glycero-3-phospho-L-serine (DOPS, Avanti Polar Lipids, Alabaster, AL) was the PS species used in all experiments unless otherwise noted. The vesicles spontaneously fused to the cleaned glass slides to form continuous SLBs. After a thirty minute incubation time, the channels were rinsed by gravity driven buffer flow for one hour to remove any remaining vesicles and experiments were subsequently commenced.

Microfluidic Procedure

Five to seven supply tubes (0.6 mm internal diameter Teflon tubing, SPC Technology) brought buffer from a reservoir to the individual microfluidic channels of the PDMS/glass device and the consumed buffer drained to a waste container (Figure 1.2). Flow through the device was gravity driven with an average flow rate on the order of 200 μ L/hour in each microfluidic channel. The total buffer consumption rates were on the order of 10 mL/hour when the buffer was being exchanged. Tris, phosphate, and

citrate buffers were tested to ensure the independence of the observed quenching reaction by specific buffers. Similar behavior was observed with each buffer.

For the flow cell experiments shown in this work, a universal buffer consisting of a 2:1:2 molar ratio of sodium citrate:MES (2-(*N*-morpholino)ethanesulfonic acid):Tris was used.⁷⁶ The buffer was adjusted to the desired pH value with NaOH and HCl. Most buffers were run at 1 mM total buffer concentration with only trace amounts of CuSO₄ and no other salts present. CuSO₄ and CuCl₂ salts were both tested as sources of Cu²⁺ and no difference was observed in the quenching reaction. Buffer was constantly flowed through the channels during all experiments. When the buffer reservoir solution was exchanged, there was a lag time of a few minutes before the fluorescence intensities inside the microchannels began to change. This was due to the dead volume in the tubing between the container and the microfluidic device. The fluorescence of the channels was intermittently observed until equilibrium was reached. When low CuSO₄ concentrations were employed (pM and below), several hours were required for equilibrium to be established.

Vesicle Titration Measurements

Fluorescence measurements at constant Cu²⁺ concentrations were recorded in a QE 65000-FL Scientific Grade Spectrometer with a DH-2000 Deuterium Tungsten Halogen Light Source (Ocean Optics, Dunedin, FL). The lipid mixture with 1 mol % TR-DHPE and 15 mol % DOPS in POPC was mixed in chloroform and dried with flowing N₂ and vacuum. It was then rehydrated with Tris/NaCl buffer (10 mM Tris, 100

mM NaCl, pH 7.4) containing serial concentrations of CuSO₄ ranging from 0 to 43 μM. This was followed by ten freeze/thaw cycles in liquid nitrogen and warm water. Finally, the vesicles were extruded through a track etched polycarbonate membrane with 100 nm pores (Whatman, Florham Park, NJ). In this way, CuSO₄ should be distributed both inside and outside the vesicles, which is important to insure that fluorophores on both leaflets can be accessed by Cu²⁺. Fluorescence measurements were performed with 1.5 mL aliquots of these 100 nm vesicle solutions at 0.17 mg/mL.

Results

Cu²⁺-PS Binding in Flowing Buffer inside Microfluidic Channels

In a first set of experiments, fluorescence imaging of supported lipid bilayers was performed in two parallel microfluidic channels. The bilayers contained 0.1 mol % TR-DHPE and were interrogated at pH 3.6 and 8.0 in the presence and absence of 800 pM CuSO₄ (Figure 2.2). The left channel of each channel pair contained no PS, while the right channel had 20 mol% PS in the bilayer. As can be seen, the fluorescence intensity was uniform under most conditions. However, in the presence of both PS and Cu²⁺ the fluorescent response of the TR-DHPE was quenched by a factor of 5 under basic conditions. If any one of the three necessary components (PS, Cu²⁺, and basic pH) for quenching were missing, very little or no quenching was observed. As will be explored below, the quenching was the result of Cu²⁺-PS complex formation, as illustrated in

Figure 2.1. The complex localized Cu^{2+} near the bilayer surface, which in turn quenched the fluorophore.

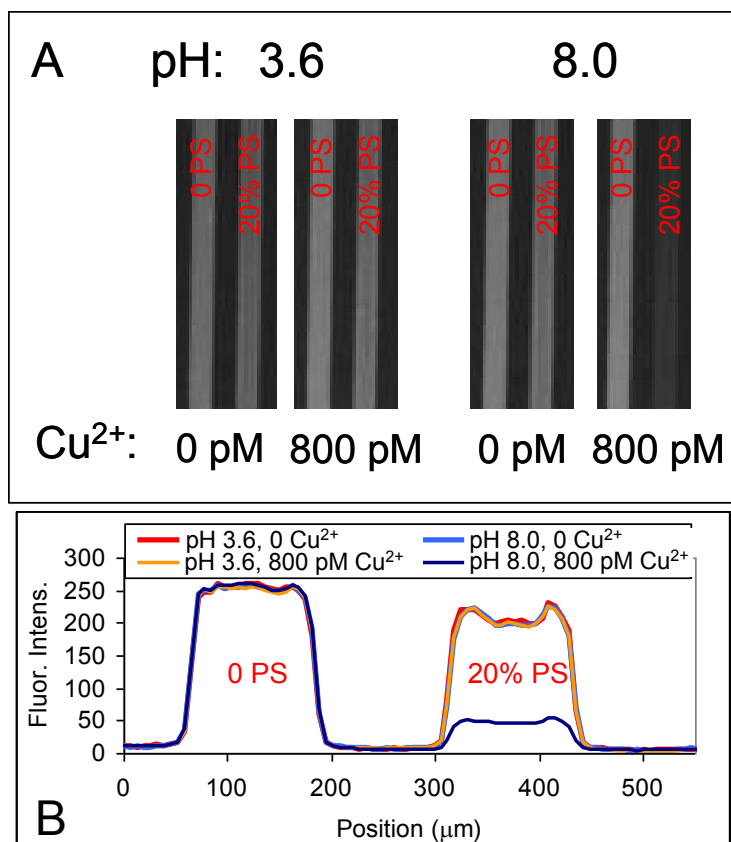


Figure 2.2. Fluorescence images from parallel lipid bilayers in a microfluidic device. (A) Fluorescence images and (B) line scans from microfluidic devices when no DOPS (left channel) and 20 mol% DOPS (right channel) were present in SLBs along with 0.1 mol % TR-DHPE. The fluorescence is shown in the presence and absence of 800 pM CuSO_4 at both pH 3.6 and 8.0 with 1 mM citrate/MES/Tris buffer. The increased fluorescence intensity observed on the sides of the channels in the line scans with the 20 mol% DOPS channel is an edge effect from where the glass floor of the microchannels met the PDMS walls.⁷⁷

To explore the pH response of this process, the pH of the buffer flowing over the SLBs was varied between pH 3 and pH 10 with 800 pM CuSO₄ and the DOPS concentration in the SLBs was varied from 0 to 30 mol % (Figure 2.3A). Each data set was normalized to its own maximum intensity over the pH range to better illustrate the pH at which the fluorescence began to be quenched at a given amount of DOPS. The midpoint of the titration curve occurred near pH 5.5 when 30 mol% DOPS was present. This titration point shifted to higher pH and became much less pronounced as the concentration of DOPS was lowered. Also, at a given pH, increasing the amount of PS in the SLB increased the quenching that occurred. The dye employed in these experiments, TR-DHPE, consisted of *ortho* and *para* isomers. The *ortho* dye, which is usually no more than a quarter of the mixture, is reversibly quenched at basic pH values.⁷⁷ This accounts for a small decrease in fluorescent signal observed at pH 10.5 even in the absence of DOPS. Moreover, it should be noted that dequenching occurred above pH 11. This is due to the formation of a copper hydroxide complex, most likely [Cu(OH)₄]²⁻.⁷⁸

Stern-Volmer plots in Figure 2.3A show near linear dependence as the DOPS concentration was increased until at least 20 mol % DOPS (Figure 2.3B). F₀ was the fluorescence intensity when no quencher was added and F was the observed fluorescence intensity at the indicated quencher concentration. In this and subsequent figures, the error bars represent the standard deviation of multiple measurements. The fluorescence increase became somewhat nonlinear above 20 mol % DOPS at pH 9.0. This may be because essentially all of the TR-DHPE molecules could already be quenched with just 20 mol % DOPS. The quenching constant (slope of the line)

increased with increasing pH, but even at relatively acidic pH values there was modest quenching of the TR-DHPE. Of course, the degree of quenching can also be seen to diminish as the DOPS concentration was lowered, which is consistent with a greater average distance between Cu^{2+} -PS complexes and TR-DHPE molecules under these conditions. Control experiments using UV-visible spectroscopy demonstrated that quenching occurs under conditions where the adsorption of the fluorophore neither shifts nor attenuates (Figure 2.4). As such, a dynamic rather than a static quenching mechanism should be involved.^{79,80}

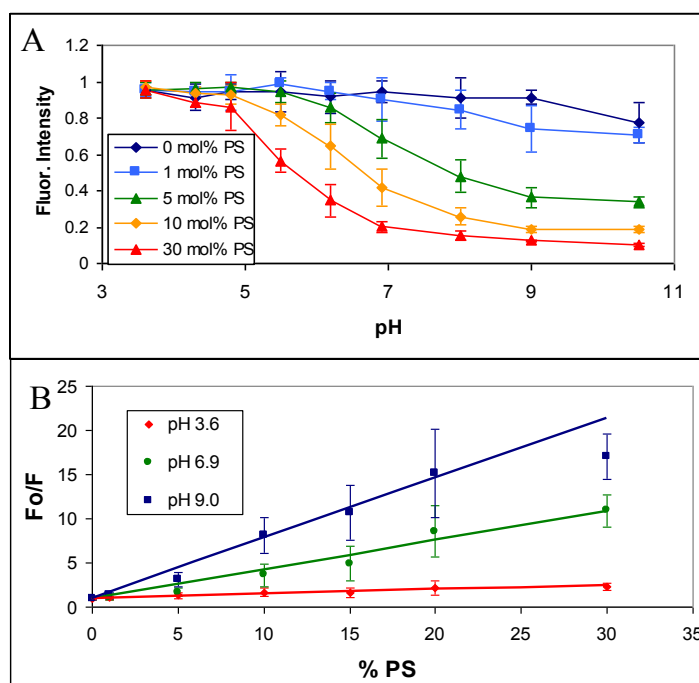


Figure 2.3. The Cu^{2+} -PS quenching response as a function of pH. In (A) the fluorescence intensity is shown as a function of pH. In (B) a Stern-Volmer plot of the data is shown at pH 3.6, 6.9, and 9.0. Both plots are for SLBs consisting of 1.0 mol % TR-DHPE and 0 to 30 mol % DOPS in POPC with a 1 mM citrate/MES/Tris buffer and 800 pM Cu^{2+} .

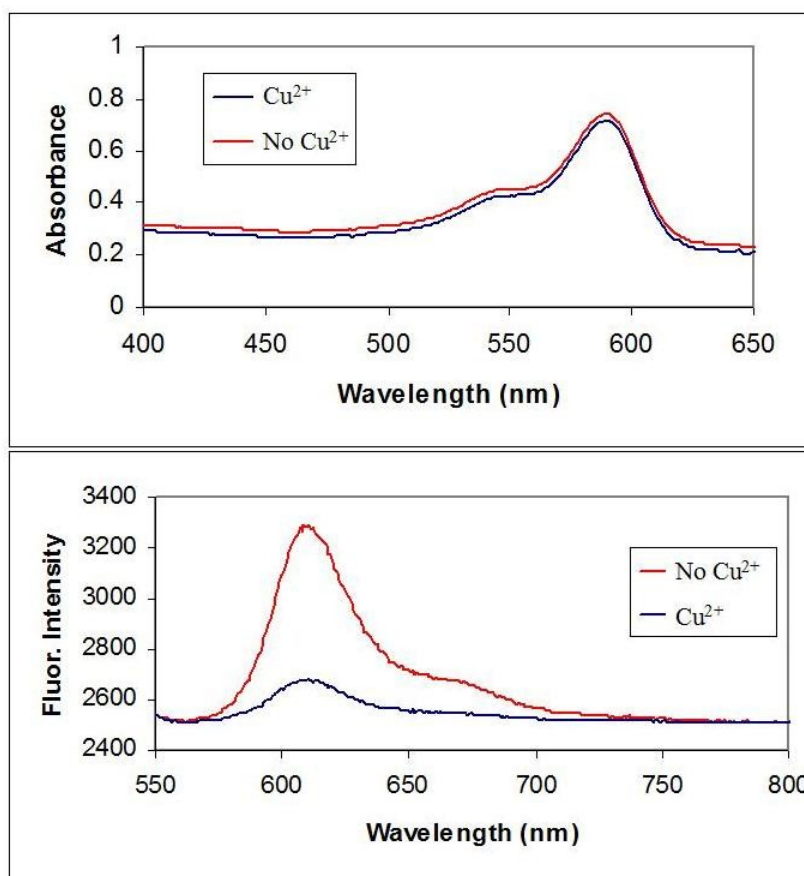


Figure 2.4. UV/Vis and fluorescence spectra of vesicles containing PS. (Top) Absorbance and (bottom) fluorescence emission spectra are from 100 nm vesicles composed of 1 mol % TR-DHPE, 15 mol % DOPS and 84 mol % POPC at 1 mg/mL. The experiments were performed in 10mM Tris buffer containing 100 mM NaCl, at pH 7.4. The red spectra show no addition of CuSO₄, while the blue spectra were taken with the addition of 100 μ M CuSO₄. Fluorescence excitation was performed at \sim 525 nm.

Results at Fixed Total Cu²⁺ Concentrations

In the microfluidic experiments discussed above, a continual flow of buffer above the SLBs ensured that a constant Cu²⁺ concentration was maintained in the bulk solution even as Cu²⁺ bound to the DOPS lipids. In the next set of experiments, measurements were performed with bulk vesicle solutions in a cuvette to determine the

quenching behavior as the DOPS was titrated with a fixed amount of Cu^{2+} (Figure 2.5). In these experiments, the added Cu^{2+} was consumed to form Cu^{2+} -DOPS complexes and thus the fluorescence response decreased as a function of time before leveling off. The data were obtained at multiple CuSO_4 concentrations in well mixed solutions.

CuSO_4 solution was added to aqueous solutions containing 100 nm vesicles with 15 mol % DOPS and 1 mol % TR-DHPE at pH 7.4. The total lipid concentration was 0.17 mg/ml; hence, the DOPS concentration was approximately 33 μM . Monitoring the extent to which the fluorescence was ultimately quenched as a function of CuSO_4 concentration produced a nearly linear rise in the Stern-Volmer plot at lower Cu^{2+} concentrations before reaching a plateau as the concentration was further increased (Figure 2.5). The crossover between these regimes occurred at about 16 μM CuSO_4 . This concentration represented a Cu^{2+} to PS ratio of approximately 1 to 2. In addition to the Stern-Volmer data, the Job's method of continuous concentration variation was applied to confirm the binding stoichiometry between PS and Cu^{2+} (Figure 2.6).⁸¹ Here the total molar concentration of PS and Cu^{2+} was held constant at 33 μM , while their mole fractions were varied. The fraction of the quenched fluorescence, which is related to the amount of complex formed, was plotted against the mole fraction of Cu^{2+} . The inflection point of the Job's plot yielded the binding stoichiometry of the complexes formed. As can be seen, the maximum in fluorescence quenching occurs when the mole fraction of Cu^{2+} is about 0.33. This is consistent with the Stern-Volmer plot to give a 1:2 binding ratio for the Cu^{2+} -PS complex.

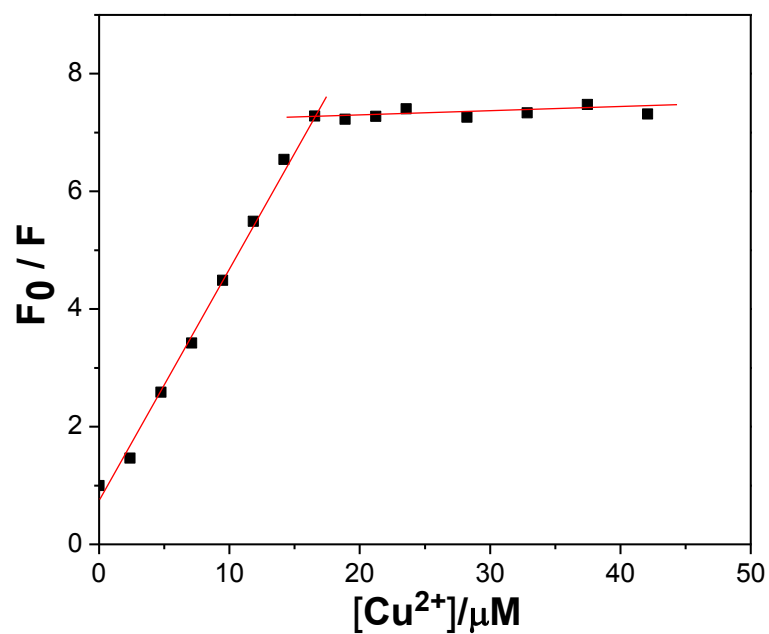


Figure 2.5. A Stern-Volmer plot to determine Cu^{2+} -PS binding stoichiometry. A Cu^{2+} titration experiment was performed for POPC vesicle solutions containing 15 mol % DOPS and 1 mol % TR-DHPE. 10 mM Tris buffer containing 100 mM NaCl at pH 7.4 was used and the indicated amount of $CuSO_4$ was added during vesicle extrusion.

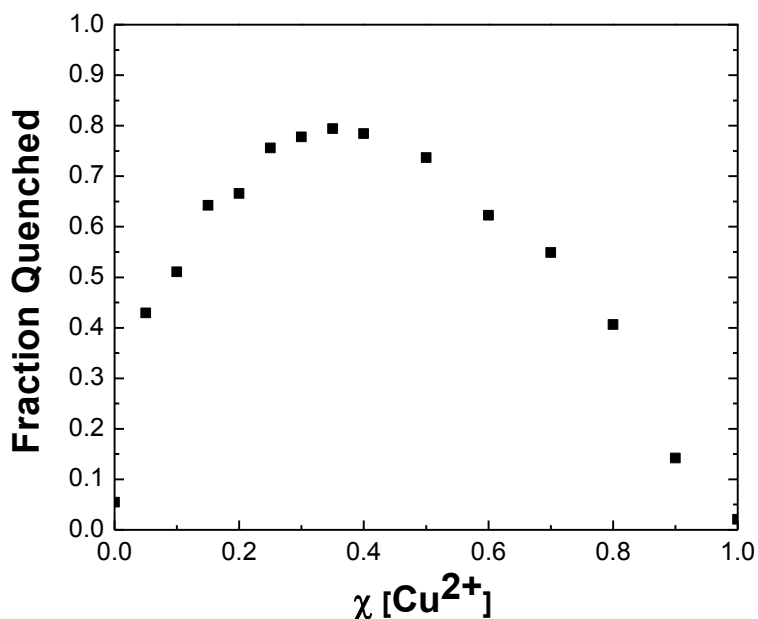


Figure 2.6. A Job's plot showing the binding stoichiometry of the Cu^{2+} -PS complex. The experiments were performed in Tris/NaCl buffer (10 mM Tris, 100 mM NaCl, pH 7.4). Serial 100 nm POPC vesicles containing 1 mol % TR-DHPE, 0 to 15 mol % DOPS at 0.17 mg/mL were used and the serial concentrations of CuSO_4 ranging from 0 to 33 μM was added during vesicle extrusion. The total molar concentration of PS and Cu^{2+} was held constant at 33 μM , while their mole fractions were varied.

The formation of a 1:2 Cu^{2+} -PS complex is in good agreement with previous spectroscopic and titration data with PS lipid and small molecule systems.^{59,82,83} For example, a 1:2 complex has been shown to be formed between Cu^{2+} and O-phospho-L-serine and in bulk aqueous solution at basic pH values.⁸³ EPR data from that system matched the data we got from 15 mol % DOPS in POPC vesicles with a saturation concentration of CuSO_4 .⁴⁵ Analogous CuL_2 complexes with amino acids have also been reported.^{83,84} As such, the Cu^{2+} -PS binding likely involves the amine and carboxylic acid groups of two PS molecules and results in the deprotonation of the amine.

pH-Driven Reversibility of the Quenching Process

In a next set of experiments, the reversibility of the 1:2 Cu^{2+} -PS complex in SLBs was explored as a function of pH in microfluidic channels with continuous buffer flow. Figure 2.7A shows the response of four different DOPS concentrations ranging from 0 to 20 mol % in POPC bilayers with 0.1 mol % TR-DHPE as the pH was varied in buffers that contained 50 nM CuSO_4 . The fluorescence was initially low after rinsing at pH 7.9 for bilayers containing PS. The intensity rose when the pH was reduced to 5.1. It could then be raised and lowered reversibly by modulating the pH of the bulk solution. The fluorescence intensity of each channel was normalized to its own maximum value to facilitate comparisons among the various DOPS concentrations. The quenching was highly stable and reproducible. The light exposure was kept sufficiently low such that photobleaching was relatively minor in these experiments.

The fluorescence quenching rate was much slower than the de-quenching process, which typically took only a few minutes. Such results are consistent with the notion that the Cu^{2+} -DOPS complex formation rate is slow and probably limited by a PS diffusion process required for the one ion, two lipid complex to form. On the other hand, when the pH was lowered, the complex quickly broke up as the protonation of the negatively charged DOPS molecules was rapid. The rate of dequenching upon acidification was limited by the rate at which the pH of the buffer solution could be changed within the microfluidic device. To further investigate the complex formation process, pH jump experiments were performed as a function of CuSO_4 concentration (Figure 2.7B). As can be seen, the formation rate was significantly attenuated at the lowest Cu^{2+} concentration.

Indeed, the quenching took approximately 2 hours to come to completion when only 50 pM CuSO₄ was employed. By contrast, the unquenching reaction was essentially independent of Cu²⁺ concentration. Again, the finite time it took to measure unquenching was related to the time it took to replace the buffer in the channels.

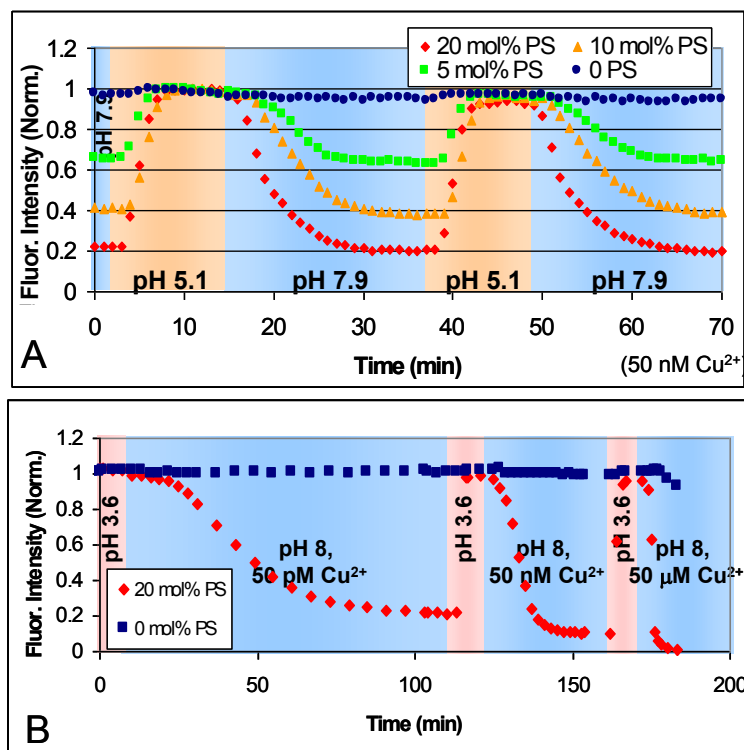


Figure 2.7. The reversible quenching-dequenching process with a varying pH. In (A) the fluorescence intensity of 0, 5, 10, and 20 mol % PS is shown as the pH is alternated between pH 5.1 (orange background) and 7.9 (blue background) in 1 mM citrate/MES/Tris with 50 nM Cu²⁺. (B) Experiments in which different concentrations of CuSO₄ solution were tested at pH 3.6 (pink background) and 8.0 (blue background) with 50 pM, 50 nM, and 50 μM levels of CuSO₄. The SLBs consisted of 0.1 mol % TR-DHPE in POPC at the labeled DOPS concentration. The buffer was 1 mM citrate/MES/Tris.

It should be noted that at 50 μM CuSO_4 some quenching was observed even when PS was absent (blue data points in Figure 2.7B). This most likely occurred because Cu^{2+} concentrations in the μM range were sufficiently high to result in some direct fluorophore-ion interactions without the need for the mediation of the Cu^{2+} -DOPS complex. Another possible source of fluorophore quenching may be the Cu^{2+} -catalyzed generation of reactive oxygen species.⁸⁵ This should result in permanent quenching independent of pH or Cu^{2+} concentration. Indeed, some permanent quenching was observed when the CuSO_4 concentration was raised to μM or mM levels, and the degree of irreversible quenching was observed to increase with time. However, below 1 μM Cu^{2+} , only reversible quenching and a very small amount of photobleaching were observed.

Metal Ion Specificity for the PS-related Quenching

In a penultimate set of experiments, we wished to explore the specificity of the quenching process to the identity of the cation. Heavy metal ion quenching of fluorophores is a common phenomenon,⁸⁰ and thus other divalent cations as well as Ag^+ were tested for their ability to bind PS and quench the TR-DHPE fluorophore. The results of these experiments are shown in Figure 2.8. 2.4 μM of each metal ion was added to solutions of vesicles containing 1 mol % TR-DHPE, 15 mol % DOPS, and 84 mol % POPC and the resulting quenching was monitored. In all cases, the metal ion was added as a chloride salt except Ag^+ , which was added as a nitrate salt. As can be seen, Cu^{2+} was the strongest quencher tested, although Ni^{2+} showed some quenching ability. It

should be noted; however, that quenching by Ni^{2+} only occurred at ion concentrations as high as μM scale compared with Cu^{2+} .

In additional microfluidic experiments, it was found that when $50 \mu\text{M}$ Ca^{2+} or Cd^{2+} were introduced after 950 pM Cu^{2+} , the fluorescence intensity was observed to increase slightly, perhaps because these ions were able to displace some Cu^{2+} already bound to the PS. Thus, it would appear that an ion has to meet two criteria to induce PS-mediated quenching. First, the ion has to form a complex with PS, as does Cu^{2+} , and to a lesser extent Ni^{2+} , Cd^{2+} and Ca^{2+} . Second, the ion has to quench the fluorophore, as do Cu^{2+} , Ni^{2+} , Sr^{2+} , and Co^{2+} .⁸⁰ Since only Cu^{2+} and Ni^{2+} fulfill both criteria, they are the only two ions tested that generated appreciable PS-mediated quenching. It should be noted that Fe^{3+} was also tested, but it was found to only moderately quench TR-DHPE regardless of the presence or absence of PS under acidic or basic conditions. This modest quenching was presumably due to direct ion-fluorophore interactions (The control experiments of direct ion-fluorophore quenching occurring at mM salt concentrations can be found in ref.45).

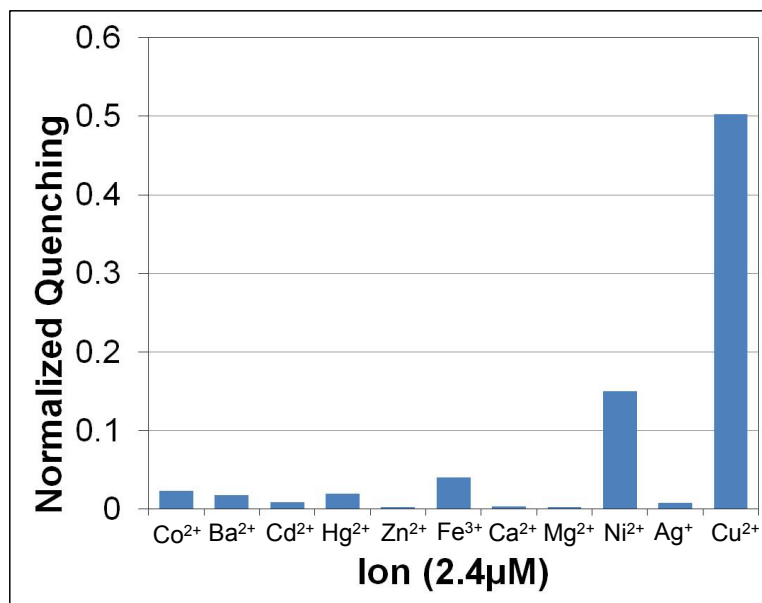


Figure 2.8. The quenching of TR-DHPE with various divalent metal chlorides and silver nitrate. The experiments were performed at pH 7.4 with 1 mM Tris and 100 mM NaCl. 2.4 μM of each metal ion was added to solutions of vesicles containing 1 mol % TR-DHPE, 15 mol % DOPS, and 84 mol % POPC.

Lipid Specificity and Fluorophore Generality

Finally, to ensure that quenching was specific to PS and general to a wide number of fluorophores, various negatively charged lipids and fluorophores were tested for pH-dependent quenching (see Table 2.1 for a summary of the fluorophores and lipids tested). All PS lipids tested (DLPS, DOPS, and DPPS) quenched lipid conjugated fluorophores in the presence of Cu²⁺, but no other lipids tested (PG, PA, PC, GM₁, and cardiolipin) produced any significant quenching.

Table 2.1. Lipids and fluorophores tested for Cu²⁺ quenching

Lipids Tested		Fluorophores Tested	
Quench TR-DHPE	Not quench TR-DHPE	Quenched by Cu ²⁺ -PS	Not quenched by Cu ²⁺ -PS
PS (DOPS, POPS, DPPS, DLPS)	PG (POPG, DOPG, DPPG)	TR-DHPE (ortho- and para-isomers, mixed or separated)	Rhodamine labeled anti-biotin IgG bound to biotin-conjugated lipids
	PA (DOPA, DSPA)		
	PC (POPC)	NBD-PC (tail labeled)	
	GM ₁	NBD-PS (tail or head labeled)	
	Cardiolipin	Rhodamine-DHPE	
		Fluorescein-DHPE	
		Bodipy-DHPE	

Fluorescence quenching was also monitored in the presence of DOPS and 800 pM Cu²⁺ for 1 mol % lipid tail group-labeled NBD-PC, tail group-labeled NBD-PS, head group-labeled NBD-PS, rhodamine-DHPE, fluorescein-DHPE, bodipy-DHPE as well as TR-DHPE concentrations from 0.1 to 5 mol % (complete names of fluorophores and lipids provided in “Nomenclature” section). All systems tested showed the similar quenching phenomenon. Moreover, the normalized Cu²⁺-PS quenching fraction from 1.0 mol % TR-DHPE was found to be essentially identical with 0.1 mol %, as was the quenching of head group-labeled lipids and tail-labeled lipids. By contrast, fluorophores attached to membrane-bound proteins showed no Cu²⁺-PS quenching, presumably

because the fluorophore was too distant from the Cu^{2+} -PS complex for quenching to occur. Thus, Cu^{2+} -PS quenching is highly specific to lipid-conjugated fluorophores which presumably have the appropriate in-plane geometry with the Cu^{2+} -PS complex to afford quenching.

Discussions

The 1:2 Cu^{2+} -PS complex observed in this work may have a number of biological implications. Given the concentrations of PS (variable, but generally μM to low mM)² and $\text{Cu}^+/\text{Cu}^{2+}$ (also variable, but $\sim 100 \mu\text{M}$ is often noted in the literature)⁶⁶ found in cells, it seems reasonable that at least under some conditions Cu^{2+} could exist in 1:2 Cu^{2+} -PS complexes *in vivo*. The distribution of both copper and PS in various cell and tissue types are often seen to roughly track one another, both being present in relatively high concentrations, for example, in human brain tissue.^{86,87} Increased PS thus may serve to complex reactive Cu^{2+} in tissues that experience high Cu^{2+} concentrations. This complexation ability may be particularly important in mitigating copper poisoning. Alternatively, PS may attract Cu^{2+} to tissues that require greater quantities of Cu^{2+} , although this seems less likely as Cu^+ should be the dominant species involved in copper ion transport.⁶⁵ The 1:2 Cu^{2+} -PS complex may also provide insights into observations that copper ions and PS both play roles in many biological processes, such as fibril formation in neurodegenerative diseases and wound healing.^{68,69}

As noted above, PS is known to bind a number of different metal ions. Ca^{2+} -PS interactions have been the most extensively studied. These interactions are generally believed to involve high μM to low mM range equilibrium dissociation constants.^{58,59,88} This interaction mediates a number of different protein-PS interactions, specifically the membrane binding of C2 domain proteins, annexin proteins, and γ -carboxyglutamic acid domain proteins such as prothrombin. Thus, it seems reasonable that the observed 1:2 Cu^{2+} -PS complex might also be involved (interfere or aide) in PS-protein interactions even in the presence of trace Cu^{2+} concentrations.

In addition to other roles, Cu^{2+} may also be involved in oxidation reactions. However, the quenching of fluorophores observed in the present experiments was almost perfectly reversible as illustrated by Figure 2.7. As oxidation is largely observed at relatively high Cu^{2+} concentrations, it may be possible that at trace Cu^{2+} concentrations, 1:2 Cu^{2+} -PS complexes help mitigate Cu^{2+} mediated oxidation. On the other hand, at higher Cu^{2+} concentrations, the complex should become saturated and excess Cu^{2+} may mediate oxidation. It should be noted, however, that the high Cu^{2+} concentrations required to saturate the 1:2 Cu^{2+} -PS complexes are well outside the normal physiological range for common healthy cells and tissues.

CHAPTER III

UNQUENCHABLE SURFACE POTENTIAL DRAMATICALLY ENHANCES Cu^{2+}

BINDING TO PHOSPHATIDYLSERINE LIPIDS

Introduction

Ligand-receptor interactions on cell membranes underlie many fundamental biological processes such as cell signaling, pathogen recognition and inflammatory response.^{3,4,41,89} In multivalent binding systems, a higher surface concentration of membrane receptors does not merely provide more sites for interactions, but also can increase binding avidity and induce receptor clustering.^{41,89,90} Curiously, however, increasing the surface density of receptors typically leads to only modest changes in binding avidity.^{3,9,41,90} One example is the bivalent interaction between lipid membrane-conjugated haptens and antibodies, where K_{Dapp} tightens by a factor of only 12 as the ligand density is increased sufficiently to switch the binding from predominantly monovalent to overwhelmingly bivalent.⁹⁰ In this bivalent binding model, the dissociation constant for the overall process K_{Dapp} changes with the varying membrane receptor density $[\text{R}]_s$ which has a unit of mol/m^2 (Eq. 3.1).⁹⁰ The individual dissociation constant K_{D1} and K_{D2} for this two-step binding model are interpreted by Eqns. 3.2 & 3.3, where $[\text{B}]$ represents the concentration of bivalent ligands at equilibrium.⁹⁰

$$K_{\text{Dapp}} = \frac{K_{\text{D1}}K_{\text{D2}}}{K_{\text{D2}} + 2[\text{R}]_s} \quad (3.1)$$

$$K_{\text{D1}} = \frac{[\text{B}][\text{R}]_s}{[\text{BR}]_s} \quad (3.2)$$

$$K_{D2} = \frac{[BR]_s [R]_s}{[BR_2]_s} \quad (3.3)$$

The change of K_{Dapp} with $[R]_s$ can be fitted to a hyperbolic function to abstract the K_{D1} and K_{D2} values. When $[R]_s$ is increased by 20-fold from $[R]_s$ to $20[R]_s$, the ratio of new K_D ' over the old K_D can be represented as $\{K_{D2} + 2[R]_s\} / \{K_{D2} + 40[R]_s\}$. If $K_{D2} \gg [R]_s$, the ratio equals 1 which shows almost no change in the binding affinity. If $K_{D2} \ll [R]_s$, the ratio equals 1/20. Therefore, the 20-fold increase of membrane receptor density can only cause no more than 20-fold change of binding affinity. Increasing the interfacial charge by tuning the pH of the bulk solution can also enhance the binding of negatively charged antibodies to membranes.⁹¹ This, however, also leads to only about an order of magnitude tightening in the K_{Dapp} value as the positive charge on the surface is rapidly attenuated as the protein molecules become attached. In fact, most effects of ligand density, ligand presentation or modulations of the surface charge lead to only modest effects on the apparent dissociation constant.^{41,92-94}

When it comes to the binding of charged ligands to charged receptors, the surface charges also vary with the receptor densities. The concentration of the ligands in the double layer of the membrane surface could be lower or higher than the bulk concentration when the ligands are coulombically repelled or attracted to the surface.⁹⁵ The Coulombic effects might cause the binding affinity of charged ligands and surface receptors to change much more drastically than predicted by the previously-established bivalent binding model. This phenomenon should be especially evident for the ligands that bind to the membrane receptors without attenuating the surface charges.

Herein, we demonstrate that the dissociation constant between Cu^{2+} and PS lipid is highly sensitive to PS density in the membrane. Strikingly, the apparent K_{Dapp} value of Cu^{2+} for PS in SLBs tightens by a factor of 17,000 when the PS density is increased from 1.0 mol % to 20 mol %. This change is significantly larger than what would be expected for changing from largely monovalent to predominantly bivalent binding.^{9,90} Rather, this dramatic increase in affinity is largely caused by the increased charge on the membrane, which leads to an increase in Cu^{2+} in the double layer (Figure 3.1). Significantly, the binding of Cu^{2+} to PS lipids causes little if any attenuation in the surface potential, unlike the binding of other divalent metal ions such as Ca^{2+} and Mg^{2+} .^{25,28} This is a result of the deprotonation of the two PS lipids upon Cu^{2+} binding (Figure 3.1). These results may have implications for Cu^{2+} -PS interactions in cellular membranes, where the PS concentration on the outer leaflet of the plasma membrane increases dramatically upon apoptosis. Note that in this chapter, monovalently bound complex will be referred to as $\text{Cu}(\text{PS})$ and bivalently bound complex is referred to as $\text{Cu}(\text{PS})_2$ while Cu^{2+} -PS represents the metal-lipid complexes in general.

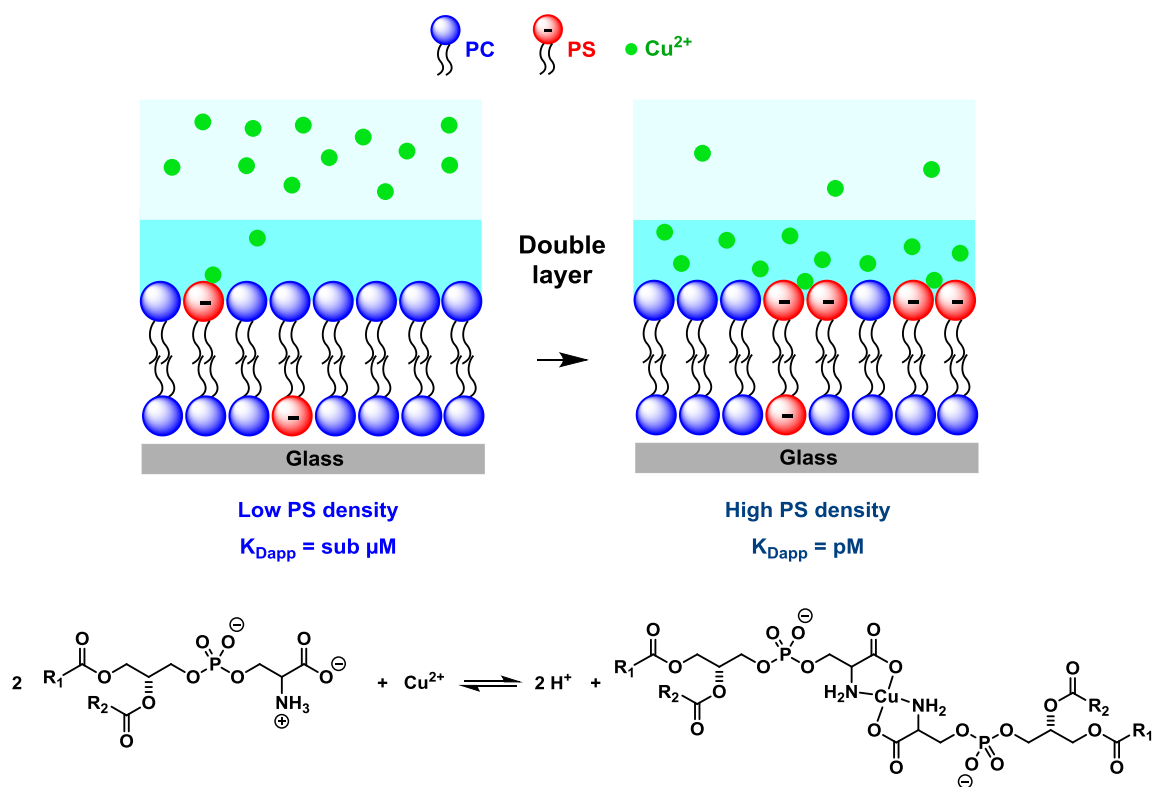


Figure 3.1. Schematic representation of the change of K_{Dapp} with PS density on SLBs (top) and the binding reaction equation (bottom). The binding of Cu^{2+} to 2 PS lipids causes the release of 2 protons leaving the net surface charge unchanged.

Experimental Section

Materials

1-Palmitoyl-2-oleoyl-*sn*-glycero-3-phosphocholine (POPC), 1-palmitoyl-2-oleoyl-*sn*-glycero-3-phospho-L-serine (POPS), 1,2-dioleoyl-*sn*-glycero-3-phospho-L-serine (DOPS) and 1,2-dipalmitoyl-*sn*-glycero-3-phospho-L-serine (DPPS) were purchased from Avanti Polar Lipids (Alabaster, AL). The fluorescent sensor used in this paper, Texas Red 1,2-dihexadecanoyl-*sn*-glycero-3-phosphoethanolamine (TR-DHPE) was

purchased from Invitrogen (Eugene, OR). The vesicles were prepared and stored in 10 mM tris(hydroxymethyl)aminomethane (Tris) buffer containing 100 mM NaCl. The pH of the Tris/NaCl buffer was set to 7.4 by dropwise addition of 1.0 M HCl. The chemicals used such as Tris, NaCl, HCl, CuCl₂, ethylenediaminetetraacetic acid (EDTA) and nitrilotriacetic acid trisodium salt (NTA) were purchased from Sigma-Aldrich (St. Louis, MO). Most of these chemicals have $\geq 99.999\%$ purity while NTA has $\geq 98\%$ purity. Purified water (18.2 M Ω •cm) for the experiments was acquired from a NANOpure Ultrapure Water System (Barnstead, Dubuque, IA). Borosilicate glass coverslips (24 \times 40 mm, No. 1.5, Corning Inc.) were used as planar solid supports for SLBs. PDMS (polydimethylsiloxane, Dow Corning Sylgard Silicone Elastomer-184) was purchased from Krayden, Inc (El Paso, TX).

Vesicle Preparation, Microfluidic Device Fabrication and Bilayer Formation

The experiment methods for preparing small unilamellar vesicles (SUVs), fabricating microfluidic devices and forming lipid bilayers in the devices were all described in Chapter II.

Binding Measurements through Fluorescence Microscopy

Binding measurements with SLBs containing different PS concentrations were performed inside the microfluidic devices described above. The experimental set-up scheme is shown in Figure 1.2. First, SLBs with a specific PS mol % were made in 6 or 7 parallel microfluidic channels. 10 mM Tris buffer (pH 7.4) containing 400 μ M EDTA

was introduced into each channel to remove any possible heavy metal ion contaminants. Then Tris buffer containing different Cu^{2+} concentrations was flown through individual channels of the PDMS/glass microfluidic device through each inlet port using 0.6 mm internal diameter Teflon tubing (SPC Technology). Flow through the device was gravity driven with an average flow rate of $\sim 100 \mu\text{L/h}$ in each microfluidic channel. The consumed buffer drained from each outlet port to a waste container. Buffer was constantly flowed through the channels during all experiments. The fluorescence of each channel was monitored by an inverted epifluorescence Nikon Eclipse TE2000-U microscope until equilibrium was reached. When low Cu^{2+} concentrations were employed (less than nM scale), several hours were required for equilibrium to be established. The fluorescent images of the channels were captured by a MicroMax 1024 CCD camera (Princeton Instruments), collected using MetaMorph software (Universal Imaging) and then processed with Origin 7.5 software (OriginLab Corporation). For competitive binding method experiments, 1 or 10 μM NTA was introduced into the channel accompanied by 10 mM Tris buffer containing different Cu^{2+} concentrations while the rest of the experiment set-up and the data processing remained the same.

Vibrational Sum-Frequency Spectroscopy (VSFS) Characterization of the Cu^{2+} -PS Complex

VSFS is a surface-specific non-linear optical technique.^{46,47} In our setup, a fixed wavelength visible (516 nm) laser beam and a tunable wavelength IR laser beam are spatially overlapped on lipid/water interfaces. Photons from the two laser beams mix at

the interface to form a sum frequency beam. The intensity of this sum frequency beam is proportional to the intensity of the visible and IR laser beams and the square of the second-order non-linear susceptibility.^{46,47} As the second order non-linear susceptibility is non-zero only in media that lack inversion symmetry, VSFS is inherently surface specific. The intensity of the sum frequency beam is increased when the IR beam is resonant with molecular vibrations at the lipid/water interface. To generate a vibrational spectrum of the lipid/water interface, the intensity of the sum frequency beam can be monitored with a changing IR beam frequency.

The VSFS experimental setup (purchased from EKSPLA, Lithuania) consisted of a 1064 nm Nd:YAG laser (pulse duration: 30 ps; pulse energy: 40 mJ; maximum repetition rate 50 Hz), which was directed to the harmonic unit (H500). The second harmonic (532 nm) and fundamental beams from the harmonic unit pump the optical parametric generator/ difference frequency generator (PG501/DFG) unit. The infrared frequency can be tuned between 1000 cm^{-1} and 4000 cm^{-1} and the spectral resolution is < 6 cm^{-1} . For VSFS experiments at the air/water interface, a PTFE Langmuir trough (NIMA technology, England) equipped with pressure sensor and controllable barriers was used. The trough had an area of 65 cm^2 and subphase volume of 35 mL. A Langmuir monolayer of lipid molecules was formed at the air/water interface and the VSFS spectra were collected in the absence and presence of metal ions in the subphase. The IR and visible beams were spatially and temporally overlapped at air/water interface and the sum frequency signal was collected at an angle of 59°. The incident angles of the IR and Visible beams on to the monolayer/water interface were of 55° and 60°

respectively. The energy of visible beam at the sample stage was 400 μJ and the infrared beam was 150 μJ at 2875 cm^{-1} . The VSFS signal was collected at 3 cm^{-1} intervals and each point on the spectrum is an average of 150 laser pulses. The intensity of the collected VSFS signal was normalized to the corresponding IR and visible intensities.

VSFS spectra of the air/water interface were obtained on lipid monolayers composed of 100 mol % DPPS. 100 mM Tris buffer at pH 7.4 was used in the subphase for all experiments. The Tris buffer containing 100 μM CuCl_2 or 100 μM CaCl_2 were used as subphase solution to compare with the buffer without divalent metal ions. The monolayers were studied at a surface pressure of 17 mN/m at 21°C.

Surface Potential Measurements by Kelvin Probe

Surface potential measurements on DPPS monolayers with 100 μM CuCl_2 or 100 μM CaCl_2 in the subphase were made in a Langmuir trough (KSV 5000, KSV Instruments, Ltd., Helsinki, Finland). This trough was equipped with a Kelvin probe for performing vibrating capacitor measurements.^{96,97} Similar to the VSFS experiments, a Langmuir monolayer of DPPS molecules was formed at the air/water interface and 100 mM Tris buffer at pH 7.4 was used in the subphase for all experiments. Tris buffer containing 100 μM CuCl_2 or 100 μM CaCl_2 were used as subphase solution to compare with the buffer without divalent metal ions. Each measurement was carried out after waiting 20 min to stabilize the reading from the Kelvin probe. The surface potential values were determined from the average of 4 measurements.

Electrospray Ionization Mass Spectrometry (ESI-MS) Characterization of the Cu²⁺-PS Complex

The ESI-MS spectra were acquired on a Waters Synapt HDMS G2 mass spectrometer (Waters UK Ltd., Manchester, U.K.). Negatively charged ions were formed by nano-ESI using a source temperature of ~80°C and a capillary voltage of -1.8–2.0 kV. The sampling cone voltage was set at 25 kV and the extraction cone voltage was 2.0 kV. The SUVs containing 80 mol % POPC and 20 mol % POPS were firstly prepared in 1 mM concentration in 10 mM ammonium acetate buffer (pH 7.4) and then diluted by 100 times in H₂O for ESI-MS experiments.

Results

Cu²⁺-PS Fluorescence Quenching Assay

The fluorescence quenching assay used for binding measurements was applied inside the microfluidic devices.⁴⁵ To measure the Cu²⁺ binding affinity at different PS concentrations, various vesicle solutions containing 0 to 20 mol % POPS, 1.0 mol % TR-DHPE and POPC were incubated inside microfluidic devices to form SLBs. The SLBs containing 0.5 mol % TR-DHPE were also tested, which gave similar binding results. Besides POPS, other PS lipids with different acyl chains such as DPPS and DOPS in POPC SLBs were also tested and they showed similar binding affinity with copper ions. Buffer solutions containing different Cu²⁺ concentrations were introduced into each channel and flowed continuously until the fluorescence signal stabilized. At sub-nM

concentration of Cu^{2+} , it took several hours for equilibrium to be established. Figure 3.2 shows fluorescence images and the corresponding line scans of SLBs containing 0, 5.0, 10, 15 and 20 mol % POPS without (left) and with (right) 10 nM CuCl_2 . As can be seen, the fluorescence response of each channel was essentially identical in the absence of Cu^{2+} . Upon introducing 10 nM CuCl_2 to the solution, the fluorescence of TR-DHPE was quenched to a greater degree at higher PS concentrations. Moreover, no quenching was observed without POPS in the bilayer. Such quenching has been attributed to the formation of complex between Cu^{2+} and PS, which can, in turn, quench a wide variety of fluorophores.⁴⁵ Such quenching is employed below to quantitatively investigate the interaction between Cu^{2+} and PS on lipid bilayer surface.

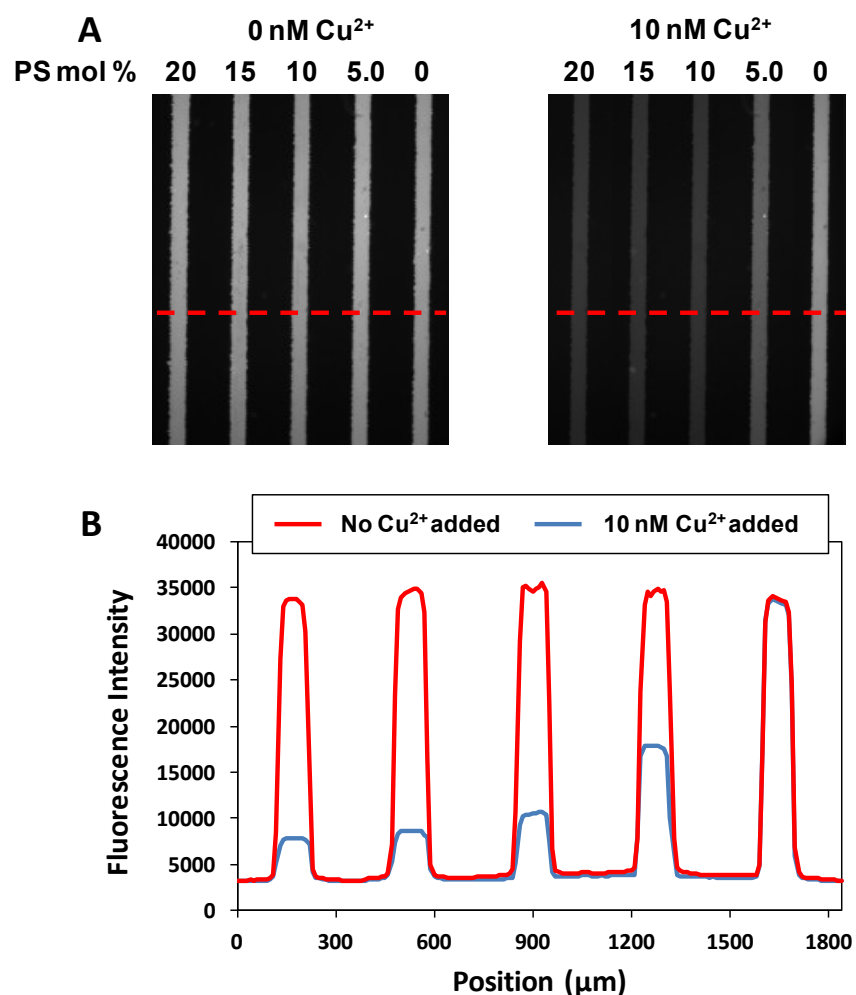


Figure 3.2. (A) Fluorescence images and (B) line scans from lipid bilayers in a multi-channel microfluidic device. The POPC SLBs contain 0 to 20 mol % POPS along with 1.0 mol % TR-DHPE. The fluorescence is shown in the absence of CuCl₂ (left panel in A and red line scan in B) and in the presence of 10 nM CuCl₂ (right panel in A and blue line scan in B) at pH 7.4 with 10 mM Tris buffer. The fluorescence line scans in B are taken from the regions along the dotted red lines shown in A.

Non-competitive Binding Measurement

In the next set of experiments, the multi-channel microfluidic devices containing SLBs were used to measure binding isotherms for Cu²⁺ to PS for membranes containing 1.0~7.5 mol % POPS (Figure 3.3). The maximum fraction of fluorophores that were

quenched increased with an increasing POPS concentration. This is expected as the average distance between Cu²⁺-PS complexes and fluorophores becomes shorter at higher complex concentration and, therefore, the quenching becomes more efficient.⁹⁸ More significantly, these curves reveal a tighter binding between Cu²⁺ and PS with increasing concentrations of POPS. The data were fit to Langmuir isotherms using Eq.3.4 in order to abstract an apparent equilibrium dissociation constant, K_{Dapp}.^{90,99,100}

$$\Delta F = \Delta F_{\max} \times \frac{[\text{Cu}^{2+}]}{[\text{Cu}^{2+}] + K_{\text{Dapp}}} \quad (3.4)$$

In this case, ΔF is the fraction of lipid-bound dye molecules that are quenched by the Cu²⁺-PS complex at each Cu²⁺ concentration, while ΔF_{\max} represents the maximum fraction quenched at the saturation concentration. $[\text{Cu}^{2+}]$ represents the free Cu²⁺ concentration in the bulk solution when equilibrium is established. It should be noted that buffer containing CuCl₂ is continuously flowed over the SLBs throughout the experiment so the bulk Cu²⁺ concentration will not be depleted once equilibrium is established. Moreover, equilibrium is determined to have been reached when the fluorescence response from the membrane stops changing as a function of time as the buffer is continuously flowing. The values of K_{Dapp} determined at each POPS concentration in Figure 3 are listed in the “K_{Dapp} (M, non-competitive)” column in Table 3.1.

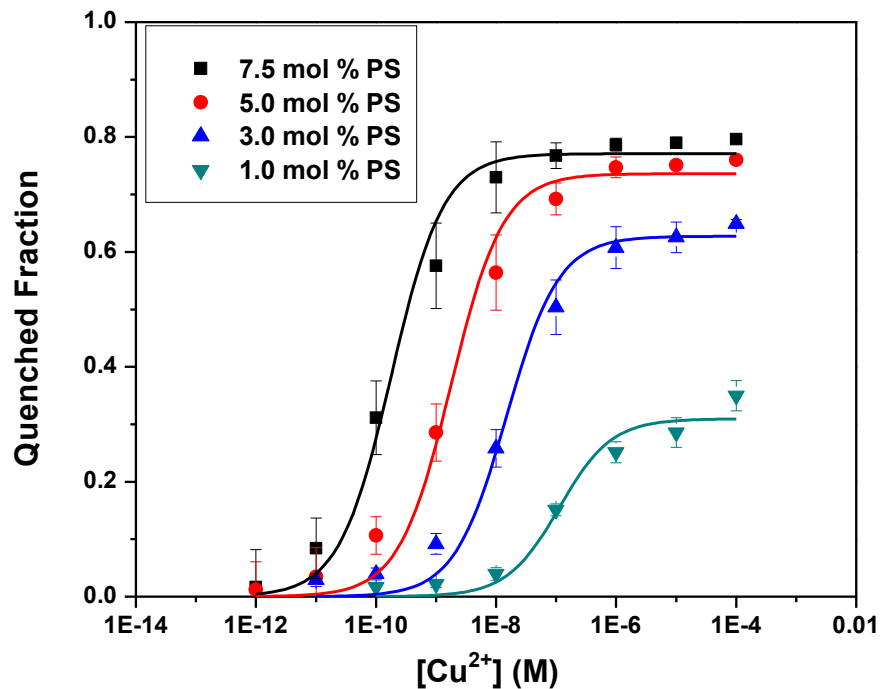


Figure 3.3. Non-competitive binding curves of SLBs containing 1.0 to 7.5 mol % PS. The quenching response of SLBs composed of 1.0 mol % TR-DHPE in POPC with 1.0 to 7.5 mol % POPS were plotted as a function of Cu^{2+} concentration. The fluorescence intensities with different Cu^{2+} concentrations at pH 7.4 were normalized to the fluorescence response without Cu^{2+} at the same pH where 400 μM EDTA was added into the system to chelate the metal ions. The fraction of fluorescent dye that was quenched (one minus the normalized fluorescence intensity) was plotted here as a function of Cu^{2+} concentration along with a solid line fit of the data using Eq. 3.4.

Table 3.1. Binding Constants of non-competitive binding curves for 1.0 to 7.5 mol % PS and competitive binding curves for 7.5 to 20 mol % PS

PS mol % in SLBs	K_{Dapp} (M, non-competitive)	K_{Dapp} (M, competitive)	K_{Dcom} (M)
1.0	1.1×10^{-7}	-	-
3.0	1.5×10^{-8}	-	-
5.0	2.7×10^{-9}	-	-
7.5	1.8×10^{-10}	5.1×10^{-11}	5.1×10^{-6}
10	-	1.6×10^{-11}	1.6×10^{-6}
15	-	9.7×10^{-12}	9.7×10^{-7}
20	-	6.4×10^{-12}	6.4×10^{-7}

Competitive Binding Measurements

Binding curves could not be established for SLBs containing more than 7.5 mol% POPS because the value of K_{Dapp} continued to tighten and quenching measurements needed to be made with ever lower concentrations of $CuCl_2$ in the buffer. This was problematic because trace Cu^{2+} contamination in the buffer began to affect the results as the K_{Dapp} value continued to tighten. Therefore we switched to a competitive binding method to obtain K_{Dapp} values from SLBs containing 7.5 to 20 mol % POPS (Figure 3.4). Such methods are routinely applied to measuring the binding affinity of transition metal

ions to proteins and peptides when the binding constant is below nM.¹⁰¹⁻¹⁰³ Herein, 10 μM of a metal ion chelator, nitrilotriacetic acid (NTA), was used to shift the binding curves into the μM range where the background Cu^{2+} contamination was negligible.^{102,104}

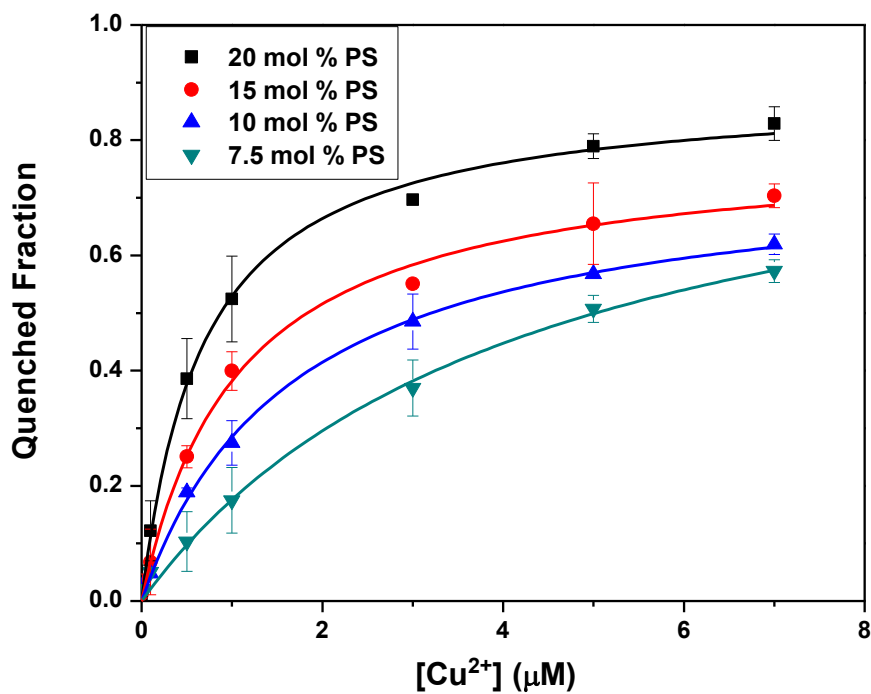


Figure 3.4. Competitive binding curves of SLBs containing 7.5 to 20 mol % PS. The quenching response of SLBs containing 1.0 mol % TR-DHPE, 7.5 to 20 mol % POPS in POPC with 10 μM NTA. The quenched fraction was normalized to the fluorescence response without Cu^{2+} at the same pH (pH=7.4) where 400 μM EDTA was added to the system. The solid lines represent least square fits of the data using Eq. 3.5. Moreover, buffers containing 1 μM NTA were also tested to confirm the K_{Dapp} values and gave similar results.

In the NTA-containing buffers, observable quenching only occurs when more than 0.1 μM Cu^{2+} was introduced into the system. Therefore the x-axis here was plotted

as a linear axis to show the quenching response within $\mu\text{M Cu}^{2+}$. In these competitive binding measurements, the original Langmuir isotherm binding model (Eq. 3.4) needs to be modified based on the actual “available” Cu^{2+} concentrations. In NTA- Cu^{2+} binding $[\text{CuNTA}^-] \rightleftharpoons [\text{Cu}^{2+}]_{\text{avail}} + [\text{NTA}^{3-}]$, the equilibrium dissociation constant for this binding:

$$K_L = \frac{[\text{Cu}^{2+}]_{\text{avail}} [\text{NTA}^{3-}]}{[\text{CuNTA}^-]} \quad (3.5)$$

Therefore, with NTA^{3-} in solutions, it can be regarded as a “ Cu^{2+} buffer” and the “available” free Cu^{2+} concentration for PS can be represented as:

$$[\text{Cu}^{2+}]_{\text{avail}} = \frac{K_L [\text{CuNTA}^-]}{[\text{NTA}^{3-}]} \quad (3.6)$$

As we generally used relatively high Cu^{2+} concentration in this competitive binding method (sub- μM to $10 \mu\text{M}$ scale), the background contaminate Cu^{2+} concentration (around sub-nM) in buffer can be ignored, thus total Cu^{2+} concentration:

$$[\text{Cu}^{2+}] \approx [\text{Cu}^{2+}]_{\text{background}} + [\text{Cu}^{2+}] \quad (3.7)$$

Since total Cu^{2+} concentration can be represented as: $[\text{Cu}^{2+}] = [\text{Cu}^{2+}]_{\text{avail}} + [\text{CuNTA}^-]$

(3.8)

Combining Eq. 3.6 and Eq. 3.8 gives:

$$[\text{Cu}^{2+}]_{\text{avail}} = \frac{[\text{Cu}^{2+}]}{1 + \frac{[\text{NTA}^{3-}]}{K_L}} \quad (3.9)$$

which is the available Cu^{2+} concentration in the buffer when NTA^{3-} exists. The quenched fraction of fluorescence intensity is correlated with the binding between Cu^{2+} and PS and follows Langmuir binding model (Eq. 3.4).^{99,100} Thus the quenched fraction can be

related to the equilibrium dissociation constant (K_{Dapp}) for the Cu^{2+} -PS complex by Eq. 3.10:

$$Q = \frac{\Delta F}{\Delta F_{max}} = \frac{[Cu^{2+}]_{avail}}{[Cu^{2+}]_{avail} + K_{Dapp}} \quad (3.10)$$

where ΔF is the fraction of TR-DHPE quenched by Cu^{2+} -PS complex, while ΔF_{max} represents the maximum fraction which can be quenched and $[Cu^{2+}]_{avail}$ is the equilibrium (unbound) Cu^{2+} concentration when equilibrium is established. Since we continuously flow buffer containing Cu^{2+} into the system, the added “available” Cu^{2+} concentrations represent the equilibrium Cu^{2+} concentrations. Applying Eq. 3.9 into Eq. 3.10 gives:

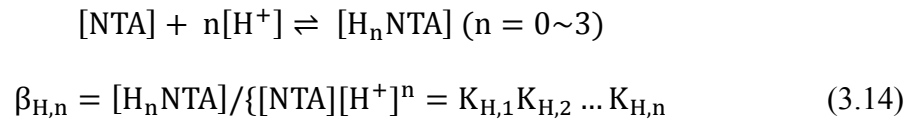
$$Q = \frac{\Delta F}{\Delta F_{max}} = \frac{[Cu^{2+}]}{[Cu^{2+}] + K_{Dapp}\{1 + \frac{[NTA^{3-}]}{K_L}\}} \quad (3.11)$$

Now we can see that the apparent dissociation constant with the competitor, K_{Dcom} , which is extracted from the competitive binding curve when NTA^{3-} is present, can be represented as:

$$K_{Dcom} = K_{Dapp}\{1 + \frac{[NTA^{3-}]}{K_L}\} \quad (3.12)$$

$$K_{Dapp} = \frac{K_{Dcom}}{1 + \frac{[NTA^{3-}]}{K_L}} \quad (3.13)$$

The protonation of NTA should be also considered to make correction of the pH-dependent NTA- Cu^{2+} binding constant K_L . Since



where $\beta_{H,n}$ is defined as the accumulated protonation constant of $H_n\text{NTA}$ where $K_{H,n}$ is the n -th protonation constant. The corrected NTA-Cu^{2+} binding constant K_L can be represented as:

$$K_L = K_{\text{NTA}}\{1 + \beta_{H,1}[\text{H}^+] + \beta_{H,2}[\text{H}^+]^2 + \beta_{H,3}[\text{H}^+]^3\} \quad (3.15)$$

where K_{NTA} is the absolute affinity of NTA^{3-} for binding Cu^{2+} , which is $10^{-13.1}\text{M}$ according to the ref.^{105,106} When $\text{pH}=7.4$, we can calculate K_L at this pH based on K_{NTA} and $K_{H,n}$ from the reference ($K_{H,1} = 10^{10.3}\text{M}$, $K_{H,2} = 10^{2.9}\text{M}$, $K_{H,3} = 10^{1.7}\text{M}$)^{106,107}, which gives $K_L \approx 10^{-10}\text{M}$.

Now based on Eq. 3.13 and the NTA-Cu^{2+} binding constant, we can deduce the intrinsic dissociation constant K_{Dapp} of Cu^{2+} -PS binding. The quenching curves were fit to a modified Langmuir isotherm binding model (Figure 3.4) based on the actual “available” Cu^{2+} concentrations (Eq. 3.16) then K_{Dapp} can be calculated by Eq. 3.13:

$$\Delta F = \Delta F_{\text{max}} \times \frac{[\text{Cu}^{2+}]}{[\text{Cu}^{2+}] + K_{\text{Dcom}}} \quad (3.16)$$

Using these equations, the K_{Dapp} values for 7.5~20 mol % PS were calculated and listed in “ K_{Dapp} (M, competitive)” column in Table 3.1 along with the K_{Dcom} values in each condition.

To confirm that the competitive binding experiments provided accurate K_{Dapp} values, the K_{Dcom} value for a membrane containing 7.5 mol % PS was also measured. In this case, the calculated K_{Dapp} value from competitive binding was $5.1 \times 10^{-11}\text{M}$, which differs by a factor of less than three from non-competitive binding measurements. One might have wished to use the competitive method to compare dissociation constants with even lower concentrations of POPS. However, K_{Dcom} values under those circumstances

were larger than 10 μM . Of course, adding more than 10 μM Cu^{2+} exceeds the metal-buffering capacity of the 10 μM NTA solution. Therefore, the NTA-based competitive binding method was only used for the range of POPS concentration from 7.5 to 20 mol %.

Characterization of the Negatively-charged Cu^{2+} -PS Complex

The data in Figures 3.3 and 3.4 are fits to isotherms that assume non-cooperative binding. This assumption is unusual for cation binding at an interface. Indeed, cation binding would normally be expected to anti-cooperative because earlier binding events would normally make subsequent ones less favorable due to increasing electrostatic repulsion. For example, Ca^{2+} and Mg^{2+} bind with phosphate and carboxyl groups on PS^{26,108,109} and this attenuates the negative charge on the bilayer.^{25,30} This is not expected to be the case, however, for Cu^{2+} -PS binding where 2 protons should be released for every Cu^{2+} that binds bivalently to phosphatidylserine (Figure 3.1). To verify this difference, we performed several experiments to test the change in interfacial potential upon Cu^{2+} and Ca^{2+} binding.

First, vibrational sum frequency spectroscopy (VSFS) was used to measure the change in interfacial water structure⁴⁶⁻⁴⁸ upon the introduction of 100 μM CuCl_2 and 100 μM CaCl_2 to the aqueous subphase below a Langmuir monolayer of DPPS lipids (Figure 3.5). The sharper peaks at 2880 and 2950 cm^{-1} are CH stretch modes from the lipid acyl chains,^{48,96} while the broader peaks at 3200 cm^{-1} and 3400 cm^{-1} arise from the alignment of interfacial water below the monolayer.¹¹⁰ The oscillator strength in the OH stretch

region has been shown to vary strongly with changes in the interfacial potential of monolayers composed of lipids, surfactants or macromolecules.^{46,48,111} Specifically, highly charged surfaces order more water molecules, resulting in a larger OH stretch oscillator strength.⁴⁶ In fact, the relatively large peak intensities in the OH stretch region in the absence of added divalent metal cations comes from the negative charge on the lipids (black plot in Figure 5). This peak is expected to be attenuated by the addition of metal cations if the interface potential is reduced. Indeed the oscillator strength of the 3200 cm^{-1} resonance decreased 48% upon the introduction of Ca^{2+} (blue plot in Figure 5). However, the addition of $100\text{ }\mu\text{M Cu}^{2+}$ only causes a reduction of 7% in the oscillator strength in the OH stretch region (red plot in Figure 5). The greater reduction in water structure upon introduction of Ca^{2+} is consistent with the greater attenuation of the negative charge.¹¹² By contrast, the more modest change upon the addition of Cu^{2+} supports the idea that the surface charge is less perturbed upon Cu^{2+} binding. It should be noted that some attenuation in the 3200 cm^{-1} resonance is expected with $100\text{ }\mu\text{M Cu}^{2+}$ because this concentration is fairly high enough to lead to some Cu^{2+} binding with the phosphate. Also, the 3400 cm^{-1} resonance was perturbed by both Ca^{2+} and Cu^{2+} as this resonance reflects the water molecules directly bound to the lipid headgroup.¹¹³

The surface potential of the DPPS monolayer was also measured directly using a Kelvin probe.^{96,97} Adding $100\text{ }\mu\text{M Ca}^{2+}$ caused the surface potential to raise 116 ± 3.5 mV, whereas adding $100\text{ }\mu\text{M Cu}^{2+}$ only caused an increase of 42 ± 2.8 mV. As such, the change in the surface potential upon the addition of Ca^{2+} was almost three times greater for Cu^{2+} . Given that the binding affinity for Cu^{2+} to PS is much tighter than Ca^{2+} while

the measured potential change is considerably smaller, the result is again consistent with only a small change in surface charges as Cu^{2+} is added.

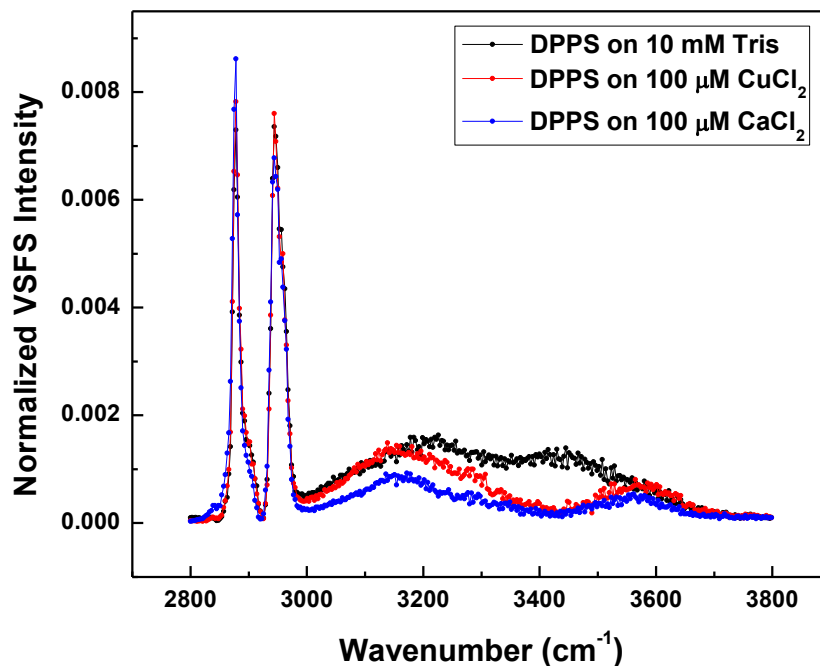


Figure 3.5. VSFS spectra of DPPS monolayers with divalent metal ions. 100 μM CuCl_2 (red data points) and 100 μM CaCl_2 (blue data points) were introduced in the subphase. The figure also contains a plot with 10 mM Tris buffer, but without any divalent metal salts for comparison (black data points). All measurements were made at pH 7.4 with a surface pressure of 17 mN/m at 21 $^\circ\text{C}$. The spectra were fitted to a Voigt profile to obtain the peak frequency, width and oscillator strength of each vibrational band.

Electrospray mass spectrometry (ESI-MS) was utilized as a final method to confirm the Cu^{2+} binding model. The results revealed dominant m/z peaks corresponding to Cu^{2+} -PS binding complex consisting of one metal ion and two lipids with a net charge of -2 (Figure 3.6, $m/z=791.2$). This is again consistent with the idea that the PS lipids are deprotonated upon Cu^{2+} binding.

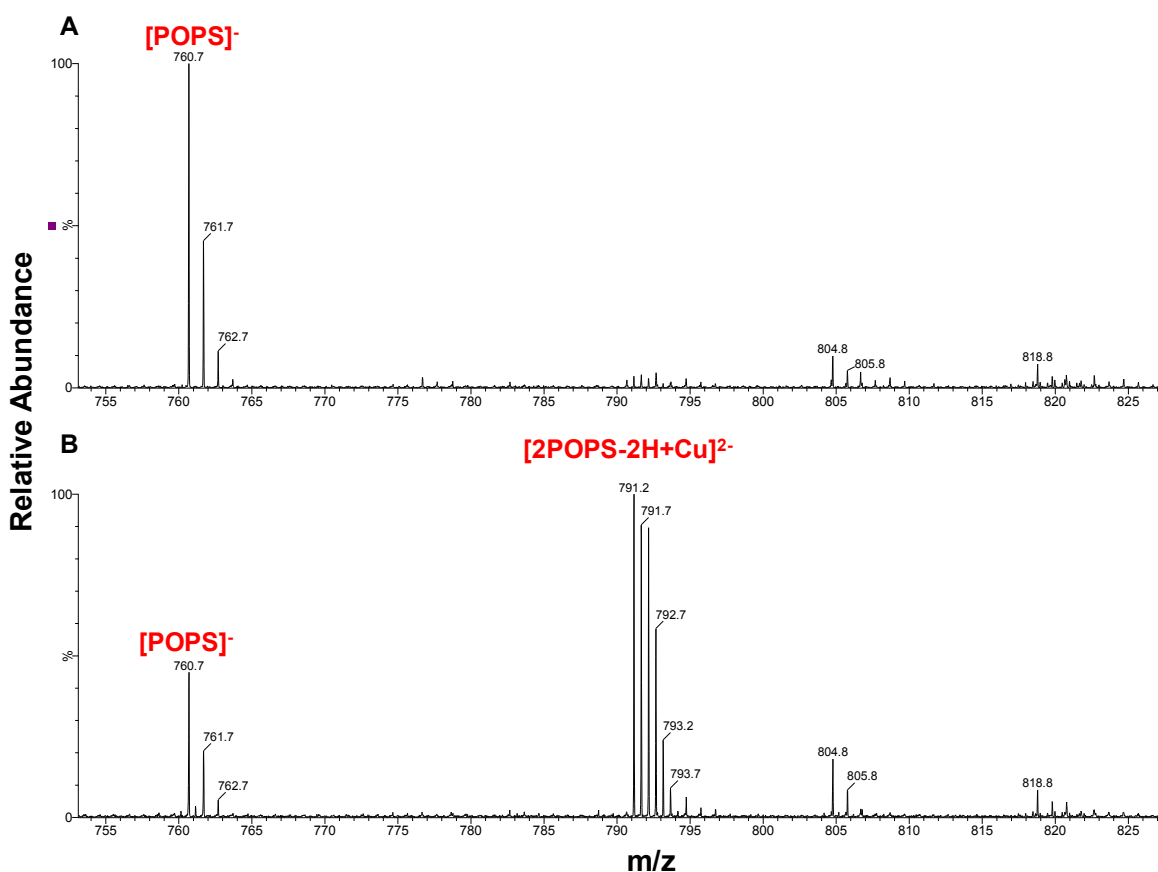


Figure 3.6. The negative mode ESI-MS spectra of PS-contained vesicles without or with Cu^{2+} . The vesicles are 10 μM 80 mol % POPC /20 mol % POPS (A) with 2 μM EDTA or (B) with 2 μM CuCl_2 . The m/z peaks at 760.7 correspond to POPS with 1 negative charge while the peak series around 791.2 represent $[\text{2POPS-2H+Cu}]^{2-}$ ions which carry 2 negative charges.

Discussions

The Change of Cu²⁺-PS Binding Affinity with PS Density

As demonstrated above, the affinity of Cu²⁺ for SLBs containing 1.0 to 20 mol % PS increases by a factor of 17,000. This apparent enhancement in affinity is predominantly due to the increase in surface charge with a small contribution from bivalent binding at higher POPS concentrations. First, because the surface charge increases 20 fold from 1.0 to 20 mol% POPS, the concentration of Cu²⁺ in the double layer goes up substantially. This can be quantified using the Grahame equation (Eq. 3.17).⁹⁵

$$\sigma = 0.117 \sinh\left(\frac{\psi_0}{51.4}\right) \times \left\{ [\text{Tris}^+] + [\text{CuCl}_2] \left[2 + \exp\left(\frac{-\psi_0}{25.7}\right) \right] \right\}^{1/2} \quad (3.17)$$

where σ is the surface charge density (C/m²), ψ_0 is the surface potential (mV) and [Tris⁺] and [CuCl₂] are the concentrations of protonated Tris and CuCl₂ in the buffer (M). [Tris⁺] was calculated by the Henderson-Hasselbalch equation¹¹⁴ using a pKa of 8.0,¹¹⁵ a pH of 7.4 and a total Tris concentration of 10 mM, which gives a [Tris⁺] equal to 8 mM. [CuCl₂] used in Eq. 3.17 was equivalent to the measured K_{Dapp} value for each SLBs containing PS. The derivation of Eq. 3.17 can be found in reference 95. It should be noted that this form of the Grahame equation assumes that the counter ion for [Tris⁺] is Cl⁻ as the pH of the Tris buffer was adjusted using HCl. The equation also ignores the addition of NTA used for the competitive binding curves. As the NTA concentration is three orders of magnitude lower than [Tris⁺], this simplification should not affect the output of the equation. The surface charge density σ was determined using Eq. 3.18,

$$\sigma = \frac{-e}{S} \times (\chi_{PS} + \chi_{TR}) \quad (3.18)$$

where the lipid headgroup area S was taken to be 70 \AA^2 .¹¹⁶ Here e is the fundamental unit of charge and χ_{PS} and χ_{TR} represent the mole fractions of PS and TR-DHPE in the SLBs while the PS and TR-DHPE lipid each possess one negative charge. Note that this calculation does not take into account the surface charge of the glass. This assumption is reasonable as it has been shown that the supported bilayers will shield the objects in solution above the bilayer from being affected by the surface charge of the glass, even at the modest salt concentrations used in these experiments.¹¹⁷⁻¹¹⁹ The calculated σ values from Eq. 3.18 were plugged in Eq. 3.17 to solve for ψ_0 by MATLAB. Using the surface potential ψ_0 together with the K_{Dapp} values measured in Figures 3.3 & 3.4, it is possible to calculate the intrinsic dissociation constant, K_{Dint} , which takes into account the adjustment for charge (Eq. 3.19),^{30,95}

$$K_{Dint} = K_{Dapp} \times \exp\left(\frac{-2e\psi_0}{kT}\right) \quad (3.19)$$

The calculated K_{Dint} values are listed in Table 3.2 and are plotted as a function of POPS density in Figure 3.7B.

Table 3.2. The calculated σ , ψ_0 and surface charge-adjusted dissociation constants K_{Dint} for Cu^{2+} binding of SLBs containing 1.0~20 mol % PS

PS mol %	σ (C/m ²)	Ψ_0 (mV)	K_{Dint} (M)
1.0	-4.6×10^{-3}	-22	6.1×10^{-7}
3.0	-9.1×10^{-3}	-40	3.4×10^{-7}
5.0	-1.4×10^{-2}	-56	2.1×10^{-7}
7.5	-1.9×10^{-2}	-71	4.5×10^{-8}
10	-2.5×10^{-2}	-83	1.0×10^{-8}
15	-3.7×10^{-2}	-101	2.5×10^{-8}
20	-4.8×10^{-2}	-115	4.9×10^{-8}

The results show that the surface charge on the bilayer has a dramatic effect on K_{Dapp} for Cu^{2+} -PS binding, while K_{Dint} only varies slightly with the mol % of POPS in the membrane. The remaining one order of magnitude change in K_{Dint} arises from the shift from monovalent to divalent binding at higher mol % POPS. Similar to the bivalent binding model described in “Introduction” by Eqns.3.1 to 3.3, Cu^{2+} -PS binding also consists of two sequential steps which have individual dissociation constants K_{D1} and K_{D2} , respectively. The measured K_{Dapp} and K_{Dint} values were both fit as a function of PS surface density to Eq. 3.1 (Figure 3.7). Figure 3.7A shows that the changing K_{Dapp} with increasing PS surface density cannot fit to Eq. 3.1 while in Figure 3.7B, the change of K_{Dint} with PS surface density fits well to Eq. 3.1, yielding a K_{D1} of 1.8 μ M and a K_{D2} of 0.026 μ moles/m².

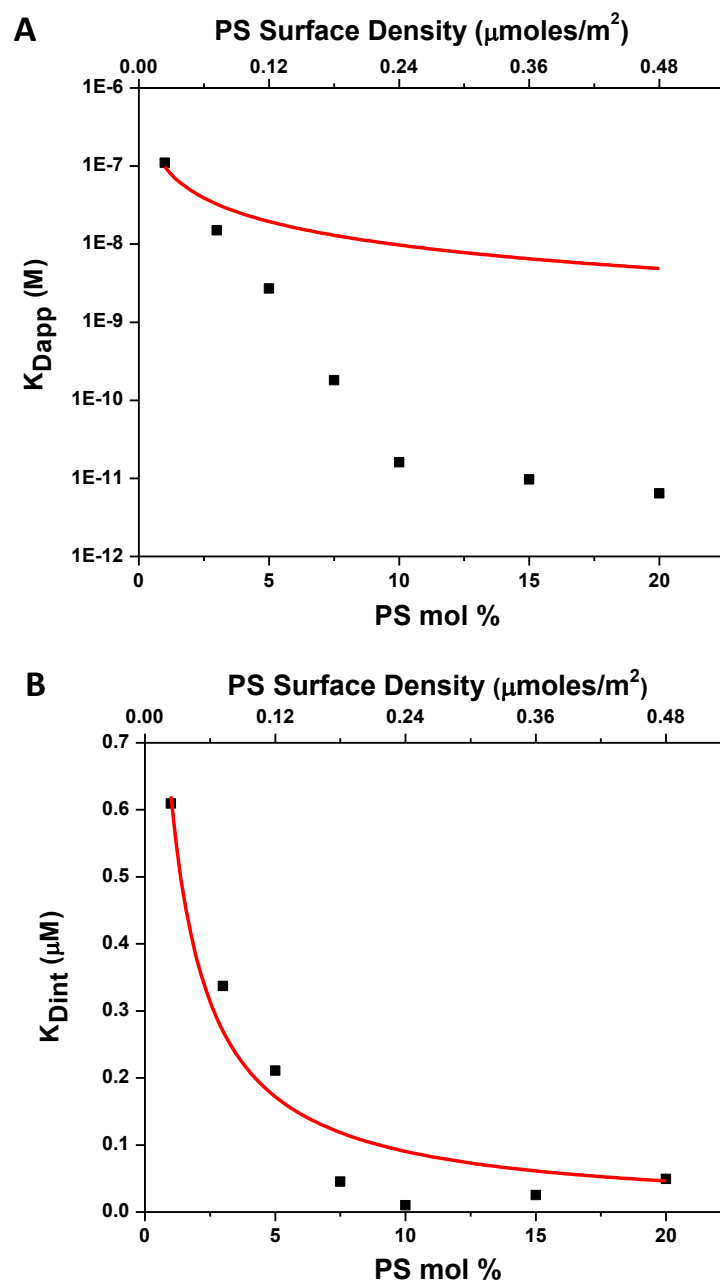


Figure 3.7. K_{Dapp} and K_{Dint} values plotted as a function of PS surface density. The data points (black dots) are plotted as PS surface density in units of $\mu\text{moles}/\text{m}^2$ (top x-axis) and PS mol % (bottom x-axis). The red line in each panel is a fit of Eq. 1 to the data. To clearly present the data points, the y-axis in (A) is plotted as a logarithmic scale while the y-axis in (B) is linear.

As noted above, the lack of change in surface charge with Cu^{2+} binding to PS is dramatically different from the binding of other divalent cations such as Ca^{2+} and Mg^{2+} .^{25,28,30} In other words, the accumulation of Cu^{2+} in double layer of the negatively-charged surface should take main responsibility for the tightening in K_{Dapp} with PS concentration as it causes nearly four orders of magnitude change in apparent binding affinity while the monovalent-to-bivalent binding only contributes one order of magnitude change.

Physiological Implications of Cu^{2+} -PS Binding

As the third most abundant transition metal in human body, copper is necessary for the activity of various proteins and is tightly regulated by chaperons and enzymes in healthy cells.^{32,33} In healthy tissues, the total copper concentration is generally around 0.1 mM.³² Moreover, there is little uncomplexed copper ($\sim 10^{-18}$ M) in the cytoplasm.⁶⁶ This can change in diseased tissue. Previous report concerning the “free” copper concentration in the cytoplasm are mainly based on studies in bacteria and yeast.⁶⁶ It has been argued that the situation in higher organisms with specialized tissues, such as human neuron systems, might be different, especially under specific pathological conditions.³² For example, it has been found that a build-up of labile Cu^{2+} is probably toxic to cells and closely linked to neurodegenerative disorders such as Wilson’s disease and Alzheimer’s disease.^{33,34}

Various approaches have been employed to study Cu^{2+} -protein interactions and Cu^{2+} is generally found to bind negatively charged moieties on proteins as well as the

lone electron pairs of nitrogen on histidine, lysine, arginine and N-terminus.³⁵⁻³⁸ There has been little discussion as to how Cu^{2+} interacts with lipids or the possibility of lipid membranes serving as metal ion reservoirs when homeostasis breaks down. As one of the most abundant negatively charged phospholipids in human membranes, PS lipids play important roles in cell apoptosis, blood clotting and embryonic development.^{2,20-23} The interactions between Cu^{2+} and PS have numerous biological implications, such as the PS-dependent protein-membrane binding and the oxidative damage of cell membranes.^{2,39} The consequences of these interactions are probably more pronounced when PS lipids are flipped from the inner to outer leaflets of plasma membranes during cell apoptosis or other biological events, which increase the exposed PS density on cell surfaces and bring PS into direct contact with a Cu^{2+} -rich environment.^{24,40} With a relatively high negatively-charged PS density on the cell surface, the apparent binding affinity to Cu^{2+} are likely to be enhanced, which might entitle PS to be a candidate for copper ion reservoir.

Additionally, the intriguing results shown in this paper also inspire us to consider the possibility of PS co-binding multiple divalent metal ions such as Cu^{2+} and $\text{Ca}^{2+}/\text{Mg}^{2+}$,²⁶ as well as the co-binding for PS-related proteins.^{2,120,121} Since Cu^{2+} -PS complexes still possess negative charges to attract other metal ions and proteins, it is appealing to investigate if these Cu^{2+} -PS interactions can affect or disrupt the PS binding of other molecules under physiological conditions.

CHAPTER IV

BETA AMYLOID-METAL ION-MEMBRANE INTERACTIONS UNDER COPPER-DEFICIENT PATHOLOGICAL CONDITIONS

Introduction

Alzheimer's disease (AD) is a neurodegenerative disorder characterized by memory loss, cognitive decline and physical deterioration.^{33,122} It is typically marked by the extracellular accumulation of amyloid β -peptides ($A\beta$) and neuron cell death. $A\beta$ is a peptide of 40~42 amino acids which derives from the proteolytic cleavage of the transmembrane amyloid precursor protein (APP).¹²² $A\beta$ monomers tend to self-assemble into neurotoxic soluble oligomers or even fibril aggregates through their hydrophobic domains while various approaches have been employed to indicate that this pathologic deposition process is promoted by transition metal ions such as Cu^{2+} and Zn^{2+} .¹²³⁻¹²⁶ Interestingly, total Cu^{2+} concentration is generally reported to decrease in AD brain tissues, probably because Cu^{2+} is abnormally redistributed, leaving the cells deficient in copper.¹²⁷⁻¹²⁹ However the Cu^{2+} level in lipid rafts is adversely associated with total Cu^{2+} concentration as people found that copper are concentrated ($\mu M \sim mM$) in lipid rafts.¹²⁸ Concurrently in these AD tissues, $A\beta$ localize on lipid rafts in neural membranes whereas a large quantity of aggregated $A\beta$ are observed to associate with negatively-charged lipids such as phosphatidylserine (PS).¹³⁰⁻¹³⁵ Under these conditions, $A\beta$ - Cu^{2+} deposits on cell surface can aggravate cell death by causing lipid oxidation damage due

to the redox activity of copper. Despite a general understanding of these events, several fundamental questions with regard to the underlying mechanisms remained to be answered. Where can A β obtain Cu²⁺ in these copper-deficient AD tissues? Do specific negatively-charged lipids actually serve as metal ion reservoirs for A β to oligomerize? Is the attachment of A β to the cell surface mediated by metal ions? How is that association process related to membrane oxidation stress and the progression of AD disease? Driven by these appealing questions, we decided to further study the function of copper ions in A β assembly at membrane surface.

Recently, we have developed a fluorescence assay to investigate the formation/dissociation of the Cu²⁺-PS complex in lipid membranes by a fluorescence quenching/dequenching detection (Chapter II).⁴⁵ As one of the most abundant negatively-charged lipids in humans, PS preferentially resides in the inner leaflet of plasma membrane facing cytosol.² The externalized PS is regarded as an essential marker in the recognition and clearance of apoptotic cells.^{2,21,24} Our results showed that Cu²⁺ can tightly bind PS in lipid bilayers and the apparent equilibrium dissociation constant is highly dependent upon the PS densities in supported lipid bilayers (SLBs) (shown in Chapter II and III). The consequence of this interaction is probably more remarkable when PS lipids are flipped from the inner to outer leaflet of plasma membranes during apoptosis. Given previous observations of the apoptotic neuron cells in AD brains by several groups,^{133,136-138} cellular membranes containing PS-Cu²⁺ complex might play significant roles in the formation of A β deposits as well as the lipid

oxidation neurotoxicity since PS-enriched membrane might promote localized accumulation of Cu^{2+} and become a copper supply for $\text{A}\beta$.

Herein we employed a combined technique of fluorescence microscopy and mass spectrometry to explore if Cu^{2+} can be “stolen” by $\text{A}\beta$ from PS lipids in the membrane (Scheme shown in Figure 4.1). To the best of our knowledge, there are few previous reports of such ternary interaction of $\text{A}\beta$ -metal ion-membrane on surface while most of the studies are focused upon the ion channels formed by $\text{A}\beta$ within the membranes.^{135,139,140} Using our newly-developed fluorescence quenching assay based on a microfluidic platform, the transfer of Cu^{2+} from PS in supported lipid bilayers (SLBs) to $\text{A}\beta$ was detected by measuring the fluorescence intensity recovery after the quenching caused by PS- Cu^{2+} complex. Since the fluorophores were embedded in the SLBs to monitor the fluorescence signals affected by the nearby binding/unbinding events, this fluorescence-based assay enables a high-throughput label-free detection of native $\text{A}\beta$ peptides and how they interact with membranes. These interactions can be further characterized and confirmed by electrospray ionization-mass spectrometry (ESI-MS). The MS spectra verified the formation of the $\text{A}\beta$ - Cu^{2+} complex as well as the dissociation of PS- Cu^{2+} complex. It should be noted that we used $\text{A}\beta_{1-16}$ and $\text{A}\beta_{1-42}$ as our model peptides. The shorter one $\text{A}\beta_{1-16}$ preserves the Cu^{2+} -binding sites but excludes the hydrophobic domain in other longer $\text{A}\beta$ peptides such as $\text{A}\beta_{1-40}$ and $\text{A}\beta_{1-42}$.¹⁴¹⁻¹⁴³ As will be shown, our results reveal that, in fact, they share similar ability to bind Cu^{2+} and swipe them off the lipid surface. There is no need for $\text{A}\beta$ to partition into the membrane to abstract Cu^{2+} , which might assist clarifying this peptide-membrane interaction

pathway. It will also help us achieve a better understanding about how apoptosis participate in these chronic diseases such as AD.

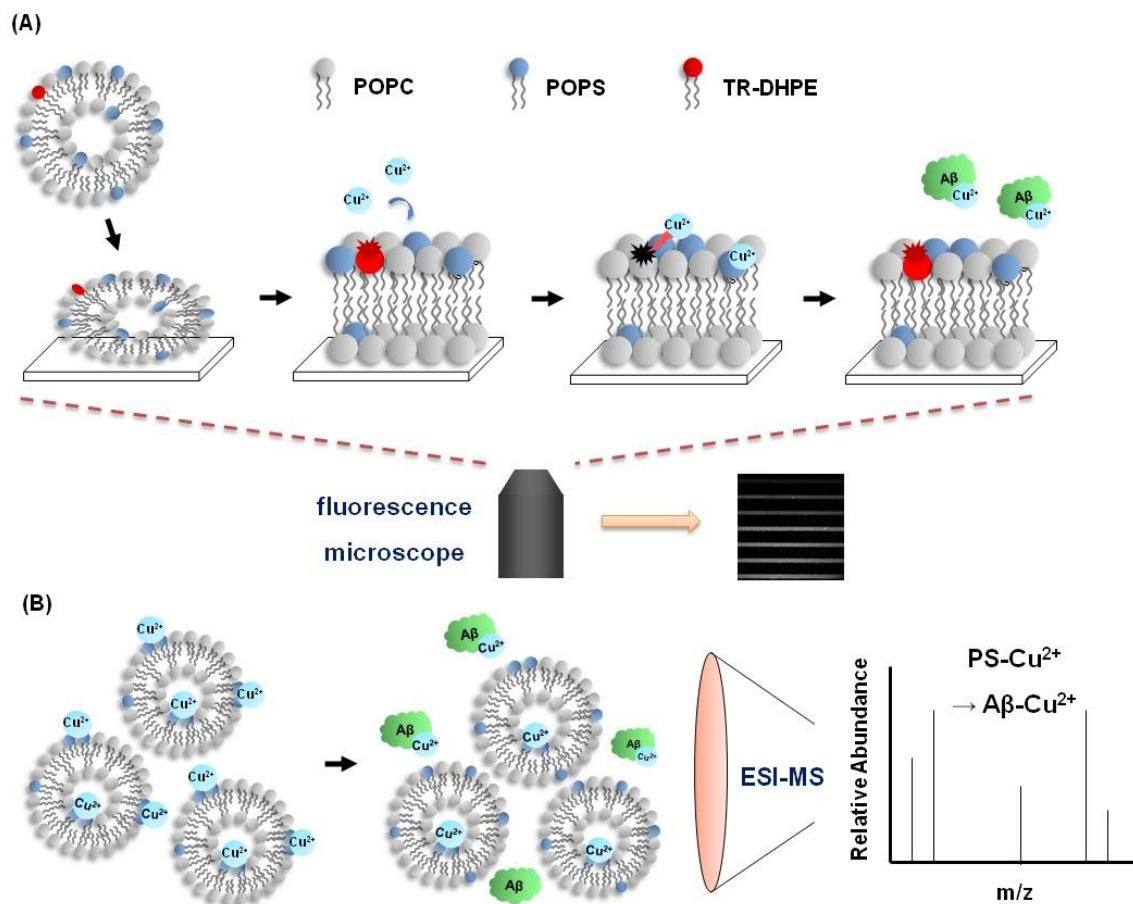


Figure 4.1. Schematic diagram of the proposed mechanism of $A\beta$ - Cu^{2+} -membrane interactions. In AD brain tissues, PS lipids in plasma membrane probably serve as Cu^{2+} reservoir as they have fairly high binding affinity to trap Cu^{2+} . Thus $A\beta$ needs to “steal” Cu^{2+} from PS, which might facilitate $A\beta$ oligomerization. The “stealing” process can be monitored by a combination of fluorescence quenching assay and mass spectrometry: (A) when Cu^{2+} binds PS in lipid bilayers, the resulting Cu^{2+} -PS complex quenches the nearby lipid-bound fluorophore while the fluorescence can be recovered when $A\beta$ swipes Cu^{2+} from PS. (B) ESI-MS spectra also prove the formation of the $A\beta$ - Cu^{2+} complex along with the dissociation of Cu^{2+} -PS complex.

Experimental Section

Materials

The lipids, the buffer and the microfluidic device used in fluorescence experiments in this chapter were listed and described in Chapter II. The vesicles used for mass spectrometry experiments were prepared and stored in 10 mM ammonium acetate buffer. The pH of this buffer solution was adjusted to 7.4 by dropwise addition of 30% ammonium hydroxide solution. Tris, NaCl, HCl, ammonium acetate, ammonium hydroxide and CuCl₂ were purchased from Sigma-Aldrich (St. Louis, MO). A β ₁₋₁₆ and A β ₁₋₄₂ were purchased from AnaSpec Inc. (Fremont, CA) in lyophilized powder form. A β ₁₋₁₆ was dissolved in 18 M Ω •cm ultrapure water at 0.5 mg/mL, aliquoted out and stored at -80 °C. Then these stock solutions were diluted by 1 mM Tris buffer to 1 μ M upon using. A β ₁₋₄₂ was dissolved in 1,1,1,3,3,3-hexafluoro-2-isopropanol (HFIP) at 0.5 mg/mL, aliquoted out and stored at -20 °C. Immediately prior to use, HFIP was evaporated, and the peptides were redissolved in 1 mM Tris buffer at concentrations of 1 μ M.

Vesicle Preparation, Microfluidic Device Fabrication and Bilayer Formation

The experiment methods for preparing small unilamellar vesicles (SUVs), fabricating microfluidic devices and forming lipid bilayers in the devices were all described in Chapter II.

Monitoring A β -Cu²⁺-PS Interactions through Fluorescence Microscopy

Fluorescence quenching/dequenching measurements of SLBs were performed inside the microfluidic devices described above. The experiment set-up scheme is shown in Figure 1.2. 1 mM Tris buffer solution (pH 7.4) containing 1 μ M CuCl₂ was provided by supply tubes (Teflon tubing with 0.6 mm internal diameter, SPC Technology) to individual channels of the microfluidic device through each inlet port. The flow through the device was gravity driven with an average flow rate at \sim 100 μ L/h in each microfluidic channel. The fluorescence of each channel was intermittently monitored by an inverted epifluorescence Nikon Eclipse TE2000-U microscope until equilibrium was reached. Then, the flow direction was reversed by switching the inlet and outlet ports. 1 μ M A β ₁₋₁₆ or A β ₁₋₄₂ in 1 mM Tris buffer was injected into the channels through outlet ports and the pipette tips filled with A β solutions were left at the outlet ports. The original inlet supply tubes and supply solution were subsequently laid to a level which is lower than the device to cause a reverse flow driving force. In this way, A β ₁₋₁₆ solutions were flowed into the channels at an average rate of 70 μ L/h. The fluorescent images of the channels were captured by a MicroMax 1024 CCD camera (Princeton Instruments) and collected by MetaMorph software (Universal Imaging).

Characterization of PS-Cu²⁺ Complex and A β -Cu²⁺ Complex by ESI-MS

The ESI-MS spectra of all the samples in this paper were acquired on a Waters Synapt HDMS G2 mass spectrometer (Waters UK Ltd., Manchester, U.K.). The samples were first prepared in 10 mM ammonium acetate buffer at pH=7.4 and then diluted by

100 times in 20 vol % methanol in water immediately before MS experiments. When preparing the SUVs with Cu^{2+} for the experiments, the buffer containing Cu^{2+} was used to re-hydrate the vacuum-dried lipids. In this way, Cu^{2+} can be distributed both inside and outside of the vesicles. The Cu^{2+} concentration in the buffer is half of the concentration of the PS in vesicles which can make it saturated at $\text{Cu}(\text{PS})_2$ complex. Negatively charged ions were formed by nano-ESI using a source temperature of $\sim 80^\circ\text{C}$ and a capillary voltage of -1.8 – 2.0 kV. The sampling cone voltage was set at 25 kV and the extraction cone voltage was 2.0 kV.

Results and Discussions

Firstly, the ability of $\text{A}\beta$ to swipe Cu^{2+} from lipid bilayers containing PS was investigated with fluorescence quenching/dequenching method. We employed supported lipid bilayers (SLBs) made of 89 mol % POPC, 10 mol % POPS and 1.0 mol % lipid-bound fluorophore Texas Red-DHPE (TR-DHPE) as a model membrane to investigate the ability of PS to serve as a bridge for $\text{A}\beta$ and metal ions. Buffer containing $1\ \mu\text{M}$ Cu^{2+} flowed into the channel continuously until the fluorescence signal became unchanged. Figure 4.2 shows the fluorescence images and line scans of SLBs containing 10 mol % POPS with (left channel) or without (right channel) Cu^{2+} . In the presence of $1\ \mu\text{M}$ Cu^{2+} , the fluorescence of TR-DHPE was quenched by $\sim 80\%$ but then got almost totally recovered after introducing $1\ \mu\text{M}$ $\text{A}\beta_{1-16}$ continuously while the fluorescence response of the channel without Cu^{2+} was uniform. It has been found previously that the quenching

phenomenon is attributed to the complex formation between Cu^{2+} and PS.⁴⁵ When PS lipids attract Cu^{2+} from the solution to SLBs, Cu^{2+} ions accumulate close to the bilayer surface, thus quenching the fluorophores nearby. The quenched fraction of the fluorophores reflects the Cu^{2+} -PS binding. This quenching process can be reversibly recovered by using low pH buffer or strong metal ion-binding ligands such as ethylenediaminetetraacetic acid (EDTA) and nitrilotriacetic acid (NTA) to swipe off Cu^{2+} , which inspired us to create a label-free detection of A β . A variety of approaches have shown that A β peptides can bind Cu^{2+} via three histidine residues and N-terminus^{36,143} while previous reports reveal comparable binding constants for the binding between Cu^{2+} and A β_{1-16} , A β_{1-40} or A β_{1-42} , indicating that these peptides share the same Cu^{2+} binding region which is located in N-terminal hydrophilic portion.^{127,144} The measured binding constant for A β_{1-16} and Cu^{2+} is around nM^{-1} .^{127,144-147} The binding affinity of A β - Cu^{2+} is stronger than the intrinsic affinity of PS- Cu^{2+} interaction (10^{-7} to 10^{-8} M, shown in Chapter III). Since A β_{1-16} was continuously flowed over the lipid bilayer surface, it pushed the equilibrium towards the dissociation of PS- Cu^{2+} complex along with the association of A β - Cu^{2+} , which enables it to competitively swipe Cu^{2+} from PS in SLBs visualized by fluorescence quenching recovery. This flowing assay is well representative of what possibly happened on cell surface. Free A β monomers are continuously generated from the amyloid precursor protein (APP) and upon forming complex with Cu^{2+} , they tend to form oligomers or fibril aggregates, resulting in an overall free Cu^{2+} reduction.

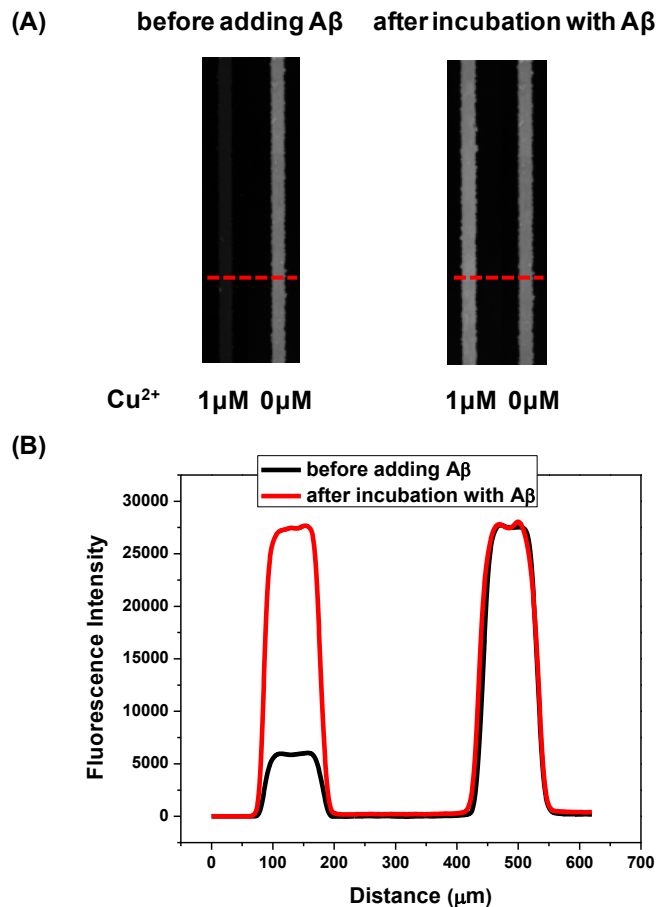


Figure 4.2. (A) Fluorescence images and (B) line scans from two parallel microfluidic channels with Cu²⁺ and A β ₁₋₁₆. These two channels have 1 μ M (left channel) and 0 μ M (right channel) CuCl₂ introduced. The SLBs in these two channels both consist of 10 mol % POPS, 89 mol % POPC and 1.0 mol % TR-DHPE. The fluorescence is shown both before and after incubation with continuously flowing 1 μ M A β ₁₋₁₆ in 1 mM Tris buffer at pH 7.4 for about 2 hours.

To explore the process of A β -Cu²⁺-PS interaction, the time course of changes in fluorescence signals was subsequently shown in Figure 4.3, which also verifies that the dequenching issue was caused by Cu²⁺ detachment from the SLBs instead of other interactions between peptides and lipid membranes. When A β is previously saturated

with Cu^{2+} , it will lose the ability to bind Cu^{2+} thus losing the effect on fluorescence signals. As shown in the pink region of Figure 4.3, the fluorescence of TR-DHPE embedded in SLBs was firstly quenched by 75% or 85% in the presence of Cu^{2+} at 5.0 mol % or 15 mol % PS concentrations. However, upon introducing metal-free $\text{A}\beta$ into the channels, the fluorescence signal got recovered gradually to the original intensity without Cu^{2+} (black and red plots in the yellow region of Figure 4.3). As a comparison, when $\text{A}\beta$ flowed in together with the same concentration of Cu^{2+} , the quenched fluorescence level remained intact (blue and green plots in the yellow region of Figure 4.3). As indicated by previous studies, $\text{A}\beta$ can employ His6, His13, His14 and Asp1 to bind Cu^{2+} in 1:1 stoichiometry.^{141,142} When $\text{A}\beta$ is already Cu^{2+} -saturated, there are no extra binding sites available on these $\text{A}\beta$ for copper ions, leaving copper ions as Cu^{2+} -PS complex on the membrane without a dequenching process. Moreover, the kinetics of this “stealing” Cu^{2+} process was also revealed by comparison of the fluorescence response from different PS mol % over time, e.g. 5.0 mol % and 15 mol % PS in Figure 4.3. For SLBs containing 5.0 mol % PS (black plot), it took about 1.5 hour for $\text{A}\beta_{1-16}$ to remove all the Cu^{2+} and restore the maximum fluorescence intensity. When it comes to 15 mol % PS condition (red plot), the recovery time is elongated to around 2.5 hours. The time scale to dequench by $\text{A}\beta$ (in hours) is longer than that to quench the fluorescence by the same concentration of Cu^{2+} (in minutes). These results suggest that this Cu^{2+} -transfer event is a much slower process compared with Cu^{2+} -PS binding and the competence of $\text{A}\beta$ over PS turns out to be weakened with an increasing PS density. During this process, $\text{A}\beta$ peptides need to push the equilibrium towards the dissociation of PS-Cu^{2+} complex

along with the association of $A\beta$ - Cu^{2+} . It was found in our previous report that with an increasing surface PS concentration, the binding affinity between PS and Cu^{2+} was greatly enhanced (Chapter III), which might slow down the rate of $A\beta$ to swipe Cu^{2+} from the surface, since the apparent driving force (the binding affinity difference between $A\beta$ - Cu^{2+} complex and PS- Cu^{2+} complex) deteriorates significantly.

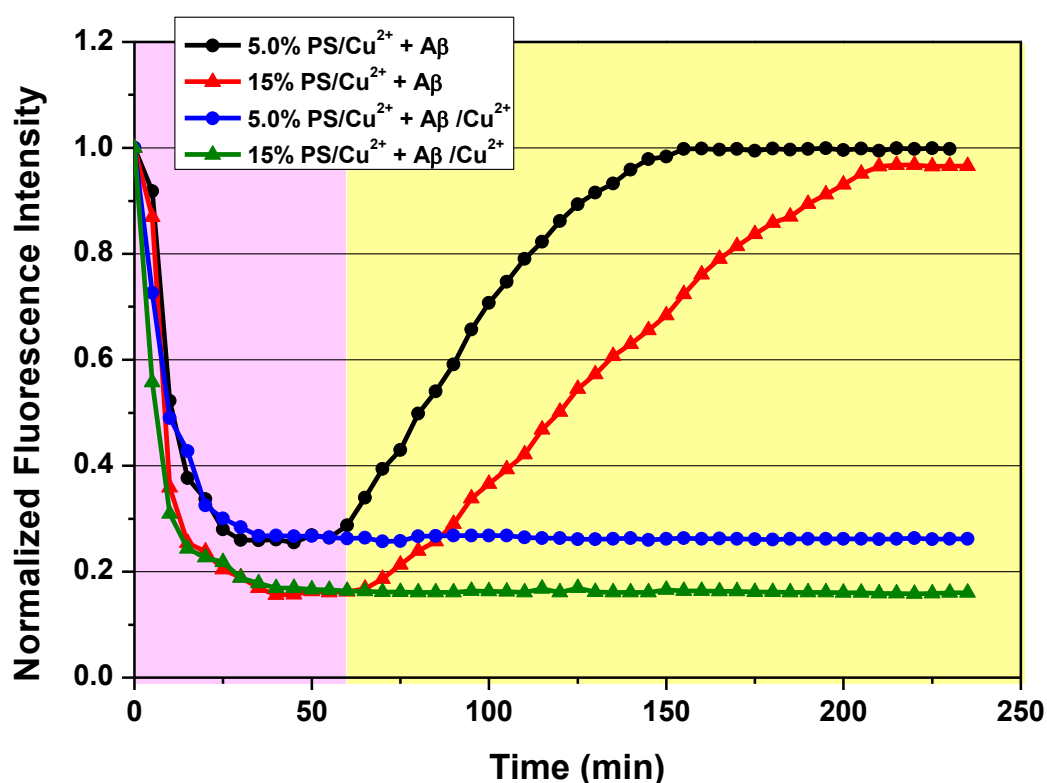


Figure 4.3. Fluorescence response over time showing fluorescence dequenching caused by $A\beta$ swiping Cu^{2+} . POPC SLBs containing 1.0 mol % TR-DHPE and 5.0 or 15 mol % POPS were firstly incubated with $1 \mu M Cu^{2+}$ (pink background), followed by $1 \mu M A\beta_{1-16}$ without or with $1 \mu M Cu^{2+}$ (yellow background). The black and red data plots showed the conditions where $1 \mu M A\beta_{1-16}$ was introduced into SLBs containing 5.0 or 15 mol % POPS while the blue and green data plots showed the conditions where $1 \mu M A\beta_{1-16}$ was applied with $1 \mu M Cu^{2+}$. The experiments were performed in 1 mM Tris buffer at pH 7.4.

In the next set of experiments, the multi-channel microfluidic device containing SLBs with various PS mol % was applied to mimic biological environments with different PS densities at cell surface. Buffer containing 1 μM Cu^{2+} was introduced into the SLBs containing 0, 3.0, 5.0, 7.5, 10, 15 and 20 mol % POPS, which were then rinsed by 1 μM $\text{A}\beta_{1-16}$. A graphical summary of the results was shown in Figure 4.4. Normalized fluorescence intensities after quenching at the indicated PS percentage were plotted in black columns and the fluorescence signals after dequenching by 1 μM $\text{A}\beta_{1-16}$ were shown in gray. It can be seen that the degree of quenching caused by Cu^{2+} was enhanced with higher PS concentrations, which, as expected, is consistent with an increasing number of Cu^{2+} -PS complex as effective quenchers and a lower dynamic distance between the quenchers and lipid-bound fluorophores. After a continuous flow of $\text{A}\beta_{1-16}$ solution, the quenched fluorescence was able to recover completely for most conditions, except for 15 or 20 mol % PS, in which the average final fluorescence signal reached 95% or 90% of the original intensity and the error bars showed more uncertainty in this range. This is probably because of the background Cu^{2+} contamination in buffer solutions, as discussed in our previous paper (Chapter III). To validate this assumption, 1 nM EDTA was added into $\text{A}\beta_{1-16}$ solutions to chelate the background heavy metal ions and a full recovery in fluorescence intensity was observed for 15 and 20 mol % PS conditions. Therefore $\text{A}\beta$ swiping is effective for all these conditions with various PS surface densities.

To compare with $\text{A}\beta_{1-16}$, $\text{A}\beta_{1-42}$ peptides were also tested, which gave us similar fluorescence change results. (Figure 4.5) We also tested if $\text{A}\beta$ can stick around the

membrane after swiping Cu^{2+} from the PS by applying HiLyte Fluor 488-labeled $\text{A}\beta_{1-16}$ and $\text{A}\beta_{1-42}$ to the SLBs containing 10 to 20 mol % PS. However, by monitoring the fluor-tagged $\text{A}\beta$ using total internal reflection fluorescence microscope (TIRFM), there was little if any peptide insertion observed. These results suggest that although the three negative charges of $\text{A}\beta$ attenuate upon Cu^{2+} binding, it might still be repelled from the negatively-charged surface owing to the remaining negative charges on $\text{A}\beta$. The formation of lipid raft or domain probably can help the peptide insertion by hydrophobic interactions.^{128,148}

Although the apparent binding affinity for Cu^{2+} to the SLBs containing 7.5~20 mol % PS (sub nM ~ pM scale) is stronger than $\text{A}\beta\text{-Cu}^{2+}$ (nM scale), the tight apparent binding affinity between Cu^{2+} and PS is indeed caused by the increased Cu^{2+} concentration in double layer of the negatively-charged surface due to Coulombic effect. The surface charge-adjusted intrinsic binding affinity of PS to Cu^{2+} turns out to be weaker than $\text{A}\beta$. (Chapter III) Therefore, $\text{A}\beta$ peptides are able to steal copper ions by a continuous approach to the membrane to alter the binding equilibrium.

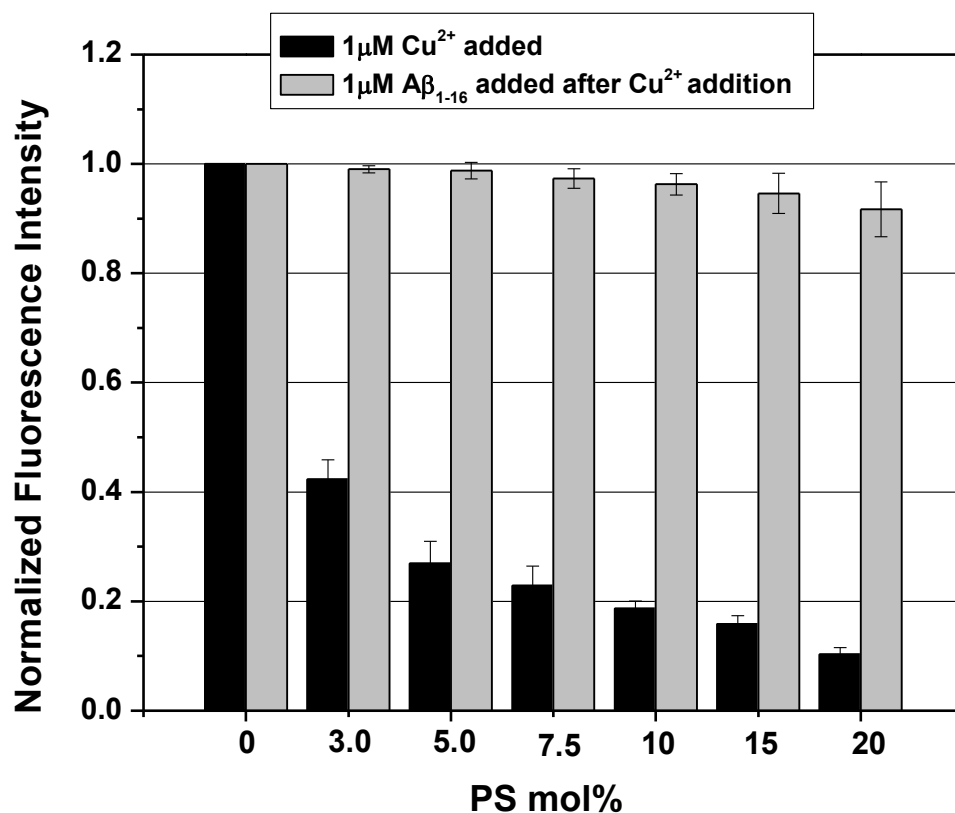


Figure 4.4. The graphic summary of normalized fluorescence intensity of SLBs containing PS with Cu²⁺-quenching and Aβ₁₋₁₆ dequenching. The POPC SLBs contained 0 to 20 mol % POPS and 1.0 mol % TR-DHPE. The black columns were plotted as the normalized fluorescence intensities after buffer containing 1 μM Cu²⁺ flowed into the channels and caused quenching at the indicated PS percentage and the gray columns were the fluorescence signals after dequenching by 1 μM Aβ₁₋₁₆. The error bars represent the standard deviation of three to five experiments.

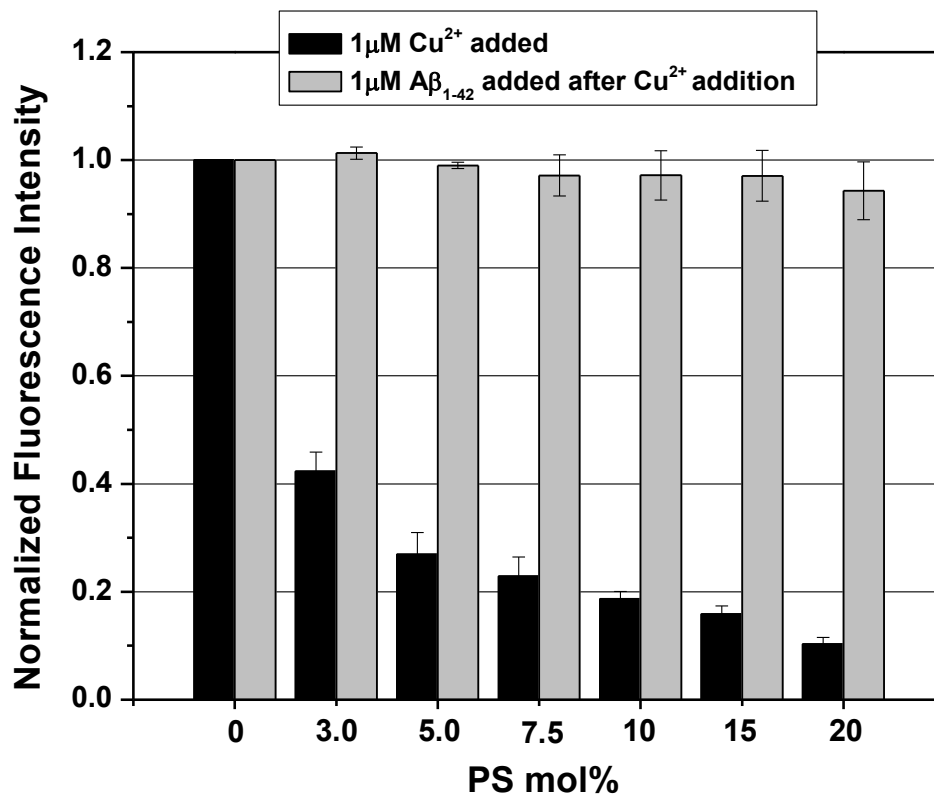


Figure 4.5. The graphic summary of normalized fluorescence intensity showing Aβ₁₋₄₂ has the similar ability to grab Cu²⁺ compared with Aβ₁₋₁₆. The black columns were plotted as the normalized fluorescence intensities from POPC SLBs containing 0 to 20 mol % POPS and 1.0 mol % TR-DHPE observed after quenching by 1 μM Cu²⁺-quenching at the indicated PS percentages and the gray columns were the fluorescence signals after dequenching by 1 μM Aβ₁₋₄₂. The error bars represent the standard deviation of three to five measurements.

Finally, ESI-MS was utilized as a supplementary label-free method to reveal the identification of the complexes during this association/dissociation process. Given the ability of ESI-MS to manipulate large intact molecular ions through soft ionization mode, the copper transfer from lipids to peptides can be examined in a more straight-forward way by capturing the declining peaks of PS-Cu²⁺ complex along with the rising peaks of

$A\beta$ - Cu^{2+} complex in mass spectra. In the mass spectra shown in Figure 4.6, the specific m/z signals of PS and the $Cu(PS)_2$ complex were highlighted in pink background while the $A\beta_{1-16}$ and their corresponding Cu^{2+} -bound complexes were highlighted in blue. As can be seen, when the vesicles containing 20 mol % POPS were extruded with Cu^{2+} (Figure 4.6B), the extra peaks corresponding to $[2POPS+Cu]^{2-}$ ions ($m/z = 791$) can be observed compared with the vesicles without Cu^{2+} (Figure 4.6A). This is consistent with our previously-built model (binding reaction shown in Figure 3.1). When Cu^{2+} reacts with PS molecules, it preferentially binds the amine and carboxyl groups and forms a square-planar complex in which one proton on each of the two amine groups is displaced (Chapter III). As such, the $2POPS-Cu^{2+}$ complex possess two negative charges, which is confirmed by the negative mode mass spectra here. These characteristic peaks significantly diminished in Figure 4.6C when $A\beta_{1-16}$ was present to compete with PS for Cu^{2+} binding, while simultaneously the peaks corresponding to $[A\beta+Cu]^{3-}$ and $[A\beta+Cu]^{2-}$ appeared.

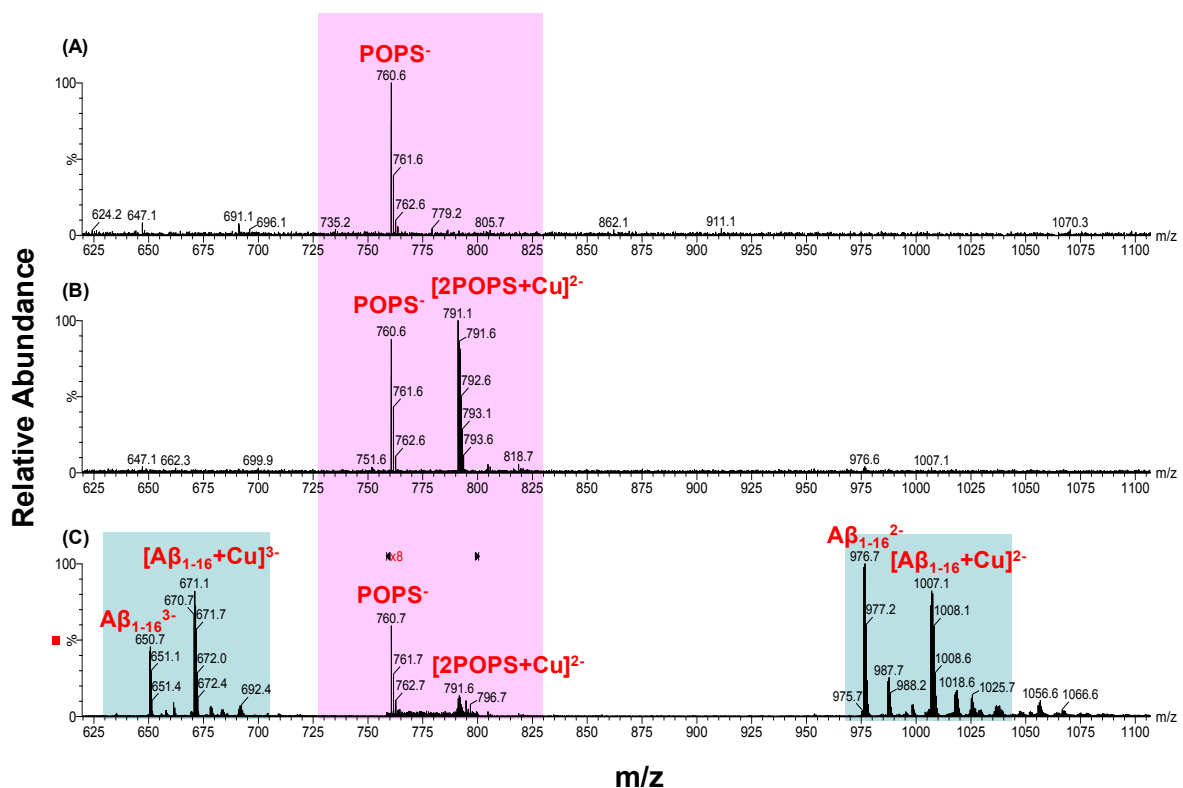


Figure 4.6. The negative mode ESI-MS spectra of PS-contained vesicles with CuCl_2 and $\text{A}\beta_{1-16}$. The vesicles were 1 mM 80 mol % POPC /20 mol % POPS vesicles (A) extruded without CuCl_2 ; (B) extruded with CuCl_2 (molar ratio of PS: Cu^{2+} = 2:1); (C) extruded with CuCl_2 and then incubated with 100 μM $\text{A}\beta_{1-16}$ for 2 hours. All the samples were firstly prepared in 10 mM ammonium acetate buffer and then diluted by 100 times in 20 vol % methanol in water solvent for MS exp. The PS and $\text{Cu}(\text{PS})_2$ peaks are highlighted in pink background while the $\text{A}\beta$ and $\text{A}\beta\text{-Cu}^{2+}$ peaks are highlighted in blue background.

Since the depression of MS signals of the Cu^{2+} -PS complex occurs along with the emergence of the $\text{A}\beta\text{-Cu}^{2+}$ complex signals, it also suggests that these complexes are formed by specific binding instead of non-specific interactions when they are sent into MS system, which further indicates the high stability of these complexes. Overall, these

spectra correlate well with the fluorescence quenching/dequenching process and validate the transfer of Cu^{2+} from PS lipids to $\text{A}\beta$ peptides.

Conclusion

In conclusion, the combination of fluorescence microscopy, microfluidic technique and mass spectrometry offers us a unique platform to mimic how $\text{A}\beta$ peptides approach cell membranes and obtain metal ions in neural systems. The results indicate that plasma membranes with exposed PS probably provide Cu^{2+} as stimulates or medium for the $\text{A}\beta$ oligomerization and assist the seeding of $\text{A}\beta$ deposits on cell surfaces. It is possible that with an additional hydrophobic domain, the longer $\text{A}\beta$ peptides such as $\text{A}\beta_{1-40}$ or $\text{A}\beta_{1-42}$ might be involved in further interactions, for example, inserting into lipid rafts to form ion channels,^{132,149} which will be studied in the future. The multi-technique label-free method described here could be extended to the analysis of more membrane-related proteins or peptides to obtain useful biological information about the membrane-ion-protein/peptide interactions.

CHAPTER V
THE EFFECTS OF Cu^{2+} -PHOSPHATIDYLSERINE BINDING ON LIPID
OXIDATIONS

Introduction

Lipid oxidations have been regarded as important factors contributing to a variety of physiological and pathological events such as cell apoptosis, atherosclerosis and Alzheimer's disease.¹⁵⁰⁻¹⁵⁴ It is typically induced by partial oxidation by reactive oxygen species (ROS) such as O_2 , O_2^- and H_2O_2 , which further brings about cellular dysfunction, enzyme inactivation and DNA damage.¹⁵⁵ It has long been known that the polyunsaturated fatty acids (PUFA) can decompose due to the slow autoxidation during storage.¹⁵⁶⁻¹⁵⁸ The reactions are usually initiated by the hydrogen abstraction from allylic or *bis-allylic* positions. The activate methylene group adjacent to the double bonds represents a critical target site where the hydrogen abstraction is easy to be achieved.^{157,158} This initiation reaction subsequently leads to an oxygenation and the formation of peroxy radicals as well as the following propagation steps. These chain reactions are likely to be catalyzed by transition metal ions.¹⁵⁷⁻¹⁵⁹ Through a similar pathway, the autoxidation of phospholipids with polyunsaturated acyl chains should take place as well in biological systems, which can cause the destruction of cell membranes. These autoxidation processes usually involve the formation of lipid radicals, oxygen uptake, rearrangement of the double bonds in unsaturated acyl chains and further

transformations to generate products such as alcohols, ketones, aldehydes and carboxylic acids.^{157,160}

Transition metal ions in human body are bound to proteins, membranes and other cell constituents and their distribution is strictly regulated by metallochaperones.³² Among these ions, the redox-active iron and copper can catalyze the redox-cycling by reducing the induction period and increasing the rate of lipid oxidation. It has been proposed that the interactions of iron and copper ions with O₂ or H₂O₂ can generate the destructive oxidants O₂⁻ or •OH through Fenton reactions or Harber-Weiss reactions.¹⁶¹⁻¹⁶³ The presence of chelating agents may promote or inhibit metal-ion-dependent ROS formation, depending on a number of factors such as the solubility of the complex, the redox potential of the Mⁿ⁺/M⁽ⁿ⁻¹⁾⁺ pair and whether or not it has a free coordination site.^{161,162,164} As the third most abundant transition metal ions in human systems, copper has a overall concentration (complexed and free) of ~100 μM in common tissues while the concentration of uncomplexed copper in the cytoplasm is extremely low (~10⁻¹⁸ M).⁶⁷ However, high concentrations of copper (mM scale) have been detected in the amyloid plaques, one of the well-recognized pathologies present in Alzheimer's disease (AD) patients' brains.¹⁶⁵ In contrast, total Cu²⁺ concentration is generally reported to decrease in AD brain tissues, probably because Cu²⁺ is abnormally redistributed, leading to the dysfunction of copper ion homeostasis.¹²⁷⁻¹²⁹ Moreover, the Cu²⁺ in AD brain systems are found accumulated in lipid rafts which are rich in anionic lipids. In consequence, amyloid-beta peptides (Aβ) might readily precipitate close to these regions on the membranes and cause further oxidative damage.^{128,130,133,134,166} In this context, it is

intriguing to see how the interactions of transition metal ions with different kinds of lipids would affect the oxidation process.

In previous studies, we have detected the formation of the Cu^{2+} -phosphatidylserine (PS) lipid complex by a fluorescence quenching-based assay on lipid bilayers (Chapter II).⁴⁵ Given this binding event, we hypothesized that the Cu^{2+} approach to the membrane surface may have some consequences on the oxidation rate of the unsaturated lipids. On one hand, when PS binds Cu^{2+} and immobilizes it at the headgroup moiety, it might limit the free motion and activity of Cu^{2+} to catalyze the lipid oxidation. On the other hand, when Cu^{2+} is attracted by PS to accumulate on the bilayers, the surface concentration of Cu^{2+} gets increased, which might promote the oxidation reaction. We wish to see how these contradictory factors contribute to lipid oxidation toxicity in a variety of physiological and pathological conditions.

Experimental Section

Materials

The following lipids were used in these experiments. 1,2-Dilauroyl-*sn*-glycero-3-phosphocholine (DLPC), 1-palmitoyl-2-oleoyl-*sn*-glycero-3-phosphocholine (POPC), 1,2-dilauroyl-*sn*-glycero-3-phospho-L-serine (DLPS), 1-palmitoyl-2-linoleoyl-*sn*-glycero-3-phosphocholine (PLiPC), 1-palmitoyl-2-linoleoyl-*sn*-glycero-3-phospho-L-serine (PLiPS), 1,2-dilauroyl-*sn*-glycero-3-phospho-(1'-*rac*-glycerol) (DLPG), 1,2-dilauroyl-*sn*-glycero-3-phosphate (DLPA) and 1,2-dilauroyl-*sn*-glycero-3-

phosphoethanolamine (DLPE) were purchased from Avanti Polar Lipids (Alabaster, AL). The vesicles used for mass spectrometry experiments were prepared and stored in 10 mM ammonium acetate buffer. The pH of the buffer was adjusted to 7.4 by dropwise addition of 30% ammonium hydroxide solution. The ammonium acetate, ammonium hydroxide, copper chloride and all the solvent (HPLC grade) used in these experiments were purchased from Sigma-Aldrich (St. Louis, MO). The purified water (18.2 M Ω •cm) used in all these experiments was acquired from a NANOpure Ultrapure Water System (Barnstead, Dubuque, IA).

SUVs Preparation and Oxidation

The experiment procedures for preparing small unilamellar vesicles (SUVs) were described in Chapter II. Oxidation treatments were carried out by adding Cu²⁺ into the SUVs solutions followed by incubations. No peroxidants such as H₂O₂ were added into the system while the only applicable oxidants are atmospheric O₂ dissolved in vesicle solution. 75 μ M CuCl₂ were added into the vesicle solution containing 300 μ M PLiPC (1 mM vesicles consisting of 70 mol % DLPC and 30 mol % PLiPC or 40 mol % DLPC, 30 mol % DLPS and 30 mol % PLiPC) and this mixture was incubated at 37 °C for different time periods.

Characterization of Oxidation Products by LC-MS and ESI-MS/MS

The oxidation products of the unsaturated lipids were separated and characterized by Surveyor HPLC system (Thermo Finnigan, San Jose, CA) interfaced with quadrupole

ion trap mass spectrometer (LCQ-DECA; Thermo Electron). The reaction products were diluted by ten times in methanol and then introduced into a Phenomenex 2.6 μm C_8 column (150 x 2.1 mm, kept at 55°C). The mobile phase consisted of acetonitrile-aqueous ammonia formate (5 mM; 60:40; eluent A) and isopropanol-acetonitrile containing ammonia formate (5 mM; 90:10; eluent B). The solvent gradient was programmed as follows: 10% B for 3 min followed by linear increase to 50% B at 10 min and then increase linearly to 66% B at 15 min and subsequently increase linearly to 97% B at 19 min and held isocratically for 4 min and then back to 10% B for 7 min. The flow rate was 200 $\mu\text{L}/\text{min}$. The ESI-MS/MS spectra of the SUVs solutions were acquired on a Waters Synapt HDMS G2 mass spectrometer (Waters UK Ltd., Manchester, U.K.). The samples were first prepared in 10 mM ammonium acetate buffer at pH=7.4 and then diluted by 100 times in 20 vol % methanol in water immediately before MS experiments. The diluted samples were directly infused into the mass spectrometer at a rate of 0.5–0.8 $\mu\text{L}/\text{min}$ and the ions were formed by nano-ESI using a source temperature of ~ 100 °C and an inlet capillary voltage of 1.8~2.0 kV. The sampling cone voltage was set at 25 kV and the extraction cone voltage was 4.0 kV. All fragmentation was carried out by collision of ions with background gas (argon) and the collision energy for collision induced dissociation (CID) of the phospholipids was generally set in a range of 28~40 V.

To compare the extent of oxidation in various samples, the relative oxidation amounts can be determined by looking at the disappearance of starting materials, the unsaturated lipid PLiPC with two double bonds. Two kinds of internal standards, DLPC and POPC, were used in this relative quantification method. DLPC was already present

in the vesicles as the main component of the vesicles while POPC could be added into the system before dilution and loading into LC-MS. The response of the target lipids is normalized to the response of the two standard lipids separately, which gave similar results. The unoxidized percentage of the PLiPC can be calculated as:

$$R \% = \frac{A_r}{A_{std}} / \frac{A_{ori}}{A'_{std}} \times 100\% \quad (5.1)$$

where A_r is the LC peak area of PLiPC in oxidized vesicle solutions while A_{ori} is the area of PLiPC in original (unoxidized) vesicle solution; A_{std} is the area of standard (DLPC or POPC) in oxidized solution while A'_{std} is the area of that standard in unoxidized solution. The relative oxidation extent can be calculated as:

$$O \% = 1 - R \% \quad (5.2)$$

Results and Discussions

Cu²⁺-catalyzed PLiPC Oxidation

After incubating with Cu^{2+} for different periods of time, the LC-MS chromatograms of vesicles consisting of 70 mol % DLPC and 30 mol % PLiPC with the internal standard POPC are obtained. Since the ESI-MS spectra of PC lipids usually share a characteristic phosphocholine head group peak at $m/z=184$,¹⁶⁷ the reconstructed-ion chromatograms (RIC) of the PC lipids with peaks at $m/z = 184$ were shown in Figure 5.1 to rule out the background contaminates for a more accurate quantification. As observed in Figure 5.1, the retention time of the non-oxidized standards DLPC and POPC lipids was around 9.6 min and 14.7 min, respectively, while the non-oxidized

target lipids PLiPC was eluted at 13.9 min. The corresponding MS spectra of these LC peaks showed the presence of characteristic molecular ions and the sodium adducts ($[M+H]^+$ and $[M+Na]^+$) of DLPC (m/z 622 and 644), POPC (m/z 760 and 782) and PLiPC (m/z 758 and 780). The chromatographic results reveal that the elution time of PC lipids increases when the molecule is more lipophilic, i.e. with longer acyl chains and fewer double bonds present. The oxidation products of PLiPC obtained after various incubation times were also shown in the RIC figure by a number of peaks evolved with retention times from 3 to 14 min, which correspond to multiple oxidation products. In the linoleic acyl chain of PLiPC, there are several vulnerable sites for oxidation reactions. The two double bonds at C-9 and C-12 present in the linoleic acyl chain can stabilize the radical intermediates at their allylic positions due to conjugation effects, thus favoring the hydrogen extraction at these positions. The loss of bis-allylic hydrogen on C-11 can generate the alkyl radical, which will be stabilized by rearrangement of the two double bonds to form a conjugated diene radical centered at C-9 or C-13 (mechanism shown in Figure 5.2). Such radical species are able to uptake O_2 to create peroxy radicals and eventually produce long-chain oxidation products by insertion of oxygen atoms. On the other hand, the initially-oxidized polyunsaturated acyl groups can undergo intramolecular rearrangement reactions or further oxidation to generate chain-shortened products such as alcohols, aldehydes or carboxylic acids.^{168,169}

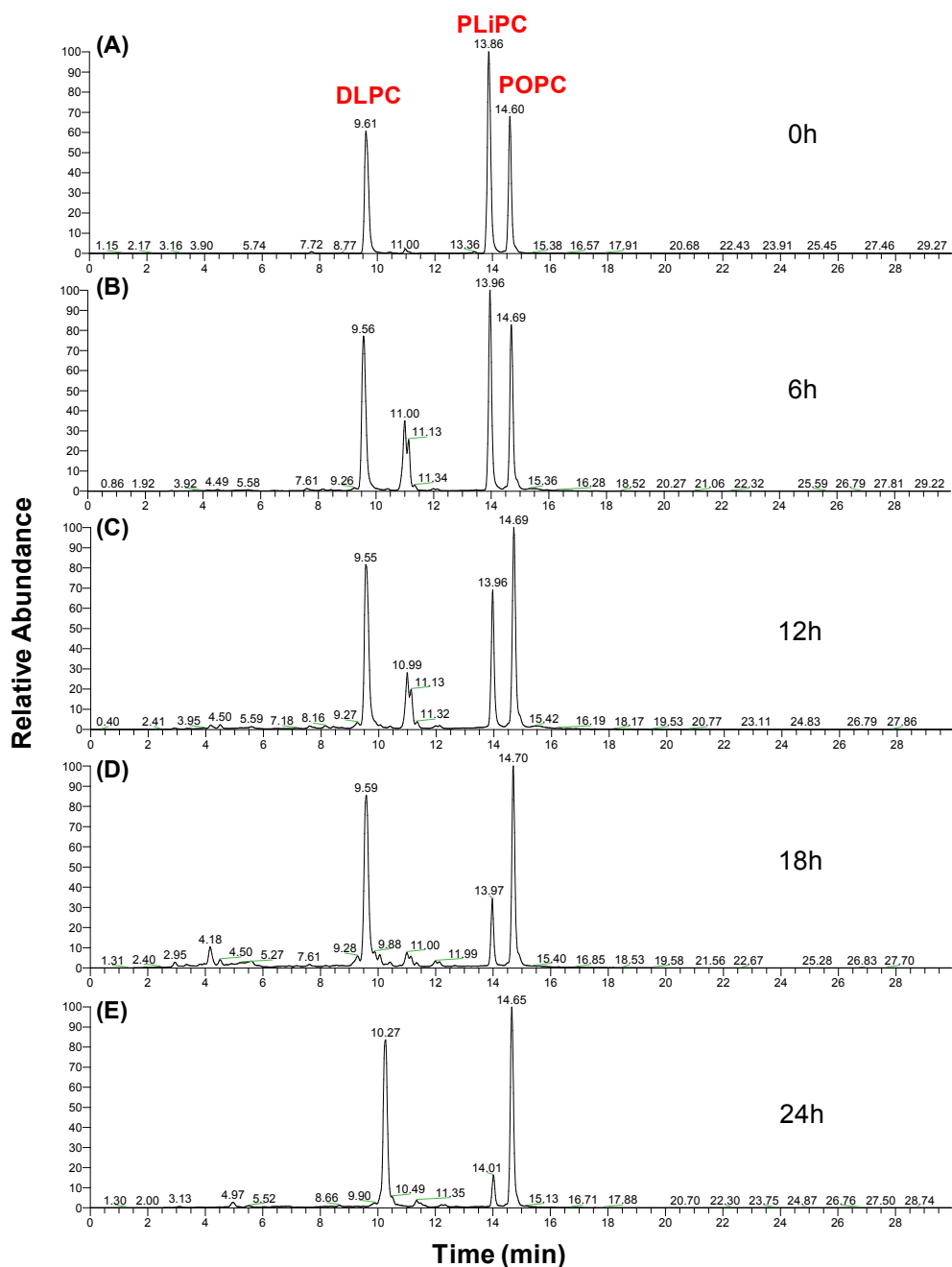


Figure 5.1. The reconstructed-ion chromatograms (RIC) of the vesicles containing 70 mol % DLPC and 30 mol % PLiPC incubated with Cu^{2+} over different time periods. 75 μM CuCl_2 was added into the 1 mM vesicle solution and incubated in 37 °C for different hours. The samples were then diluted in methanol by ten times and 10 μM POPC was added as an internal standard before LC-MS experiments. The RIC of the PC lipids were generated based on a characteristic MS peak of PC lipids ($m/z = 184$) to rule out the background contaminants.

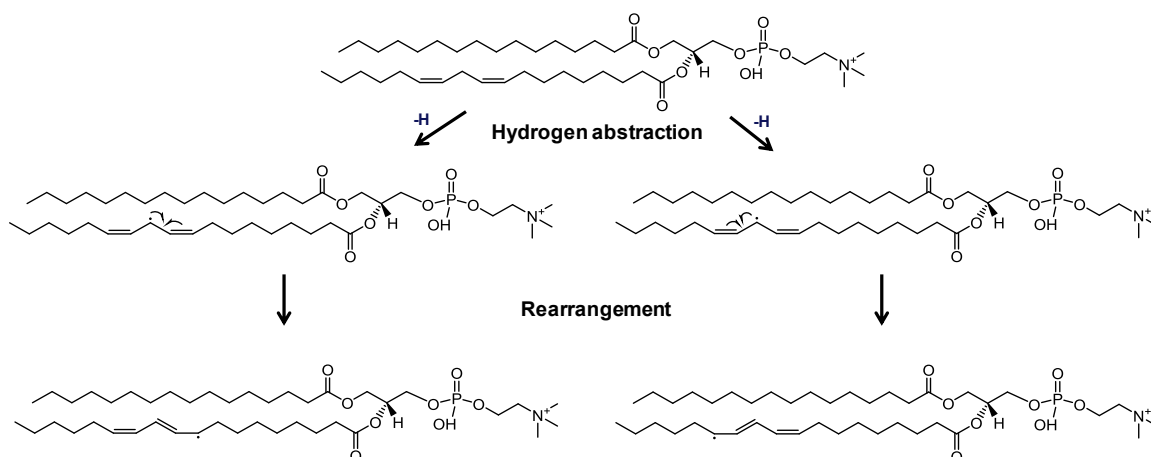
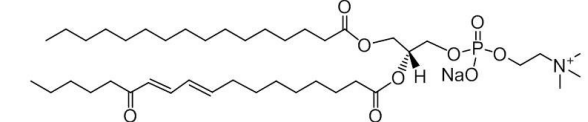
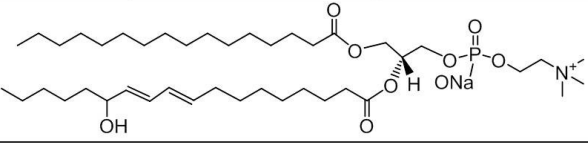
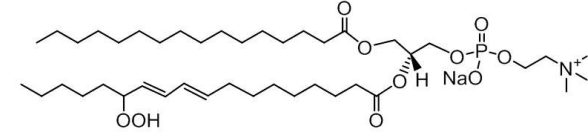
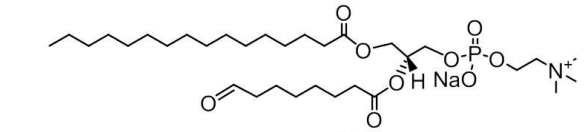
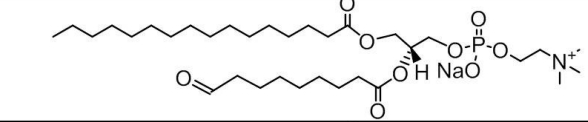
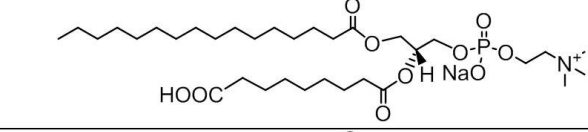
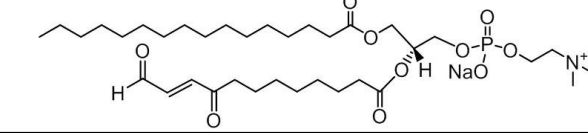
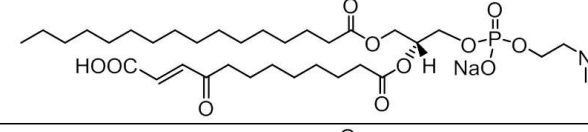
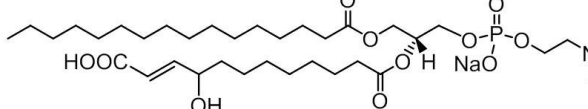


Figure 5.2. The proposed formation mechanism of PLiPC radicals susceptible to oxidations. PLiPC has two double bonds at C-9 and C-12 in the *sn*-2 linoleic acyl chain where the hydrogen extraction readily happens. The loss of bis-allylic hydrogen on C-11 generates the alkyl radical, which will be further stabilized by rearrangement of the two double bonds to form a conjugated diene radical centered at C-9 or C-13.

It is interesting to find that these long-chain and short-chain oxidation products exhibit different ionization efficiency, shown in Figure 5.1. After incubating with Cu^{2+} for 6 hours (Figure 5.1B), the predominant long-chain oxidation products were found to be eluted at 11.0, 11.1 and 11.3 min. The mass spectra of these peaks show the ions with m/z equal to 794, 796 and 812, which correspond to the sodium adducts of long-chain oxidation products, 1-palmitoyl-2-(keto-octadecadienoic acid)-*sn*-glycero-3-phosphocholine, 1-palmitoyl-2-(hydroxy-octadecadienoic acid)-*sn*-glycero-3-phosphocholine and 1-palmitoyl-2-(hydroperoxide-octadecadienoic acid)-*sn*-glycero-3-phosphocholine, respectively. Possible structures of the oxidation products were certified by comparing their ESI-MS/MS spectra with the previous reports and they were listed in Table 5.1.^{168,170} However, after 12 to 24 hours' incubation time (Figure 5.1C-E), the

peak areas of these long-chain products decrease and we observed the appearance of broad peaks of the sodium adducts of short-chain oxidation products including 1-palmitoyl-2-(8-oxo-octanoic acid)-*sn*-glycero-3-phosphocholine ($m/z = 658$), 1-palmitoyl-2-(9-oxo-nonanoic acid)-*sn*-glycero-3-phosphocholine ($m/z = 672$), 1-palmitoyl-2-(nonandioic acid)-*sn*-glycero-3-phosphocholine ($m/z = 688$), 1-palmitoyl-2-(9-keto-12-oxo-10-dodecenoic acid)-*sn*-glycero-3-phosphocholine ($m/z = 726$), 1-palmitoyl-2-(9-keto-10-dodecendioic acid)-*sn*-glycero-3-phosphocholine ($m/z = 742$) and 1-palmitoyl-2-(9-hydroxy-10-dodecendioic acid)-*sn*-glycero-3-phosphocholine ($m/z = 744$), etc, which were also found in previous lipid peroxidation research (also listed in Table 5.1).¹⁷¹ These short-chain products are more hydrophilic than the long-chain ones and eluted out of the LC column faster in a more aqueous solvent mixture, which might explain why they present lower ionization efficiency. These phenomena were also observed in previous reports by other groups although the detailed mechanism remains unclear.^{51,168}

Table 5.1. Oxidation products and their possible structures

Oxidation Products	Possible Structures of Oxidation Products
1-palmitoyl-2-(keto-octadecadienoic acid)- <i>sn</i> -glycero-3-phosphocholine	
1-palmitoyl-2-(hydroxy-octadecadienoic acid)- <i>sn</i> -glycero-3-phosphocholine	
1-palmitoyl-2-(hydroperoxide-octadecadienoic acid)- <i>sn</i> -glycero-3-phosphocholine	
1-palmitoyl-2-(8-oxo-octanoic acid)- <i>sn</i> -glycero-3-phosphocholine	
1-palmitoyl-2-(9-oxo-nonanoic acid)- <i>sn</i> -glycero-3-phosphocholine	
1-palmitoyl-2-(nonandioic acid)- <i>sn</i> -glycero-3-phosphocholine	
1-palmitoyl-2-(9-keto-12-oxo-10-dodecenoic acid)- <i>sn</i> -glycero-3-phosphocholine	
1-palmitoyl-2-(9-keto-10-dodecendioic acid)- <i>sn</i> -glycero-3-phosphocholine	
1-palmitoyl-2-(9-hydroxy-10-dodecendioic acid)- <i>sn</i> -glycero-3-phosphocholine	

To validate that free Cu^{2+} was able to catalyze the oxidation in general and the oxidation of PLiPC occurred via a radical-related mechanism, two control experiments were performed, as shown in Figure 5.3. When EDTA instead of Cu^{2+} was added into the vesicle solution and incubated for 24 hours, the detected oxidation level was low ($< 10\%$) in Figure 5.3A. The addition of EDTA chelated the unavoidable trace amounts of Cu^{2+} in contaminants found in buffer solutions and experiment apparatus (Chapter III) and could significantly inhibit the oxidation reactions. To further study the mechanism of autoxidation, a free radical scavenger was tested as an additive in this system. Herein butylated-hydroxytoluene (BHT) was applied as the radical-capturing agent.¹⁷² Compared with the results obtained from the samples without BHT in Figure 5.1E, there was little oxidation found in Figure 5.3B, which implied that the oxidation was through a free radical-mediated pathway. With radicals being scavenged by BHT, the autoxidation of polyunsaturated lipids are inhibited, even in the presence of copper ions.

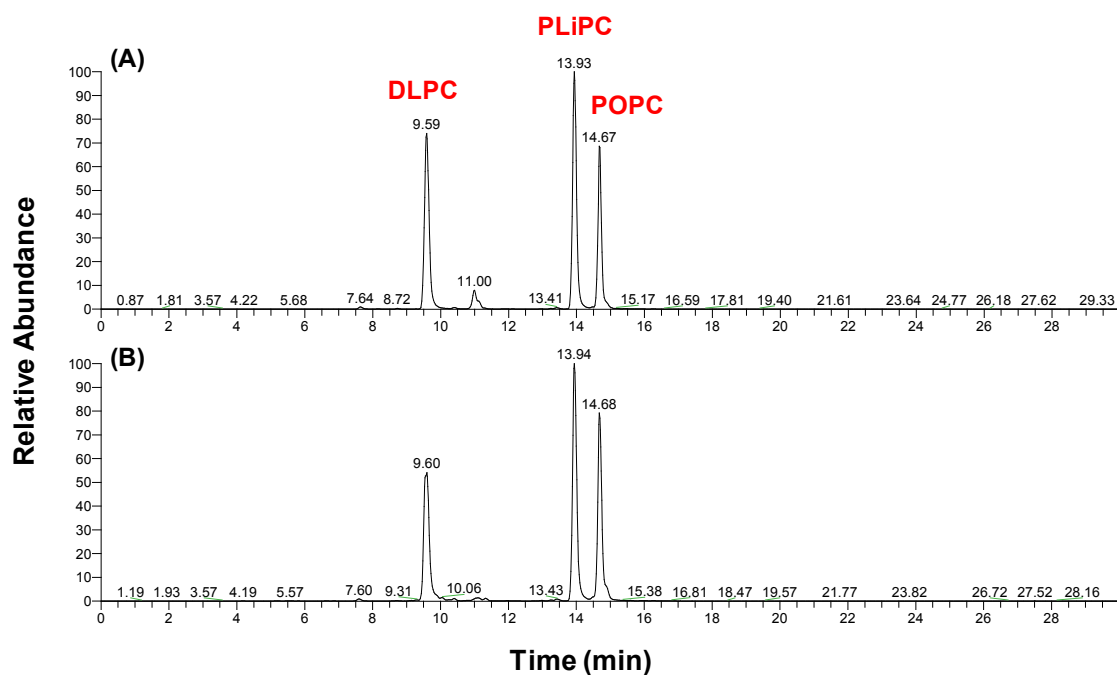


Figure 5.3. The RIC of the vesicles containing 70 mol % DLPC and 30 mol % PLiPC incubated for 24 hours without Cu^{2+} or with Cu^{2+} and BHT. The vesicles were made at 1 mM total lipid concentration in 10 mM ammonium acetate buffer at pH = 7.4. In (A), 75 μM EDTA was added into the vesicle solution while in (B), 75 μM CuCl_2 and 75 μM BHT were added into the vesicle solution simultaneously. These two samples were both incubated in 37 °C for 24 hours.

Cu^{2+} -PS Binding Inhibits Cu^{2+} -catalyzed PLiPC Oxidation

In a next set of experiments, PS lipids were introduced into the vesicles to explore their effects on Cu^{2+} -promoted PLiPC autoxidation. Vesicles containing 40 mol % DLPC, 30 mol % DLPS and 30 mol % PLiPC were compared with the ones with 70 mol % DLPC and 30 mol % PLiPC after incubating with the same Cu^{2+} concentrations for different times. The LC-MS of each condition was acquired and the oxidation percentages of PLiPC were calculated and plotted in Figure 5.4 as a function of incubation time. As shown in Figure 5.4, the oxidation extent of PLiPC without PS

significantly increased to about 85% when the incubation time was extended to 24 hours. However, in the presence of 30 mol % DLPS in the vesicles, the PLiPC oxidation remarkably slowed down while only 20% of the PLiPC got oxidized after incubation with Cu^{2+} for the same amount of time. This difference in oxidation rate was more obvious in the right panel of Figure 5.3, where the LC peaks of our target lipid PLiPC and the internal standard lipid POPC were compared for two kinds of vesicles after different incubation time. For the vesicles without PS, the PLiPC peaks shrink rapidly with time going, which is far more pronounced than the PS-containing vesicles. These results indicate that the Cu^{2+} -PS binding might have inhibitory effects on Cu^{2+} catalysis of autoxidation of the surrounding unsaturated lipids. On one hand, the Cu^{2+} -binding of PS headgroups might shift the redox potential of $\text{Cu}^{2+}/\text{Cu}^+$.¹⁷³ After the carboxyl and amino groups from two PS lipids chelate Cu^{2+} and form a stable square-planar complex, it is more difficult to reduce Cu^{2+} to Cu^+ as the ligand field-stabilized Cu^{2+} might no longer be an active electron acceptor in the redox cycling.¹⁷³ On the other hand, when Cu^{2+} ions were localized at the headgroup region of lipid bilayers, they were restricted from diffusing in solution or membranes so that the direct activation of the allylic hydrogen of the double bond was less likely to occur. Therefore, the oxidative damage of surrounding unsaturated lipids was attenuated.

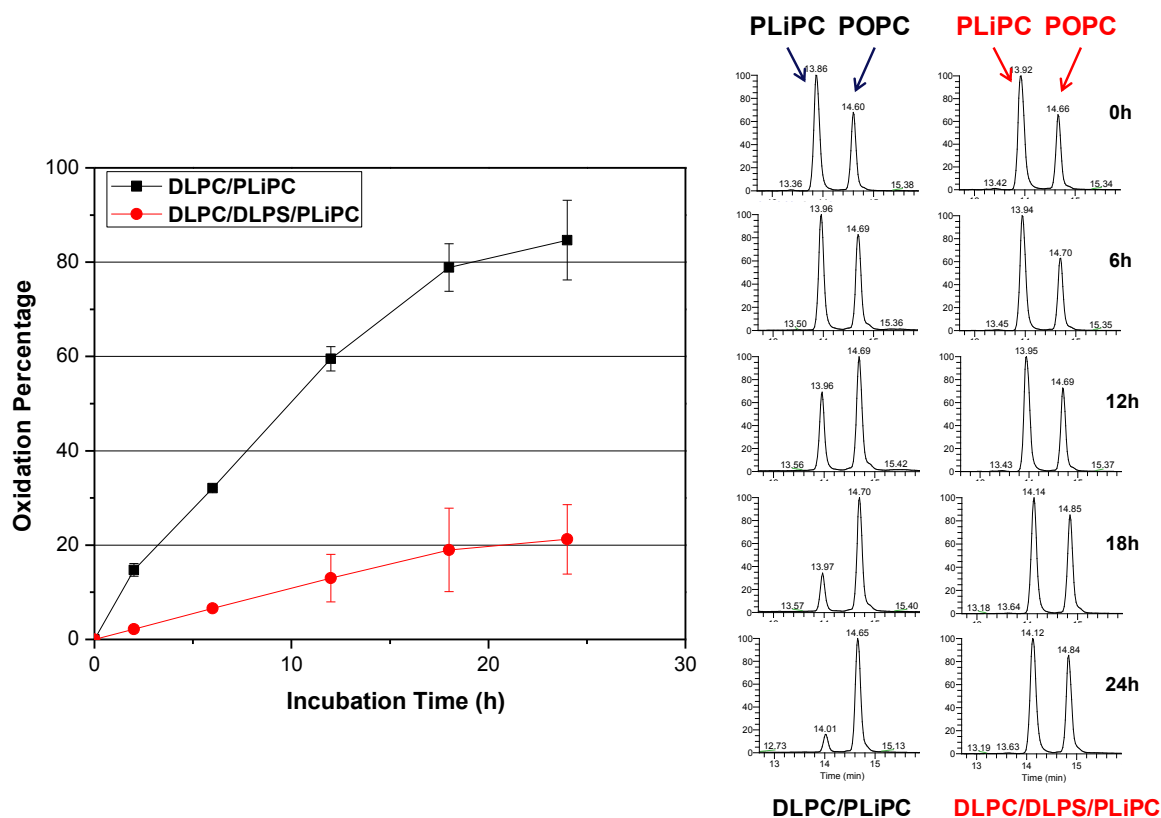


Figure 5.4. A comparison of the oxidation percentages of vesicles without or with PS over time. The vesicles noted as “DLPC/PLiPC” consist of 70 mol % DLPC and 30 mol % PLiPC while the vesicles labeled as “DLPC/DLPS/PLiPC” contain 40 mol % DLPC, 30 mol % DLPS and 30 mol % PLiPC. They were both made at 1 mM total lipid concentration in 10 mM ammonium acetate buffer at pH = 7.4. After incubation with 75 μ M CuCl_2 for different time periods, the samples were diluted in methanol by ten times and 10 μ M POPC was added as an internal standard before the LC-MS was applied. In the left panel, the oxidation percentage was plotted as a function of incubation time. The error bars represent the standard deviation of multiple measurements. In the right panel, the LC peaks of PLiPC (peak on the left) and the internal standard POPC (peak on the right) from the two different vesicle solutions were shown side by side to give a clearer presentation for comparison.

Comparisons of PS with Other Lipids

The interactions between anionic lipids and transition metal ions have been explored before for their effects on the lipid peroxidation.^{39,174} It was found that the negatively-charged lipids such as PS and PA effectively inhibited lipid peroxidation induced by iron or copper ions, which was ascribed to their binding of free iron/copper ions. However, there were no comparisons between different anionic lipids and the oxidation levels reported in these papers were generally measured by UV spectra, which was not the optimal technique to quantify all the generated oxidation products. Moreover, although the main focus of these reports are about the lipid peroxidation induced by 2,2'-azobis(2-amidinopropane) dihydrochloride (AAPH) or ascorbic acid (AA), the autoxidation process cannot be ruled out and it is hard to differentiate these complicated oxidation pathways. Therefore, questions and doubts still remain about the inhibitory effect of the anionic lipids on the lipid oxidation. Our discovery of the specific binding between PS and Cu^{2+} instead of an electrostatic attraction encouraged us to believe that PS might behave differently when compared with the other anionic lipids.

Here a variety of phospholipids were mixed with PLiPC in vesicles to compare their efficacy against oxidation damage. The vesicle containing 70 mol % DLPC and 30 mol % PLiPC incubated with Cu^{2+} for 24 hours served as a control, which was compared with the vesicles consisting of 40 mol % DLPC, 30 mol % PLiPC and 30 mol % DLPS, DLPG, DLPA or DLPE under the same conditions. A column graphic representation of the results as well as the structures of these lipids was shown in Figure 5.5. PS, PG and PA each carry one negative charge at physiological pH but PG and PA cannot

specifically bind Cu^{2+} with a high affinity as PS does.⁴⁵ As illustrated by Figure 5.5, the oxidation percentages for different anionic lipids were in the order of: $\text{PS} < \text{PA} < \text{PG}$, which means that PS has the largest inhibitory effect due to the highest binding affinity of Cu^{2+} . The difference between PA and PG might arise from the extra sterically hindered glycerol headgroup of PG that might block the Cu^{2+} -phosphate group interaction. This is similar to their electrostatic interaction behaviors with other cations.¹⁷⁵ As for PE, despite its zwitterionic property at physiological pH, it may bind metal ions through the deprotonated amine group, but only at alkaline environment. Therefore, under the neutral conditions used in the experiments, the addition of PE here showed little inhibitory effects on the PLiPC oxidations (Figure 5.5).

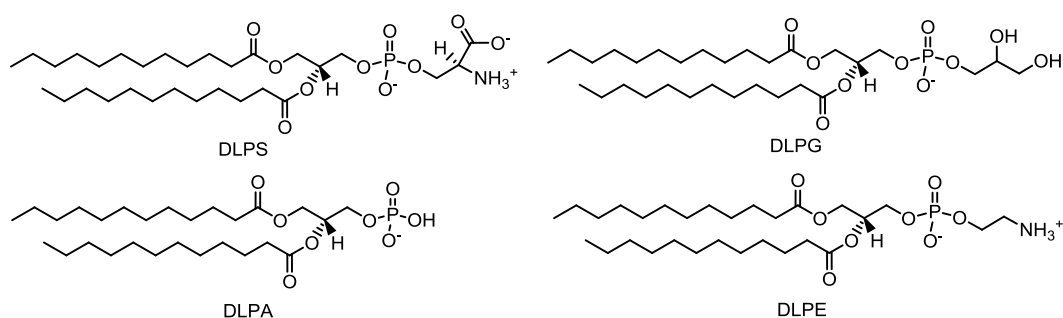
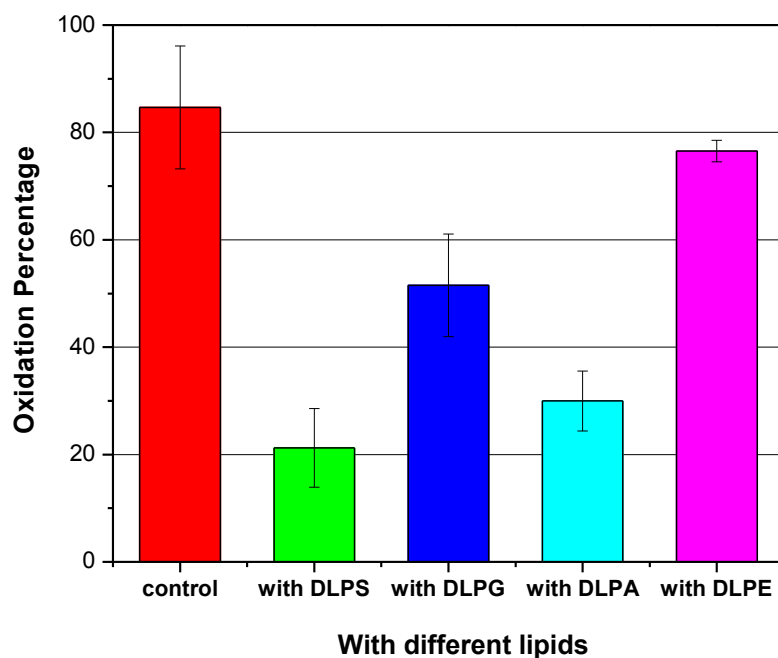


Figure 5.5. A graphic summary showing the comparison of oxidation percentages of PLiPC mixed with different kinds of lipids. The control samples are vesicles consisting of 70 mol % DLPC and 30 mol % PLiPC while the other vesicles contain 40 mol % DLPC, 30 mol % PLiPC and 30 mol % DLPS, DLPG, DLPA or DLPE. They were both made at 1 mM total lipid concentration in 10 mM ammonium acetate buffer at pH = 7.4. After incubation with 75 μ M CuCl_2 at 37 $^\circ\text{C}$ for 24 hours, the samples were diluted in methanol by ten times and 10 μ M POPC was added as an internal standard before the LC-MS was applied. The oxidation percentage of each kind of vesicle was plotted and the error bars represent the standard deviation of multiple measurements. The structures of DLPS, DLPG, DLPA and DLPE were shown at the bottom.

Comparisons of PS with Other Cu²⁺-Binding Reagents

Cu²⁺ is generally known to form complexes with amino acids such as glycine and alanine with an apparent dissociation constant of 10⁻⁸ M.¹⁷⁶ Another common Cu²⁺-binding ligand in metalloproteins is histidine. In neurodegenerative disorders such as Alzheimer's disease, Cu²⁺ has been found to tightly bind A β peptides by three histidine residues and N-terminal, which promotes the A β aggregation.^{36,102} In the last set of experiments, some of these physiological binding reagents were employed to investigate their effects on lipid autoxidation. As shown in Figure 5.6, glycine and histidine were added into the vesicles to compare with the vesicles containing PS. After incubation with the same Cu²⁺ concentration for 24 hours, the oxidation percentage of PLiPC in the presence of histidine was found to be lower than the samples containing glycine, although both of them show less inhibitory effects than PS lipids (Figure 5.6). Cu²⁺ has a higher binding affinity for histidine than glycine owing to the imidazole nitrogen at the side chain of histidine as an extra coordinating group besides the amino and carboxyl group. This chelating effect yields an apparent dissociation constant of 10⁻¹⁰ M for Cu²⁺-histidine binding.^{176,177} The binding affinity between Cu²⁺ and the SLBs containing 20 mol % PS, has been measured to be around pM scale (Chapter III). It was expected that the lipid bilayers containing high PS densities should have a higher binding affinity for Cu²⁺ relative to glycine or histidine. Moreover, compared with PS anchored on the surface of the vesicles, the amino acid-metal ion complexes in solution are more accessible because of their free diffusion, which might also promote the Cu²⁺ catalysis of the lipid autoxidation process.

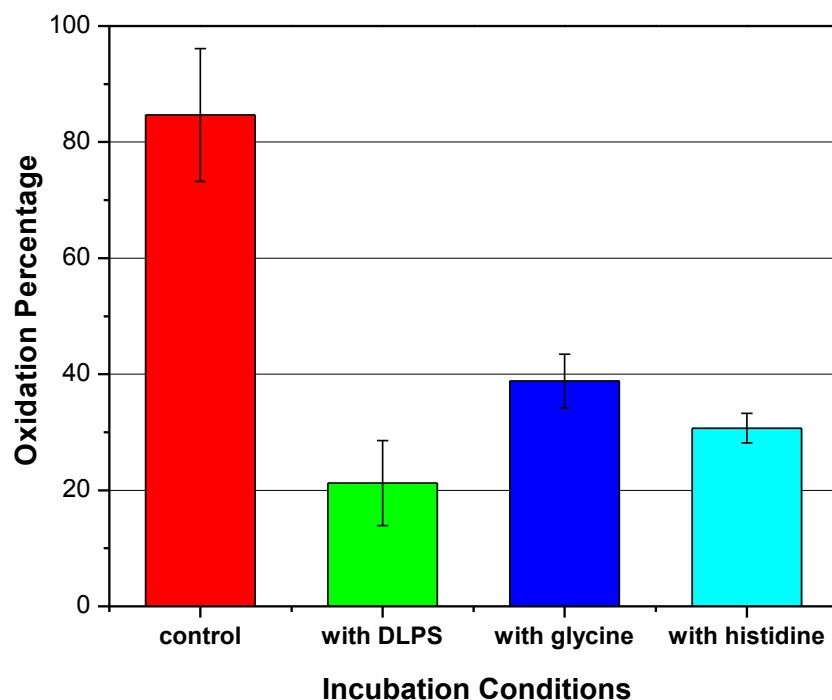


Figure 5.6. A graphic summary showing the comparison of oxidation percentages of PLiPC when different Cu^{2+} -binding reagents were added. The “control” samples are vesicles consisting of 70 mol % DLPC and 30 mol % PLiPC while the samples labeled as “with DLPS” are vesicles contain 40 mol % DLPC, 30 mol % PLiPC and 30 mol % DLPS. The samples labeled as “with glycine” and “with histidine” are vesicles of 70 mol % DLPC and 30 mol % PLiPC while 300 μM glycine or histidine was added into the samples, respectively. These vesicles were both made at 1 mM total lipid concentration in 10 mM ammonium acetate buffer at $\text{pH} = 7.4$. After incubation with 75 μM CuCl_2 at 37 $^\circ\text{C}$ for 24 hours, they were diluted in methanol by ten times and 10 μM POPC was added as an internal standard before the LC-MS was applied. The oxidation percentage of each kind of vesicle was plotted and the error bars represent the standard deviation of multiple measurements.

The mechanism of the lipid autoxidation is complicated and still unclear although they were discovered and studied in previous reports.^{157,158,160,178} The original induction might involve a radical formation by hydrogen abstraction of the bis-allylic position on the polyunsaturated acyl chain of lipids. The heavy metal and the ROS impurity in buffer solutions and UV light irradiation might generate free radicals and act as the initiators

for radical-mediated lipid oxidation while the propagation of the chain reaction can be catalyzed by transition metal ions like copper. Since PS in lipid membranes has a surface accumulation effect for Cu^{2+} and can bind Cu^{2+} tightly, it may serve as the transition metal ion reservoir on cell surface and help protecting against the lipid autoxidation and maintaining the membrane integrity. Things might be different when the double bonds are on PS lipids themselves which could change the oxidation rates and pathways. Besides, in cell membranes, the existence of other lipids such as sphingolipids, cholesterol and ganglioside may also affect the interactions of PS and metal ions by changing the fluidity of the membranes, creating lipid rafts and causing the redistribution of PS on membranes,^{179,180} which will be studied in the future.

CHAPTER VI

CONCLUSIONS

We developed a novel fluorescence quenching assay to investigate the interactions between Cu^{2+} and PS lipids in cell membranes. This assay was built upon lipid bilayer-coated microfluidic platforms, which could be combined with fluorescence microscopy and other spectroscopic techniques to detect the association/dissociation of Cu^{2+} and PS on SLBs. PS lipids were found to bind Cu^{2+} and the resulting $\text{Cu}(\text{PS})_2$ complex was able to quench a broad spectrum of lipid-bound fluorophores in a reversible and pH-dependent fashion. At acidic pH values, the fluorophores are almost completely unquenched while at basic pH, up to 90% quenching can be achieved.

This quenching assay can be used to determine the equilibrium dissociation constants between Cu^{2+} and SLBs containing different PS concentrations, since the PS concentration on cell surfaces varies during different biological events such as the cell apoptosis and blood clotting. Our results showed that with an increasing PS surface density from 1.0 to 20 mol %, the apparent binding affinity of PS-containing SLBs to Cu^{2+} was enhanced significantly by about five orders of magnitude. This binding enhancement can be attributed to the accumulated large quantities of Cu^{2+} ions in the double layer of the negatively-charged bilayer surface as well as a switch between monovalent and divalent binding. When Cu^{2+} is chelated by the deprotonated amine groups and carboxyl groups of two PS molecules, the resulting $\text{Cu}(\text{PS})_2$ complex preserves the negatively-charged character on membranes, thus causing a remarkably

high concentration of Cu^{2+} close to the surface relative to the bulk solution. These results might provide insights into the interactions between transition metal ions and PS lipids at specific physiological or pathological conditions. For example, when PS flips from the inner to the outer leaflet of plasma membranes during cell apoptosis or other biological events, they will be brought into direct contact with a Cu^{2+} -rich environment. With a significantly enhanced apparent binding affinity to Cu^{2+} at high PS densities, PS- Cu^{2+} complexes may get involved into apoptotic process and the membrane oxidative stress or affect the membrane binding of PS-relevant proteins.

In addition, this fluorescent-based detection method was further employed to explore the Cu^{2+} -mediated interactions between proteins/peptides and membrane. It was combined with mass spectrometry technique to provide a label-free way to mimic how $\text{A}\beta$ peptides approach to cell membranes to attain metal ions in neural systems. Our fluorescence and mass spectra results correspond well with each other to demonstrate the $\text{A}\beta$ - Cu^{2+} -PS interactions on lipid bilayers where Cu^{2+} could be grabbed from PS-containing membranes by $\text{A}\beta$ peptides. It indicates that plasma membranes with exposed PS probably provide Cu^{2+} as stimulates or medium for the $\text{A}\beta$ oligomerization on cell surfaces, especially when copper is deficient in AD patients' brain systems. More research about the $\text{A}\beta$ insertion into the membranes and the related oxidation damage will be studied in the future. Besides, this multi-technique label-free method described here could be extended to the analysis of more membrane-related proteins or peptides to obtain useful biological information about the membrane-ion-protein/peptide interactions.

Finally, LC-MS was applied to study how PS affects Cu^{2+} -catalyzed lipid autoxidation in vesicles. The oxidation percentage of PC lipids with double bonds was inhibited when PS was present in the vesicles and this inhibitory effect was higher than the other anionic lipids and the amino acids which can also bind Cu^{2+} . In this way, PS might be an antioxidant candidate for protecting surrounding unsaturated lipids against autoxidation

REFERENCES

- (1) Singer, S. J.; Nicolson, G. L. *Science* **1972**, *175*, 720-&.
- (2) Leventis, P. A.; Grinstein, S. *Annu. Rev. Biophys.* **2010**, *39*, 407-427.
- (3) Jayaraman, N. *Chem. Soc. Rev.* **2009**, *38*, 3463-3483.
- (4) Rihova, B. *Adv. Drug Deliver Rev.* **1998**, *29*, 273-289.
- (5) Holden, M. A.; Cremer, P. S. *Annu. Rev. Phys. Chem.* **2005**, *56*, 369-387.
- (6) Castellana, E. T.; Cremer, P. S. *Surf. Sci. Rep.* **2006**, *61*, 429-444.
- (7) Groves, J. T.; Boxer, S. G. *Acc. Chem. Res.* **2002**, *35*, 149-157.
- (8) Sackmann, E. *Science* **1996**, *271*, 43-48.
- (9) Shi, J.; Yang, T.; Kataoka, S.; Zhang, Y.; Diaz, A. J.; Cremer, P. S. *J. Am. Chem. Soc.* **2007**, *129*, 5954-5961.
- (10) Daniel, S.; Diaz, A. J.; Martinez, K. M.; Bench, B. J.; Albertorio, F.; Cremer, P. S. *J. Am. Chem. Soc.* **2007**, *129*, 8072-8073.
- (11) Jonsson, P.; Beech, J. P.; Tegenfeldt, J. O.; Hook, F. *J. Am. Chem. Soc.* **2009**, *131*, 5294-5297.
- (12) Richter, R. P.; Brisson, A. R. *Biophys. J.* **2005**, *88*, 3422-3433.
- (13) Tamm, L. K.; McConnell, H. M. *Biophys. J.* **1985**, *47*, 105-113.
- (14) Sharom, F. J.; Grant, C. W. *Biochim. Biophys. Acta.* **1978**, *507*, 280-293.
- (15) Groves, J. T.; Boxer, S. G.; McConnel, H. M. *P. Natl. Acad. Sci. USA* **1997**, *94*, 13390-13395.
- (16) Plant, A. L. *Langmuir* **1993**, *9*, 2764-2767.

- (17) Cho, N. J.; Frank, C. W.; Kasemo, B.; Hook, F. *Nat. Protoc.* **2010**, *5*, 1096-1106.
- (18) Brian, A. A.; McConnell, H. M. *P. Natl. Acad. Sci.-Biol.* **1984**, *81*, 6159-6163.
- (19) Kalb, E.; Frey, S.; Tamm, L. K. *Biochim. Biophys. Acta.* **1992**, *1103*, 307-316.
- (20) Gordesky, S. E.; Marinett, G. *Biochem. Biophys. Res. Commun.* **1973**, *50*, 1027-1031.
- (21) Li, M. O.; Sarkisian, M. R.; Mehal, W. Z.; Rakic, P.; Flavell, R. A. *Science* **2003**, *302*, 1560-1563.
- (22) Zwaal, R. F. A.; Comfurius, P.; Bevers, E. M. *Bba-Rev. Biomembranes* **1998**, *1376*, 433-453.
- (23) Huang, B. X.; Akbar, M.; Kevala, K.; Kim, H. Y. *J. Cell. Biol.* **2011**, *192*, 979-992.
- (24) Bratton, D. L.; Fadok, V. A.; Richter, D. A.; Kailey, J. M.; Guthrie, L. A.; Henson, P. M. *J. Biol. Chem.* **1997**, *272*, 26159-26165.
- (25) Hauser, H.; Darke, A.; Phillips, M. C. *Eur. J. Biochem.* **1976**, *62*, 335-344.
- (26) Shirane, K.; Kuriyama, S.; Tokimoto, T. *Biochim. Biophys. Acta.* **1984**, *769*, 596-600.
- (27) Newton, C. *Biophys. J.* **1979**, *25*, A179-A179.
- (28) Newton, C.; Pangborn, W.; Nir, S.; Papahadjopoulos, D. *Biochim. Biophys. Acta.* **1978**, *506*, 281-287.

- (29) Hendrick, H.; Fulling, J. *Biochemistry-U.S.* **1965**, *4*, 1599-1605.
- (30) Mclaughlin, S.; Mulrine, N.; Gresalfi, T.; Vaio, G.; Mclaughlin, A. *J. Gen. Physiol.* **1981**, *77*, 445-473.
- (31) Repetto, M. G.; Ferrarotti, N. F.; Boveris, A. *Arch. Toxicol.* **2010**, *84*, 255-262.
- (32) Que, E. L.; Domaille, D. W.; Chang, C. J. *Chem. Rev.* **2008**, *108*, 1517-1549.
- (33) Gaggelli, E.; Kozlowski, H.; Valensin, D.; Valensin, G. *Chem. Rev.* **2006**, *106*, 1995-2044.
- (34) Bush, A. I. *Trends Neurosci.* **2003**, *26*, 207-214.
- (35) Makinen, W. B.; Pearlmutter, A. F.; Stuehr, J. E. *J. Am. Chem. Soc.* **1969**, *91*, 4083-&.
- (36) Smith, D. P.; Smith, D. G.; Curtain, C. C.; Boas, J. F.; Pilbrow, J. R.; Ciccotosto, G. D.; Lau, T. L.; Tew, D. J.; Perez, K.; Wade, J. D.; Bush, A. I.; Drew, S. C.; Separovic, F.; Masters, C. L.; Cappai, R.; Barnham, K. J. *J. Biol. Chem.* **2006**, *281*, 15145-15154.
- (37) Lavanant, H.; Hoppilliard, Y. *Eur. Mass Spectrom.* **1999**, *5*, 41-50.
- (38) Hong, L. A.; Carducci, T. M.; Bush, W. D.; Dudzik, C. G.; Millhauser, G. L.; Simon, J. D. *J. Phys. Chem. B* **2010**, *114*, 11261-11271.
- (39) Gal, S.; Lichtenberg, D.; Bor, A.; Pinchuk, I. *Chem. Phys. Lipids* **2007**, *150*, 186-203.

- (40) Balasubramanian, K.; Mirnikjoo, B.; Schroit, A. J. *J. Biol. Chem.* **2007**, *282*, 18357-18364.
- (41) Mammen, M.; Choi, S. K.; Whitesides, G. M. *Angew. Chem. Int. Ed.* **1998**, *37*, 2755-2794.
- (42) Yang, T.; Jung, S.-y.; Mao, H.; Cremer, P. S. *Anal. Chem.* **2001**, *73*, 165-169.
- (43) Holden, M. A.; Cremer, P. S. *Biophys. J.* **2003**, *84*, 168a-168a.
- (44) Cremer, P. S.; Boxer, S. G. *J. Phys. Chem. B* **1999**, *103*, 2554-2559.
- (45) Monson, C. F.; Cong, X.; Robison, A. D.; Pace, H. P.; Liu, C. M.; Poyton, M. F.; Cremer, P. S. *J. Am. Chem. Soc.* **2012**, *134*, 7773-7779.
- (46) Richmond, G. L. *Chem. Rev.* **2002**, *102*, 2693-2724.
- (47) Shen, Y. R. *Nature* **1989**, *337*, 519-525.
- (48) Kim, J.; Kim, G.; Cremer, P. S. *Langmuir* **2001**, *17*, 7255-7260.
- (49) Fenn, J. B.; Mann, M.; Meng, C. K.; Wong, S. F.; Whitehouse, C. M. *Science* **1989**, *246*, 64-71.
- (50) Hofstadler, S. A.; Sannes-Lowery, K. A. *Nat. Rev. Drug Discov.* **2006**, *5*, 585-595.
- (51) Brouwers, J. F. *Bba-Mol. Cell Biol.* **2011**, *1811*, 763-775.
- (52) Zambrano, F.; Fleischer, S.; Fleischer, B. *Bba - Lipids and Lipid Metabolism* **1975**, *380*, 357-369.
- (53) Tyurina, Y. Y.; Shvedova, A. A.; Kawai, K.; Tyurin, V. A.; Kommineni, C.; Quinn, P. J.; Schor, N. F.; Fabisiak, J. P.; Kagan, V. E. *Toxicology* **2000**, *148*, 93-101.

- (54) Majd, S.; Estes, D. J.; Mayer, M. *Calcium Binding Proteins* **2006**, *1*, 26-29.
- (55) Bailey, R. W.; Nguyen, T.; Robertson, L.; Gibbons, E.; Nelson, J.; Christensen, R. E.; Bell, J. P.; Judd, A. M.; Bell, J. D. *Biophys. J.* **2009**, *96*, 2709-2718.
- (56) Chaurio, R. A.; Janko, C.; Munoz, L. E.; Frey, B.; Herrmann, M.; Gaipf, U. S. *Molecules* **2009**, *14*, 4892-4914.
- (57) Lentz, B. *Prog. Lipid Res.* **2003**, *42*, 423-438.
- (58) Papahadjopoulos, D. *Biochim. Biophys. Acta.* **1968**, *163*, 240-254.
- (59) Shirane, K.; Kuriyama, S.; Tokimoto, T. *Biochim. Biophys. Acta.* **1984**, *769*, 596-600.
- (60) Feigenson, G. W. *Biochemistry* **1986**, *25*, 5819-5825.
- (61) Tokutomi, S.; Lew, R.; Ohnishi, S.-I. *Biochim. Biophys. Acta.* **1981**, *643*, 276-282.
- (62) Sinn, C.; Antonietti, M.; Dimova, R. *Colloids Surf. A: Physicochemical and Engineering Aspects* **2006**, *282-283*, 410-419.
- (63) Majd, S.; Mayer, M. *Angew. Chem. Int. Ed.* **2005**, *44*, 6697-6700.
- (64) Linder, M.; Hazegh-Azam, M. *Am. J. Clin. Nutr.* **1996**, *63*, 797S-811S.
- (65) Elam, J. S.; Thomas, S. T.; Holloway, S. P.; Taylor, A. B.; Hart, P. J. *Advances in Protein Chemistry*, Academic Press: **2002**, *60*, 151-219.
- (66) Rae, T. D.; Schmidt, P. J.; Pufahl, R. A.; Culotta, V. C.; O'Halloran, T. V. *Science* **1999**, *284*, 805-808.
- (67) O'Halloran, T. V.; Culotta, V. C. *J. Biol. Chem.* **2000**, *275*, 25057-25060.

- (68) Mandinov, L.; Mandinova, A.; Kyurkchiev, S.; Kyurkchiev, D.; Kehayov, I.; Kolev, V.; Soldi, R.; Bagala, C.; de Muinck, E. D.; Lindner, V.; Post, M. J.; Simons, M.; Bellum, S.; Prudovsky, I.; Marciag, T. *P. Nati. Acad. Sci.* **2003**, *100*, 6700-6705.
- (69) Sigurdsson, E. M.; Brown, D. R.; Alim, M. A.; Scholtzova, H.; Carp, R.; Meeker, H. C.; Prelli, F.; Frangione, B.; Wisniewski, T. *J. Biol. Chem.* **2003**, *278*, 46199-46202.
- (70) Tardito, S.; Bassanetti, I.; Bignardi, C.; Elviri, L.; Tegoni, M.; Mucchino, C.; Bussolati, O.; Franchi-Gazzola, R.; Marchiò, L. *J. Am. Chem. Soc.* **2011**, 110331105304037.
- (71) Hope, M. J.; Bally, M. B.; Webb, G.; Cullis, P. R. *Biochim. Biophys. Acta. - Biomembranes* **1985**, *812*, 55-65.
- (72) Mayer, L. D.; Hope, M. J.; Cullis, P. R. *Biochim. Biophys. Acta. - Biomembranes* **1986**, *858*, 161-168.
- (73) Brian, A. A.; McConnell, H. M. *P. Nati. Acad. Sci.* **1984**, *81*, 6159-6163.
- (74) Groves, J. T.; Ulman, N.; Cremer, P. S.; Boxer, S. G. *Langmuir* **1998**, *14*, 3347-3350.
- (75) Cremer, P. S.; Groves, J. T.; Kung, L. A.; Boxer, S. G. *Langmuir* **1999**, *15*, 3893-3896.
- (76) Monson, C. F.; Pace, H. P.; Liu, C.; Cremer, P. S. *Anal. Chem.* **2011**, *83*, 2090-2096.
- (77) Jung, H.; Robison, A. D.; Cremer, P. S. *J. Am. Chem. Soc.* **2009**, *131*, 1006-1014.

- (78) Shriver, D.; Attkins, P. *Inorganic Chemistry*; 3rd Edition ed.; W. H. Freeman and Company: New York, 1999.
- (79) Crane, J. M.; Tamm, L. K. *Biophys. J.* **2004**, *86*, 2965-2979.
- (80) Lakowicz, J. R. *Principles of Fluorescence Spectroscopy*; 3rd Edition ed.; Springer Science+Business Media: New York, 2006.
- (81) Job, P. *Ann. Chim. France* **1928**, *9*, 113-203.
- (82) Gal, S.; Pinchuk, I.; Lichtenberg, D. *Chem. Phys. Lipids* **2003**, *126*, 95-110.
- (83) Jastrzab, R.; Lomozik, L. *J. Coord. Chem.* **2009**, *62*, 710-720.
- (84) Várnagy, K.; Garriba, E.; Sanna, D.; Sóvágó, I.; Micera, G. *Polyhedron* **2005**, *24*, 799-806.
- (85) Albro, P. W.; Corbett, J. T.; Schroeder, J. L. *J. Inorg. Biochem.* **1986**, *27*, 191-203.
- (86) Cross, J.; Leslie, A.; Smith, H. *J. Forensic Sci.* **1976**, *16*, 311-315.
- (87) Yorek, M. A. *Phospholipids Handbook*; Cevc, G., Ed.; Marcel Dekker, Inc.: New York, **1993**, 745-775.
- (88) Hauser, H.; Darke, A.; Phillips, M. C. *Euro. J. Biochem.* **1976**, *62*, 335-344.
- (89) Heldin, C. H. *Cell* **1995**, *80*, 213-223.
- (90) Yang, T. L.; Baryshnikova, O. K.; Mao, H. B.; Holden, M. A.; Cremer, P. *S. J. Am. Chem. Soc.* **2003**, *125*, 4779-4784.

- (91) Leckband, D. E.; Kuhl, T.; Wang, H. K.; Herron, J.; Muller, W.; Ringsdorf, H. *Biochemistry-Us* **1995**, *34*, 11467-11478.
- (92) Jung, H.; Robison, A. D.; Cremer, P. S. *J. Struct. Biol.* **2009**, *168*, 90-94.
- (93) Pisarchick, M. L.; Thompson, N. L. *Biophys. J.* **1990**, *58*, 1235-1249.
- (94) Kalb, E.; Engel, J.; Tamm, L. K. *Biochemistry-Us* **1990**, *29*, 1607-1613.
- (95) Israelachvili, J. N. *Intermolecular and Surface Forces*, 3rd Edition; **2011**, 1-674.
- (96) Chen, X.; Yang, T.; Kataoka, S.; Cremer, P. S. *J. Am. Chem. Soc.* **2007**, *129*, 12272-12279.
- (97) Adamson, A. W.; Gast, A. P. *Physical Chemistry of Surfaces*; 6th ed.; Wiley: New York, 1997.
- (98) Lakowicz, J. R.; *Principles of Fluorescence Spectroscopy*; 3rd Edition ed.; Springer Science+Business Media: New York: 2006.
- (99) Matthews, J. C. *Fundamentals of receptor, enzyme, and transport kinetics*; CRC Press: Boca Raton, 1993.
- (100) Tamm, L. K.; Bartoldus, I. *Biochemistry-Us* **1988**, *27*, 7453-7458.
- (101) Zhang, L.; Koay, M.; Mahert, M. J.; Xiao, Z.; Wedd, A. G. *J. Am. Chem. Soc.* **2006**, *128*, 5834-5850.
- (102) Atwood, C. S.; Scarpa, R. C.; Huang, X. D.; Moir, R. D.; Jones, W. D.; Fairlie, D. P.; Tanzi, R. E.; Bush, A. I. *J. Neurochem.* **2000**, *75*, 1219-1233.
- (103) Perrin, D. D.; Dempsey, B. *Buffers for pH and metal ion control*; Chapman and Hall; Wiley: London, New York, 1974.

- (104) Sarell, C. J.; Syme, C. D.; Rigby, S. E. J.; Viles, J. H. *Biochemistry-US* **2009**, *48*, 4388-4402.
- (105) Dawson, R. M. C. *Data for biochemical research*; 3rd ed.; Clarendon Press: Oxford, 1986.
- (106) Anderegg, G. *Pure Appl. Chem.* **1982**, *54*, 2693-2758.
- (107) Motekaitis, R. J.; Martell, A. E. *J. Coord. Chem.* **1994**, *31*, 67-78.
- (108) Pedersen, U. R.; Leidy, C.; Westh, P.; Peters, G. H. *Bba-Biomembranes* **2006**, *1758*, 573-582.
- (109) Bockmann, R. A.; Grubmuller, H. *Angew. Chem. Int. Ed.* **2004**, *43*, 1021-1024.
- (110) Shen, Y. R.; Ostroverkhov, V. *Chem. Rev.* **2006**, *106*, 1140-1154.
- (111) Schultz, Z. D.; Levin, I. W. *Annu. Rev. Anal. Chem.* **2011**, *4*, 343-366.
- (112) Chen, X. K.; Hua, W.; Huang, Z. S.; Allen, H. C. *J. Am. Chem. Soc.* **2010**, *132*, 11336-11342.
- (113) Covert, P. A.; Jena, K. C.; Hore, D. K. *J. Phys. Chem. Lett.* **2014**, *5*, 143-148.
- (114) Henderson, L. J. *Am. J. Physiol.* **1908**, *21*, 173-179.
- (115) Weast, R. C. *CRC handbook of chemistry and physics*; 1st Student ed.; CRC Press: Boca Raton, FL, 1988.
- (116) White, S. H.; King, G. I. *P. Natl. Acad. Sci. USA* **1985**, *82*, 6532-6536.
- (117) Poyton, M. F.; Cremer, P. S. *Anal. Chem.* **2013**, *85*, 10803-10811.

- (118) Monson, C. F.; Pace, H. P.; Liu, C. M.; Cremer, P. S. *Anal. Chem.* **2011**, *83*, 2090-2096.
- (119) Cunliffe, J. M.; Baryla, N. E.; Lucy, C. A. *Anal. Chem.* **2002**, *74*, 776-783.
- (120) Swairjo, M. A.; Concha, N. O.; Kaetzel, M. A.; Dedman, J. R.; Seaton, B. *A. Nat. Struct. Biol.* **1995**, *2*, 968-974.
- (121) Huang, M. D.; Rigby, A. C.; Morelli, X.; Grant, M. A.; Huang, G. Q.; Furie, B.; Seaton, B.; Furie, B. C. *Nat. Struct. Biol.* **2003**, *10*, 751-756.
- (122) Rauk, A. *Dalton T.* **2008**, 1273-1282.
- (123) Faller, P. *Chembiochem* **2009**, *10*, 2837-2845.
- (124) Hardy, J.; Selkoe, D. J. *Science* **2002**, *297*, 353-356.
- (125) Faller, P.; Hureau, C.; Berthoumieu, O. *Inorg. Chem.* **2013**, *52*, 12193-12206.
- (126) Walsh, D. M.; Klyubin, I.; Fadeeva, J. V.; Cullen, W. K.; Anwyl, R.; Wolfe, M. S.; Rowan, M. J.; Selkoe, D. J. *Nature* **2002**, *416*, 535-539.
- (127) Kepp, K. P. *Chem. Rev.* **2012**, *112*, 5193-5239.
- (128) Hung, Y. H.; Robb, E. L.; Volitakis, I.; Ho, M.; Evin, G.; Li, Q. X.; Culvenor, J. G.; Masters, C. L.; Cherny, R. A.; Bush, A. I. *J. Biol. Chem.* **2009**, *284*, 21899-21907.
- (129) Roberts, B. R.; Ryan, T. M.; Bush, A. I.; Masters, C. L.; Duce, J. A. *J. Neurochem.* **2012**, *120*, 149-166.
- (130) Lee, G.; Pollard, H. B.; Arispe, N. *Peptides* **2002**, *23*, 1249-1263.

- (131) Zhao, H. X.; Tuominen, E. K. J.; Kinnunen, P. K. J. *Biochemistry-US* **2004**, *43*, 10302-10307.
- (132) Arispe, N.; Diaz, J. C.; Simakova, O. *Bba-Biomembranes* **2007**, *1768*, 1952-1965.
- (133) Simakova, O.; Arispe, N. J. *J. Neurosci.* **2007**, *27*, 13719-13729.
- (134) Matsuzaki, K. *Bba-Biomembranes* **2007**, *1768*, 1935-1942.
- (135) Lau, T. L.; Ambroggio, E. E.; Tew, D. J.; Cappai, R.; Masters, C. L.; Fidelio, G. D.; Barnham, K. J.; Separovic, F. *J. Mol. Biol.* **2006**, *356*, 759-770.
- (136) Mattson, M. P. *Nat. Rev. Mol. Cell Bio.* **2000**, *1*, 120-129.
- (137) Cotman, C. W.; Anderson, A. J. *Mol. Neurobiol.* **1995**, *10*, 19-45.
- (138) Behl, C. *J. Neural. Transm.* **2000**, *107*, 1325-1344.
- (139) Bahadi, R.; Farrelly, P. V.; Kenna, B. L.; Curtain, C. C.; Masters, C. L.; Cappai, R.; Barnham, K. J.; Kourie, J. I. *Am. J. Physiol.-Cell Physiol.* **2003**, *285*, C873-C880.
- (140) Weber, D. K.; Gehman, J. D.; Separovic, F.; Sani, M. A. *Aust. J. Chem.* **2012**, *65*, 472-479.
- (141) Drew, S. C.; Noble, C. J.; Masters, C. L.; Hanson, G. R.; Barnham, K. J. *J. Am. Chem. Soc.* **2009**, *131*, 1195-1207.
- (142) Ali-Torres, J.; Marechal, J. D.; Rodriguez-Santiago, L.; Sodupe, M. *J. Am. Chem. Soc.* **2011**, *133*, 15008-15014.
- (143) Minicozzi, V.; Stellato, F.; Comai, M.; Dalla Serra, M.; Potrich, C.; Meyer-Klaucke, W.; Morante, S. *J. Biol. Chem.* **2008**, *283*, 10784-10792.

- (144) Hatcher, L. Q.; Hong, L.; Bush, W. D.; Carducci, T.; Simon, J. D. *J. Phys. Chem. B* **2008**, *112*, 8160-8164.
- (145) Xiao, Z. G.; Wedd, A. G. *Nat. Prod. Rep.* **2010**, *27*, 768-789.
- (146) Hong, L.; Bush, W. D.; Hatcher, L. Q.; Simon, J. *J. Phys. Chem. B* **2008**, *112*, 604-611.
- (147) Guilloreau, L.; Damian, L.; Coppel, Y.; Mazarguil, H.; Winterhalter, M.; Faller, P. *J. Biol. Inorg. Chem.* **2006**, *11*, 1024-1038.
- (148) Curtain, C. C.; Ali, F. E.; Smith, D. G.; Bush, A. I.; Masters, C. L.; Barnham, K. J. *J. Biol. Chem.* **2003**, *278*, 2977-2982.
- (149) Arispe, N.; Rojas, E.; Pollard, H. B. *P. Natl. Acad. Sci. USA* **1993**, *90*, 567-571.
- (150) Adibhatla, R. M.; Hatcher, J. F. *Antioxid. Redox Signal* **2010**, *12*, 125-169.
- (151) Axelsen, P. H.; Komatsu, H.; Murray, I. V. *J. Physiology* **2011**, *26*, 54-69.
- (152) Kagan, V. E. *Lipid peroxidation in biomembranes*; CRC Press: Boca Raton, Fla., 1988.
- (153) Kagan, V. E.; Fabisiak, J. P.; Shvedova, A. A.; Tyurina, Y. Y.; Tyurin, V. A.; Schor, N. F.; Kawai, K. *Febs Lett.* **2000**, *477*, 1-7.
- (154) Esterbauer, H.; Ramos, P. *Rev. Physiol. Biochem. Pharmacol.* **1996**, *127*, 31-64.
- (155) Halliwell, B.; Gutteridge, J. M. C. *Met. Enzymology* **1990**, *186*, 1-85.
- (156) Logani, M. K.; Davies, R. E. *Lipids* **1980**, *15*, 485-495.

- (157) Repetto, M.; Semprine, J.; Boveris, A. *Biochemistry, Genetics and Molecular Biology*; Catala, A., Ed.; InTech Publisher: Winchester, UK., 2012.
- (158) Gardner, H. W. *Free Radical Bio. Med.* **1989**, *7*, 65-86.
- (159) Miller, D. M.; Buettner, G. R.; Aust, S. D. *Free Radical Bio. Med.* **1990**, *8*, 95-108.
- (160) Ishida, M.; Yamazaki, T.; Houjou, T.; Imagawa, M.; Harada, A.; Inoue, K.; Taguchi, R. *Rapid Commun. Mass Spec.* **2004**, *18*, 2486-2494.
- (161) Prousek, J. *Pure Appl. Chem.* **2007**, *79*, 2325-2338.
- (162) Urbanski, N. K.; Beresewicz, A. *Acta. Biochimica. Polonica* **2000**, *47*, 951-962.
- (163) Kehrer, J. P. *Toxicology* **2000**, *149*, 43-50.
- (164) Kasprzak, K. S. *Free Radical Bio. Med.* **2002**, *32*, 958-967.
- (165) Lovell, M. A.; Robertson, J. D.; Teesdale, W. J.; Campbell, J. L.; Markesbery, W. R. *J. Neurol. Sci.* **1998**, *158*, 47-52.
- (166) Chauhan, A.; Ray, I.; Chauhan, V. P. *Neurochem. Res.* **2000**, *25*, 423-429.
- (167) Murphy, R. C.; Axelsen, P. H. *Mass Spectrom. Rev.* **2011**, *30*, 579-599.
- (168) Reis, A.; Domingues, M. R. M.; Amado, F. M. L.; Ferrer-Correia, A. J. V.; Domingues, P. *Biomed. Chromatogr.* **2005**, *19*, 129-137.
- (169) Harrison, K. A.; Davies, S. S.; Marathe, G. K.; McIntyre, T.; Prescott, S.; Reddy, K. M.; Falck, J. R.; Murphy, R. C. *J. Mass Spectrom.* **2000**, *35*, 224-236.
- (170) Reis, A.; Domingues, M. R. M.; Amado, F. M. L.; Ferrer-Correia, A. J.; Domingues, P. *J. Chromatogr. B* **2007**, *855*, 186-199.

- (171) Reis, A.; Domingues, P.; Ferrer-Correia, A. J. V.; Domingues, M. R. M. *Rapid Commun. Mass Spec.* **2004**, *18*, 2849-2858.
- (172) Burton, G. W.; Ingold, K. U. *J. Am. Chem. Soc.* **1981**, *103*, 6472-6477.
- (173) Haas, K. L.; Franz, K. J. *Chem. Rev.* **2009**, *109*, 4921-4960.
- (174) Yoshida, K.; Terao, J.; Suzuki, T.; Takama, K. *Biochem. Biophys. Res. Commun.* **1991**, *179*, 1077-1081.
- (175) Merchant, T. E.; Glonek, T. *Lipids* **1992**, *27*, 551-559.
- (176) Martell, A. E.; Smith, R. M. *Critical stability constants*; Plenum Press: New York, 1974.
- (177) Sarkar, B.; Wigfield, Y. *J. Biol. Chem.* **1967**, *242*, 5572-&.
- (178) Morita, M.; Tokita, M. *Lipids* **2006**, *41*, 91-95.
- (179) Crane, J. M.; Tamm, L. K. *Biophys. J.* **2004**, *86*, 2965-2979.
- (180) Dietrich, C.; Bagatolli, L. A.; Volovyk, Z. N.; Thompson, N. L.; Levi, M.; Jacobson, K.; Gratton, E. *Biophys. J.* **2001**, *80*, 1417-1428.